THE MINERALOGICAL MAGAZINE

AND

JOURNAL OF
THE MINERALOGICAL SOCIETY

No. 238 September, 1957 Vol. XXXI

# *Götzenite and combeite, two new silicates from the Belgian Congo.*

By Th. G. Sahama and Kai Hytönen, M.A.

Institute of Geology, University of Helsinki, Finland.

[Read 6 June 1957.]

*Summary.* A nephelinite from the extinct volcano Mt. Shaheru, North Kivu, Belgian Congo, contains two new minerals: *Götzenite* is triclinic with $a$ 10·93, $b$ 7·32, $c$ 5·74 Å., $\alpha$ 90°, $\beta$ 100°, $\gamma$ 120°; the unit-cell contents approximate to $(Ca,Na,Al)_7(Si,Ti)_5O_{15}F_{3\cdot5}$, and the optical constants are $\alpha$ 1·660, $\beta$ 1·662, $\gamma$ 1·670, $2V_\gamma$ 52°; sp.gr. 3·138. Götzenite is related to the rinkite series, and, less closely, to wollastonite and pectolite. *Combeite* is rhombohedral, space-group $R3m$, $R32$, or $R\bar{3}m$, $a$ 10·43, $c$ 13·14 Å., the unit cell containing approximately $3[Na_4(Ca,Al,Fe)_3Si_6O_{16}(O,OH,F)_2]$; optically uniaxial positive, $\epsilon = \omega = 1{\cdot}598 \pm 0{\cdot}002$; sp.gr. 2·844.

In 1954, together with Mr. André Meyer, of the Geological Survey of the Belgian Congo, the authors had the privilege of making a joint excursion to the active volcano Mt. Nyiragongo and to its extinct southern tributary Mt. Shaheru in North Kivu, Belgian Congo. On that excursion a specimen was collected from the north-eastern inner wall of the Shaheru crater and numbered S. 80 = M. 2 and 3. Later microscopic study of the rock showed that it represents a nephelinite with a rather complicated mineralogical composition. Among the principal constituents of the rock two were found that could not be identified microscopically. A detailed investigation of these two minerals proved them to be new species, now named götzenite and combeite, the description of which is given in this paper. The petrography of the rock itself will be published later in connexion with the general mineralogy and petrology of the Nyiragongo area lavas by the senior author in the papers by the Institut des Parcs Nationaux du Congo Belge, Brussels.

## *Götzenite.*

This mineral occurs as prismatic crystals that may reach a length of $\frac{1}{2}$ mm. The crystallographic axes were chosen in such a way that they

correspond to the conventional setting of wollastonite; accordingly, the axis of the prism zone was taken as $b$. Fig. 1 shows a section perpendicular to this $b$-axis. The faces shown were collected from two individual crystals and were indexed on the basis of the unit-cell data. The angles between the faces were measured with the optical goniometer with the following results: (100):(403) = 138°, (403):(001) = 143°, (001):($\bar{1}$01) = 145°, ($\bar{1}$01):($\bar{1}$00) = 113°, ($\bar{1}$00):($\bar{2}$0$\bar{1}$) = 147°, ($\bar{2}$0$\bar{1}$):(00$\bar{1}$) = 135°,

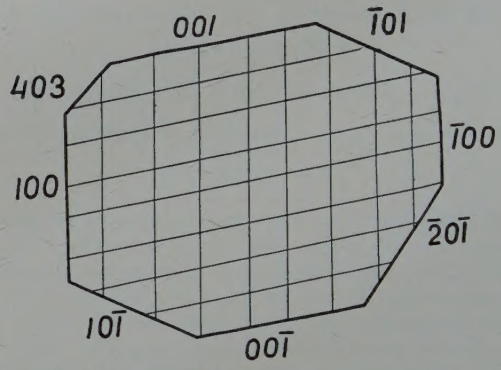


FIG. 1. Götzenite crystal. Section perpendicular to the $b$-axis.

(00$\bar{1}$):(10$\bar{1}$) = 146°, (10$\bar{1}$):(100) = 113°. Owing to the small size and poor quality of the crystals and the goniometer available for their measurement, these interfacial angles are only accurate to $\pm\frac{1}{2}°$. Faces outside the [010] zone are extremely rare and were detected only in a few crystals; and these pyramidal faces are too poorly developed to be accurately measured and indexed. There is a perfect cleavage ‖ (100), and a good one ‖ (001). Almost every crystal shows lamellar twinning, with twin axis $b$; the composition plane is perpendicular to (001).

The mineral is colourless in thin section. Under the binocular microscope with low power, the crystals lying on the surface of the specimen are glass clear. The refractive indices measured with the immersion method are: $\alpha = 1{\cdot}660$, $\beta = 1{\cdot}662$, $\gamma = 1{\cdot}670$. Birefringence weak: $\gamma - \alpha = 0{\cdot}010$ (calculated). Optically positive. $2V_\gamma = 52°$ (measured). The refractive indices given yield a value $2V_\gamma = 53\frac{1}{2}°$ (calculated). The optic axial angle is somewhat greater for red than for blue. Dispersion strong. The optical orientation for sodium light is indicated in fig. 2: the optic axial plane makes an angle of 29° with the $b$-axis, and on (010) the extinction direction $\gamma'$ makes an angle of *ca.* 58° with the trace of the $c$-axis in the obtuse angle $\beta$.

A pycnometric measurement of the specific gravity yielded $D_{4°}^{20°} = 3{\cdot}138$.

The mineral is triclinic. The lengths of the axes of the unit cell were measured from rotation photographs with the crystal rotated about the

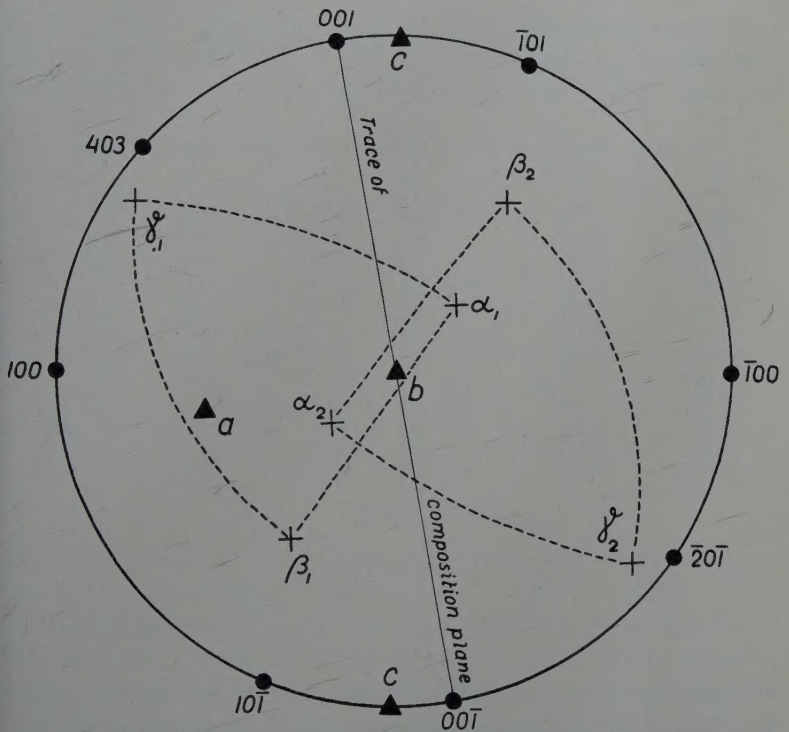


FIG. 2. Optical orientation of a götzenite twin in stereographic projection.

three axes. The interaxial angles of the reciprocal cell were measured from the three corresponding zero-layer Weissenberg photographs with the following results: $\alpha^* = 84°$, $\beta^* = 78\frac{1}{3}°$, $\gamma^* = 59\frac{1}{3}°$. To test the interaxial angle $\alpha$ of the direct cell, a first and second layer equi-inclination Weissenberg photograph was taken rotating the crystal about the *b*-axis. No deviation from 90° was detected for $\alpha$. The data obtained lead to the unit-cell dimensions (assuming $\lambda = 1{\cdot}54050$ Å. for Cu-$K\alpha_1$):

| | | |
|---|---|---|
| *a* 10·93±0·05 Å., | *b* 7·32±0·03, | *c* 5·74±0·03, |
| $\alpha$ 90°, | $\beta$ 100°±1°, | $\gamma$ 120°±1°, |

Volume 389 Å$^3$., $a:b:c::1{\cdot}493:1:0{\cdot}784$.

The rotation photograph about the $b$-axis shows very weak layer lines with $n$ odd. Hence there is a pronounced sub-cell with $b = 3{\cdot}66$ Å.

The powder pattern of götzenite was recorded with the Philips Norelco diffractometer using copper radiation and nickel filter. The result is presented in table I.

Götzenite was separated for chemical analysis by centrifuging the powdered rock in Clerici's solution. The material used for the analysis was tested under the microscope and found to be of a very high purity.

TABLE I. Powder pattern of götzenite. Filtered copper radiation.

| $2\theta$ | $d$ | $I$ | $2\theta$ | $d$ | $I$ |
|---|---|---|---|---|---|
| 22·24 | 3·994 | 15 | 43·935 | 2·059 | 5 |
| 24·70 | 3·601 | 5 | *45·575 | 1·989 | 7 |
| 28·775 | 3·100 | 100 | 47·535 | 1·911 | 50 |
| 29·90 | 2·986 | 100 | 48·495 | 1·876 | 15 |
| 31·26 | 2·859 | 10 | 49·685 | 1·833 | 15 |
| 31·68 | 2·822 | 7 | 50·72 | 1·798 | 10 |
| 33·815 | 2·648 | 40 | 54·24 | 1·690 | 25 |
| 35·725 | 2·511 | 25 | *55·815 | 1·646 | 7 |
| 38·725 | 2·323 | 10 | 57·81 | 1·594 | 10 |
| 39·83 | 2·261 | 15 | 58·635 | 1·573 | 10 |
| 40·71 | 2·214 | 7 | *59·88 | 1·543 | 10 |
| *41·945 | 2·152 | 5 | 62·635 | 1·482 | 15 |

* Line broad.

The result of the chemical analysis and the unit-cell content, calculated on the basis of the density and X-ray data, is summarized in table II. Neglecting the minor constituents, the stoichiometric net formula of götzenite may be written as $5Ca(Si,Ti)O_3.(Na,Ca,Al)_2F_{3\cdot5}$. The structural interpretation of this empirical formula must be left till the crystal structure of the mineral has been worked out. A qualitative spectrographic test revealed the absence of Ce, Yt, and Cb in the mineral.

Experiments made with the Leitz heating microscope (1954 model) revealed the fact that the birefringence of götzenite is strongly decreased on heating. At a temperature of $955° \pm 10°$ C. the mineral becomes isotropic and loses its transparency. A powder pattern of the heated material showed the mineral to be decomposed. The decomposition product consists apparently of a mixture of phases the identification of which is difficult.

Götzenite is easily soluble in hot diluted hydrochloric acid.

In chemical composition, götzenite is closely related to calcium rinkite from Yukspor, Kola. Calcium rinkite may be derived from rinkite by replacing most of the rare earths by calcium. Rare earths are not present

at all in götzenite. Accordingly, the following series with decreasing rare-earth content may be established: rinkite–calcium-rinkite–götzenite. The optical and unit-cell data for rinkite and calcium rinkite being incomplete so far, an accurate comparison of these three minerals with each other is not possible. However, the entire absence of the rare

TABLE II. Chemical composition and unit-cell content of götzenite.

| | % | | *Atomic ratio* $\times 10^4$ | *Unit-cell content* |
|---|---|---|---|---|
| $SiO_2$ | 32·50 | Si | 5409 | 3·98 |
| $TiO_2$ | 9·72 | Ti | 1217 | 0·90 |
| $Al_2O_3$ | 4·26 | Al | 836 | 0·62 |
| $Fe_2O_3$ | 0·35 | $Fe^{3+}$ | 44 | 0·03 |
| FeO | 0·45 | $Fe^{2+}$ | 63 | 0·05 |
| MnO | 0·07 | Mn | 10 | 0·01 |
| MgO | 0·29 | Mg | 72 | 0·05 |
| CaO | 41·80 | Ca | 7454 | 5·49 |
| BaO | 0·09 | Ba | 6 | 0·00 |
| SrO | 0·00 | Na | 1565 | 1·15 |
| $Na_2O$ | 4·85 | K | 30 | 0·02 |
| $K_2O$ | 0·14 | F | 4384 | 3·23 |
| $P_2O_5$ | 0·01 | Cl | 42 | 0·03 |
| $CO_2$ | 0·00 | $SO_4$ | 24 | 0·02 |
| F | 8·33 | OH | 287 | 0·21 |
| Cl | 0·15 | O | 20546 | 15·11 |
| $SO_3$ | 0·19 | | | |
| $H_2O+$ | 0·26 | | | |
| $H_2O-$ | 0·14 | | | |
| | 103·60 | | | |
| $-O$ | 3·54 | | | |
| Total | 100·06 | | | |

earths (and Cb, Sr) and the somewhat higher fluorine content of götzenite as well as its slightly differing optical properties seem to justify the mineral being distinguished from calcium rinkite. Götzenite is also formally related to wollastonite and pectolite.

The mineral is named after the German traveller, Count G. A. von Götzen, who was the first white man to climb Mt. Shaheru and Mt. Nyiragongo in 1894, together with a German companion.

### *Combeite.*

Crystals are poorly developed; in some instances stout hexagonal prisms were found, a few tenths of a millimetre in length. No terminal faces are visible, and there is no cleavage. The mineral is colourless, optically uniaxial, positive; birefringence very low. Refractive indices

by the immersion method: $\epsilon \approx \omega = 1{\cdot}598 \pm 0{\cdot}002$. $D_{4°}^{20°} = 2{\cdot}844$ (pycnometer).

A series of Weissenberg photographs proved the mineral to be rhombohedral. The unit-cell dimensions were determined from rotation photographs about the *a*- and *c*-axis, respectively. The results are:

$c = 13{\cdot}14 \pm 0{\cdot}03$ Å. $\quad c/a = 1{\cdot}260$.

$a = 10{\cdot}43 \pm 0{\cdot}03$ Å. $\quad$ Volume $= 1238$ Å$^3$.

Diffraction symbol $\bar{3}mR$—. Possible space-groups $R3m$, $R32$, and $R\bar{3}m$. The powder pattern recorded with the Philips Norelco diffractometer

TABLE III. Powder pattern of combeite. Filtered copper radiation. Indices given in hexagonal notation.

| *hkil* | *I* | 2*ϑ* | *d* | $Q_{obs.}$ | $Q_{calc.}$ | *hkil* | *I* | 2*ϑ* | *d* | $Q_{obs.}$ | $Q_{calc.}$ |
|---|---|---|---|---|---|---|---|---|---|---|---|
| $10\bar{1}1$ | 10 | 11·87 | 7·449 | 0·0180 | 0·0180 | $20\bar{2}5$ | 15 | 39·625 | 2·72 | 0·1937 | 0·1938 |
| 0003 | 30 | 20·255 | 4·380 | 0·0521 | 0·0521 | *$\bar{4}042$ | 15 | 42·28 | 2·136 | 0·2192 | 0·2192 |
| $20\bar{2}2$ | 50 | 23·89 | 3·722 | 0·0722 | 0·0722 | *$32\bar{1}5$ | 10 | 43·415 | 2·083 | 0·2305 | 0·2305 |
| $11\bar{2}3$ | 40 | 26·555 | 3·354 | 0·0889 | 0·0889 | $40\bar{4}4$ | 40 | 48·91 | 1·861 | 0·2887 | 0·2886 |
| $21\bar{3}1$ | 70 | 26·96 | 3·304 | 0·0916 | 0·0915 | $\bar{4}153$ | 10 | 50·805 | 1·795 | 0·3104 | 0·3094 |
| *$30\bar{3}0$ | 10 | 29·585 | 3·017 | 0·1099 | 0·1103 | $\bar{5}051$ | | | | | 0·3120 |
| $\bar{2}024$ | 100 | 33·70 | 2·657 | 0·1417 | 0·1416 | $\bar{2}027$ | 10 | 52·735 | 1·734 | 0·3326 | 0·3327 |
| $22\bar{4}0$ | 80 | 34·375 | 2·607 | 0·1471 | 0·1470 | $20\bar{2}8$ | 20 | 59·825 | 1·544 | 0·4195 | 0·4196 |
| $\bar{1}015$ | 10 | 35·52 | 2·525 | 0·1568 | 0·1570 | $64\bar{2}4$ | 20 | 61·125 | 1·515 | 0·4357 | 0·4356 |
| $31\bar{4}2$ | 10 | 38·43 | 2·340 | 0·1826 | 0·1824 | *$60\bar{6}0$ | 20 | 61·575 | 1·505 | 0·4415 | 0·4410 |

* Line broad.

(filtered copper radiation) is summarized in table III. The indexing is based on the unit-cell dimensions given above.

Combeite was separated from the rock for chemical analysis by centrifuging in Clerici's solution. A microscopic test revealed that the material to be analysed was of a somewhat lower purity than the analysed material for götzenite. However, the contamination consisted mostly of the alteration product of combeite to be described below. The result of the chemical analysis and the unit-cell content, calculated on the basis of the density and X-ray data, is summarized in table IV. The following simplified formula may be tentatively written for combeite: $Na_4(Ca,Al,Fe)_3Si_6O_{16}(OH,F)_2$. The unit cell contains three formula weights. A structural formula cannot be established as long as the type of the crystal structure has not been determined.

Combeite is easily soluble in hot diluted hydrochloric acid. Much of the mineral has undergone alteration, as illustrated in fig. 3. The crystals consist mostly of an alteration product in which unaltered combeite forms irregularly shaped relics resembling olivine relics in serpentine. The alteration product has a birefringence higher than that of combeite and a wavy extinction. It is uniaxial negative with the optic axis parallel to that of unaltered combeite. The refractive indices

TABLE IV. Chemical composition and unit-cell content of combeite.*

| | % | | *Atomic ratio* $\times 10^4$ | *Unit-cell content* |
|---|---|---|---|---|
| $SiO_2$ | 49·78 | Si | 8284 | 17·69 |
| $TiO_2$ | 0·32 | Ti | 40 | 0·09 |
| $ZrO_2$ | 0·44 | Zr | 35 | 0·07 |
| $Al_2O_3$ | 2·45 | Al | 480 | 1·02 |
| $Fe_2O_3$ | 1·86 | $Fe^{3+}$ | 233 | 0·50 |
| FeO | 0·54 | $Fe^{2+}$ | 75 | 0·16 |
| MnO | 0·58 | Mn | 82 | 0·18 |
| MgO | 0·41 | Mg | 102 | 0·22 |
| CaO | 22·68 | Ca | 4044 | 8·63 |
| BaO | 0·09 | Ba | 6 | 0·01 |
| SrO | 0·00 | Na | 5207 | 11·12 |
| $Na_2O$ | 16·14 | K | 250 | 0·53 |
| $K_2O$ | 1·18 | F | 984 | 2·10 |
| $P_2O_5$ | 0·02 | Cl | 85 | 0·18 |
| $CO_2$ | 0·00 | $SO_4$ | 24 | 0·05 |
| F | 1·87 | OH | 1543 | 3·29 |
| Cl | 0·30 | O | 23423 | 50·02 |
| $SO_3$ | 0·19 | | | |
| $H_2O+$ | 1·39 | | | |
| $H_2O-$ | 0·42 | | | |
| | 100·66 | | | |
| $-O$ | 0·86 | | | |
| Total | 99·80 | | | |

* A spectrographic test showed the material to be free from rare earths.

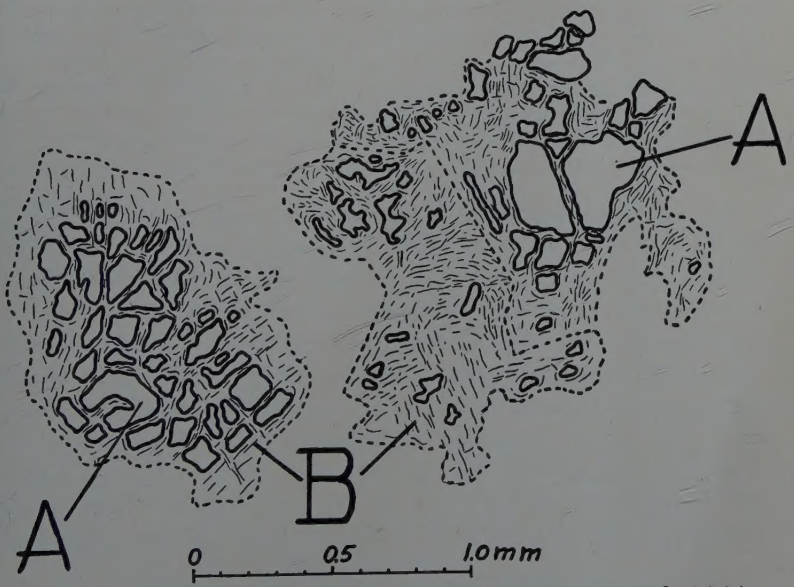


FIG. 3. Unaltered combeite relics (A) surrounded by alteration product (B) in parallel growth.

are lower than those of combeite and vary within the range of *ca.* 1·56–1·57. No noticeable difference was found in powder pattern between pure combeite and a combeite material in which the alteration product was strongly enriched. The similarity in powder pattern and homoaxial growth of combeite and alteration product indicates that the latter is structurally and probably also chemically closely related to the former.

The data for combeite given above are not consistent with any known species. Formally, it represents an analogue to eudialyte.

The mineral is named after the late Mr. A. D. Combe, of the Geological Survey of Uganda, who contributed much to the geology of the Virunga volcanic field; the name should be pronounced kōombite.

*Acknowledgements.* The authors are indebted to the following institutions and individuals: the Emil Aaltonen Foundation, Tampere, Finland, for funds covering the expenses of the two chemical analyses; Mr. Pentti Ojanperä, of the Geological Survey of Finland, for undertaking the task of chemical analysis; Mr. A. Löfgren, of the Geological Survey of Finland, for the spectrographic tests; Prof. Frans-E. Wickman, of the Swedish State Museum for Natural History, Stockholm, for critical inspection of the X-ray data; Prof. C. E. Tilley, of the University of Cambridge, England, for calling the authors' attention to the relationship between calcium rinkite and götzenite.

# *Pyroxenes from the early and middle stages of fractionation of the Skaergaard intrusion, East Greenland.*

(With Plates XVI and XVII.)

By G. M. Brown, M.A., B.Sc., D.Phil., F.G.S.

Department of Geology and Mineralogy, University Museum, Oxford.

With chemical analyses by E. A. Vincent, M.A., B.Sc., Ph.D., F.R.I.C., F.G.S.

Department of Geology and Mineralogy, University Museum, Oxford,

and

P. E. Brown, B.Sc., Ph.D., Department of Geology, University of Manchester.[1]

[Read 28 March 1957.]

*Summary.* Coexisting calcium-rich and calcium-poor pyroxenes have been separated from the gabbros and ferrogabbros of the Skaergaard layered basic intrusion and chemically analysed. Nine new analyses of augites, three of inverted pigeonites, and one of orthopyroxene are presented, together with optical properties. The trend of crystallization of the augites is different from that drawn by previous investigators. The stages at which the orthopyroxene and pigeonite begin and cease to crystallize are defined, and the sub-solidus exsolution and inversion textures of the pigeonites are examined in detail. The characters of the exsolution textures and the degree of pigeonite inversion (monoclinic to orthorhombic pyroxene) are shown to change gradually with height in the intrusion, and are related to a gradual change in the interval between the temperatures of crystallization and inversion.

SINCE the first description of the trend of crystallization of the Skaergaard clinopyroxenes by Wager and Deer (1939), and the review of the course of crystallization of pyroxenes from mafic magmas by Hess (1941), a great deal of attention has been paid to the character and composition of pyroxenes from basic igneous rocks. Hess plotted the Wo–En–Fs ratio of the chemically analysed pyroxenes of the Stillwater complex and the Skaergaard intrusion and was able to demonstrate a general trend of augite crystallization during the cooling of a mafic magma, and to place the analyses of single pyroxenes from several other igneous bodies on this trend. Up to this stage the trend-line in the ferroaugite region had been tentatively based on only two Skaergaard

[1] Present address: Geological Survey, Tanganyika.

analyses, and more analyses in this region were required. Muir (1951) made fifteen new analyses of clinopyroxenes from the Skaergaard intrusion and drew on a Ca–Mg–Fe diagram (1951, fig. 1) a trend that differed from that of Hess. The marked divergence of the trend in the augite region from that postulated by Hess for pyroxenes from mafic magmas was explained by Muir as due to the unique conditions prevalent at the middle gabbro horizon of the Skaergaard intrusion, where olivines temporarily ceased to crystallize. The trend was drawn in relation to five points believed to be the augite components of five bulk pyroxene analyses; the other component was assumed, in each case, to be a calcium-free hypersthene.

From fresh material collected on the East Greenland Geological Expedition (1953) both calcium-rich and calcium-poor pyroxenes were separated and chemically analysed. The two pyroxenes present in all rocks below, and a few within the ferrogabbro horizon were separated by a magnetic separator and Clerici solution. The trend shown by the augites from this single intrusion does not differ markedly from the composite trend drawn by Hess, and the successive augites and ferro-augites of the Skaergaard intrusion would appear to represent an almost complete series of calcium-rich clinopyroxenes resulting from extreme fractionation of a particular type of basaltic magma.

Hess (1941) clarified pyroxene relationships in slowly cooled mafic magmas by defining the approximate limits of solid solution, the orthopyroxene-pigeonite relationship, and the limit of the field of two-pyroxene crystallization, and by showing the significance of certain exsolution textures. Later Poldervaart and Hess (1951) emphasized the importance of differentiating clearly between the three different groups of pyroxenes crystallizing from basaltic magmas, and summarized the evidence that could be obtained about the cooling history of these magmas from a detailed study of the chemical compositions and textures of the pyroxenes. Muir (1954) and Kuno (1955) have since shown that, under certain physical and chemical conditions, the limits of two-pyroxene crystallization and of solid solution between calcium-rich and calcium-poor pyroxenes, defined by Hess, may not apply.

These papers have directed attention to the value of pyroxenes as a guide to the cooling history of basic magmas. The present investigation was undertaken in order to obtain more detailed information on the two coexisting pyroxene phases from the early and middle stages of fractionation of the Skaergaard intrusion. Further work is in progress on the single pyroxenes from the late fractionation stages, to demonstrate

the behaviour of the pyroxenes throughout extreme fractionation of one type of basic magma.

*The pyroxene phases present at different horizons in the intrusion.* In

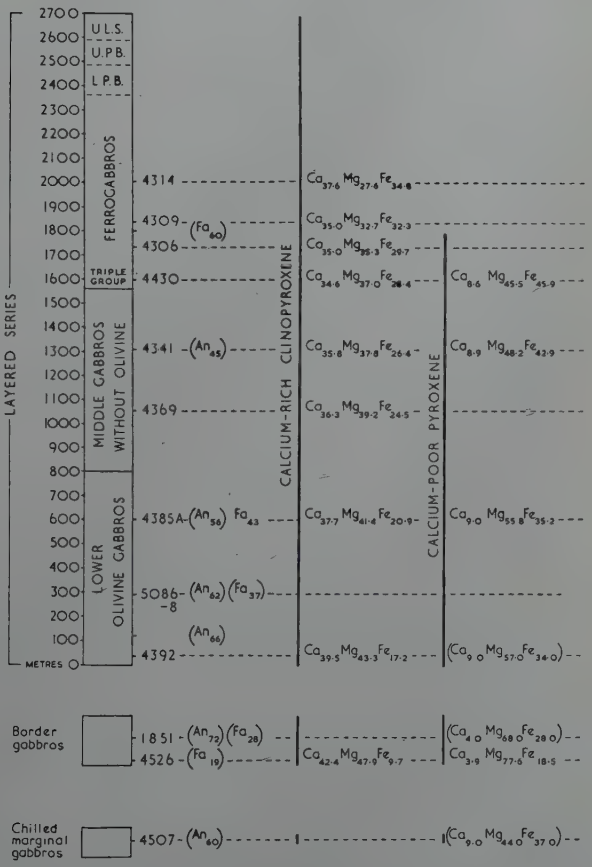


FIG. 1. The relative heights of the rocks of the Skaergaard intrusion from which pyroxenes have been analysed. Compositions of other minerals, if obtained from optical properties, are in brackets.

the chilled marginal gabbro, representing the quickly cooled initial liquid, both augite and pigeonite (subsequently inverted to orthorhombic pyroxene) have crystallized (fig. 1). Rocks formed of the earliest crystal fractions from the slow cooling of this liquid are found next to the chilled margin in the outer part of the narrow marginal border group.

A much greater thickness of similar rocks, forming part of the layered series, is believed to lie hidden below the present level of erosion. The process of formation of the marginal border group is more difficult to understand than is that of the layered series, but three important rock types were recognized by Wager and Deer (1939, p. 137): the gabbro-picrite, rich in a magnesian olivine ($Fa_{19}$); the perpendicular-felspar rock, rich in a basic plagioclase felspar ($An_{70}$); and the wavy-pyroxene rock, rich in an iron-poor augite.

The gabbro-picrite contains a diopsidic augite in small euhedral crystals together with orthopyroxene as poikilitic plates. Orthopyroxene is only found in the gabbro-picrite and the perpendicular-felspar rock, although it is reasonable to suggest that it may occur in the lower rocks of the hidden layered series. In the wavy-pyroxene rock, which occurs in a zone farther from the margin than that containing the gabbro-picrite and perpendicular-felspar rock, the calcium-poor pyroxene phase is an inverted pigeonite rather than orthopyroxene. Thus in the earliest stages of crystallization through fractionation of the Skaergaard magma, a clinopyroxene and an orthorhombic pyroxene were the pyroxene phases to crystallize in equilibrium, but the calcium-poor pyroxene later became a pigeonite rather than an orthopyroxene.

The lowest exposed rocks of the layered series contain augite and a hypersthene formed from inversion of pigeonite (see p. 529 for proof), so the name 'lower olivine gabbro' is used in this paper, in preference to the earlier-used name of 'hypersthene olivine gabbro'. From 0 to 250 m., only the olivine and felspar occur as a primary precipitate, and the pyroxenes appear to have crystallized entirely from the inter-precipitate liquid. However, this evidence does not entirely preclude their crystallization as a primary precipitate in the hidden layered rocks. Above the 250-m. level augite is certainly a primary precipitate mineral, and a little later pigeonite (now inverted) apparently became a primary precipitate phase and together with the olivine and felspar may be concentrated in thin layers.

From 800 m. to 1550 m. (the middle gabbros) olivine fails to crystallize as a primary precipitate. The absence of olivine has apparently no effect on the character of the pyroxenes, a primary precipitate augite crystallizing in equilibrium with a primary precipitate pigeonite (usually inverted) to the 1800-m. level. Towards the top of the middle gabbros and in the lower part of the ferrogabbros (1300-m. to 1800-m. level) a few of the rocks contain grains of uninverted pigeonite. The proportion of uninverted to inverted pigeonite is rarely greater than about 10 %, the highest

value being reached in the upper levels, just before the pigeonite phase disappears.

At approximately the 1800-m. level pigeonite ceased to crystallize and a ferroaugite is the only pyroxene phase present in the increasingly iron-rich ferrogabbros and later rocks. The behaviour of the ferroaugites towards the top of the intrusion has been described by Wager and Deer (1939) and Muir (1951), and further work in progress on these pyroxenes, by L. R. Wager and others, will be described in a later paper.

*Chemical analysis of selected pyroxenes.* The chemical analyses by E. A. V. (see key to table I) were made on a semi-micro scale; all main portions on samples of less than $\frac{1}{2}$ g., and nine of the twelve on samples of less than 150 mg. (the smallest sample analysed was no. 7, of 41 mg.). With this advantage it was possible to work on small fractions, usually of pure material; it would have been impracticable to separate the large amounts required for macro-analysis, of comparable purity, from the middle gabbros and lower ferrogabbros (fig. 1) where augites and pigeonites are closely intergrown.

The analyses (table I) have been recalculated into the standard formula $(WXY)_2Z_2O_6$ (table II), in order to demonstrate both the balance of charge and the variation in cation proportions throughout the fractionation sequence represented by analyses 1 to 10. In order to calculate the distribution of the cations between the $(WXY)$ group (8-fold and 6-fold coordination) and the $(Z)$ group (4-fold coordination), the method described by Hess (1949, p. 625) is believed to be of most value. Thus instead of making $Z = 2$ by adding arbitrary amounts of Al, and occasionally Ti and Fe‴, to the Si (e.g. Kuno, 1955, p. 85), the cations are allotted to groups in accordance with the balance of charge on a cation for cation basis (e.g. NaFe‴:Si; Fe‴:Al; and Al:Al). By this method it is possible to estimate the proportion of Al, $Ti^{IV}$, and Fe‴ likely to be replacing Si in the tetrahedral sites, and their effect, in this position, on the optical properties and unit-cell dimensions.

The variation in the principal cations Ca, Mg, and Fe″ during fractionation is best seen by reference to fig. 2 and is discussed in the following section. However, several of the other cations show a regular pattern in their distribution, which can be seen in table II. The Al in augites and in calcium-poor pyroxenes decreases steadily during fractionation, both in the $(Z)$ and in the $(WXY)$ groups, the decrease being more marked and regular for the augites. The augite always contains more Al in the $(Z)$ group than does the calcium-poor pyroxene from the same rock, but contains about the same (perhaps slightly less) in the $(WXY)$ group.

TABLE I. Analyses and optical properties of the pyroxenes. (All refractive indices $\pm 0{\cdot}001$; $2V \pm 1°$. Data are for the host orthopyroxene in analyses 4A, 6A, and 7A. For the key to these analyses see p. 518.)

| | 1. | 1A. | 3. | 4. | 4A. | 5. | 6. | 6A. | 7. | 7A. | 8. | 9. | 10. |
|---|---|---|---|---|---|---|---|---|---|---|---|---|---|
| $SiO_2$ | 51·17 | 53·6 | 51·25 | 50·66 | 50·35 | 51·26 | 51·26 | 50·9 | 50·58 | 50·5 | 50·33 | 50·10 | 49·73 |
| $Al_2O_3$ | 3·22 | 2·3 | 2·92 | 2·45 | 2·23 | 2·23 | 1·98 | 1·8 | 2·20 | 1·3 | 2·12 | 1·30 | 1·39 |
| $Fe_2O_3$ | 1·53 | 1·3 | 1·70 | 1·33 | 1·14 | 1·25 | 1·25 | 0·7 | 1·57 | 0·7 | 1·69 | 1·51 | 1·50 |
| FeO | 4·54 | 10·8 | 8·87 | 11·24 | 21·12 | 13·34 | 14·49 | 25·1 | 15·53 | 27·0 | 16·32 | 17·89 | 19·28 |
| MnO | 0·13 | 0·3 | 0·18 | 0·29 | 0·38 | 0·34 | 0·35 | 0·3 | 0·28 | 0·2 | 0·23 | 0·43 | 0·41 |
| MgO | 16·68 | 28·7 | 15·04 | 14·25 | 20·03 | 13·40 | 12·85 | 16·4 | 12·60 | 15·5 | 11·92 | 11·17 | 9·40 |
| CaO | 20·54 | 2·0 | 19·04 | 18·01 | 4·50 | 17·23 | 16·91 | 4·2 | 16·40 | 4·1 | 16·48 | 16·68 | 17·75 |
| $Na_2O$ | 0·65 | 0·2 | 0·37 | 0·36 | — | 0·26 | 0·26 | 0·1 | 0·24 | 0·2 | 0·25 | 0·25 | 0·24 |
| $K_2O$ | 0·05 | $0{\cdot}0_3$ | 0·05 | 0·08 | — | 0·02 | 0·02 | $0{\cdot}0_4$ | 0·03 | 0·1 | 0·03 | 0·02 | 0·02 |
| $TiO_2$ | 0·97 | 0·5 | 0·76 | 1·30 | 0·55 | 0·80 | 0·84 | 0·5 | 0·61 | 0·4 | 0·71 | 1·31 | 0·77 |
| $Cr_2O_3$ | 0·42 | 0·3 | 0·17 | n.d.* | n.d. | < 0·01 | < 0·01 | n.d. | < 0·01 | n.d. | n.d. | n.d. | n.d. |
| | 99·90 | $100{\cdot}0_3$ | 100·35 | 99·97 | 100·30 | 100·13 | 100·21 | $100{\cdot}0_4$ | 100·04 | 100·0 | 100·08 | 100·66 | 100·49 |
| $\beta$ | 1·691 | — | 1·695 | 1·697 | — | 1·700(5) | 1·702 | — | 1·704 | — | 1·707 | 1·710 | 1·714 |
| $\gamma$ | — | 1·689 | — | — | 1·714 | — | — | 1·723 | — | 1·727 | — | — | — |
| 2V | 47°(+) | 75°(−) | 45°(+) | 42°(+) | 53°(−) | 41°(+) | 41°(+) to 44°(+) | 47°(−) | 40°(+) to 42°(+) | 46°(−) | 40°(+) | 42°(+) | 46½°(+) |
| Exsolution lamellae | None | (100) | (100) and (001) | (001) | complex | (001) | (001) | complex | (001) | complex | (001) | (001) | None |
| *Atomic* % | | | | | | | | | | | | | |
| Ca | 42·4 | 3·9 | 39·5 | 37·7 | 9·0 | 36·3 | 35·8 | 8·9 | 34·6 | 8·6 | 35·0 | 35·0 | 37·6 |
| Mg | 47·9 | 77·6 | 43·3 | 41·4 | 55·8 | 39·2 | 37·8 | 48·2 | 37·0 | 45·5 | 35·3 | 32·7 | 27·6 |
| Fe | 9·7 | 18·5 | 17·2 | 20·9 | 35·2 | 24·5 | 26·4 | 42·9 | 28·4 | 45·9 | 29·7 | 32·3 | 34·8 |

* $Cr_2O_3 = 0{\cdot}06$ % in augite of 4389, of similar horizon and almost identical composition to 4385A (analyst, E. A. V.).

TABLE II. Formulae of the analysed pyroxenes (on the basis of six oxygen atoms) arranged in their order of crystallization during fractionation. (Note the changes in the amount of each cation during fractionation, and also the relative distribution of minor cations between the calcium-poor pyroxenes 1A, 4A, 6A, 7A and the corresponding calcium-rich pyroxenes 1, 4, 6, 7.)

| | | 1. | 1A. | 3. | 4. | 4A. | 5. | 6. | 6A. | 7. | 7A. | 8. | 9. | 10. |
|---|---|---|---|---|---|---|---|---|---|---|---|---|---|---|
| $Z$ | Si | 1·882 | 1·911 | 1·904 | 1·903 | 1·895 | 1·932 | 1·937 | 1·947 | 1·925 | 1·952 | 1·923 | 1·924 | 1·931 |
| $Z$ | Al | 0·099 | 0·074 | 0·097 | 0·094 | 0·081 | 0·081 | 0·078 | 0·059 | 0·080 | 0·042 | 0·081 | 0·060 | 0·063 |
| $Z$ | Ti | — | — | — | — | — | — | — | — | — | — | — | 0·020 | 0·005 |
| $WXY$ | Al | 0·040 | 0·023 | 0·030 | 0·015 | 0·018 | 0·018 | 0·010 | 0·022 | 0·018 | 0·019 | 0·013 | — | — |
| $WXY$ | $Fe'''$ | 0·042 | 0·034 | 0·047 | 0·038 | 0·032 | 0·036 | 0·036 | 0·021 | 0·046 | 0·021 | 0·048 | 0·044 | 0·044 |
| $WXY$ | $Fe''$ | 0·139 | 0·321 | 0·277 | 0·354 | 0·665 | 0·421 | 0·458 | 0·801 | 0·494 | 0·873 | 0·521 | 0·574 | 0·625 |
| $WXY$ | Mn | 0·004 | 0·009 | 0·007 | 0·009 | 0·011 | 0·011 | 0·011 | 0·011 | 0·009 | 0·007 | 0·007 | 0·014 | 0·014 |
| $WXY$ | Mg | 0·915 | 1·526 | 0·833 | 0·797 | 1·124 | 0·751 | 0·724 | 0·935 | 0·716 | 0·891 | 0·684 | 0·639 | 0·543 |
| $WXY$ | Ca | 0·809 | 0·077 | 0·759 | 0·725 | 0·181 | 0·695 | 0·685 | 0·172 | 0·668 | 0·169 | 0·675 | 0·685 | 0·739 |
| $WXY$ | Na | 0·046 | 0·015 | 0·027 | 0·027 | n.d. | 0·018 | 0·018 | 0·009 | 0·018 | 0·014 | 0·018 | 0·018 | 0·019 |
| $WXY$ | K | 0·002 | 0·002 | 0·002 | 0·004 | n.d. | — | — | 0·002 | 0·002 | 0·004 | 0·002 | — | — |
| $WXY$ | Ti | 0·027 | 0·013 | 0·022 | 0·036 | 0·016 | 0·023 | 0·025 | 0·014 | 0·018 | 0·012 | 0·021 | 0·017 | 0·019 |
| $WXY$ | Cr | 0·013 | 0·009 | 0·004 | n.d.* | n.d. | — | — | n.d. | — | n.d. | n.d. | n.d. | n.d. |
| $Z$ | | 1·981 | 1·985 | 2·001 | 1·997 | 1·976 | 2·013 | 2·015 | 2·006 | 2·005 | 1·994 | 2·004 | 2·004 | 1·999 |
| $WXY$ | | 2·037 | 2·029 | 2·008 | 2·005 | 2·047 | 1·973 | 1·967 | 1·987 | 1·989 | 2·010 | 1·989 | 1·991 | 2·003 |
| % Al in $Z$ | | 5·0 | 3·7 | 4·8 | 4·7 | 4·1 | 4·0 | 3·9 | 2·9 | 4·0 | 2·1 | 4·0 | 3·0 | 3·2 |
| % Ti in $Z$ | | — | — | — | — | — | — | — | — | — | — | — | 1·0 | 0·3 |

* Cr = 0·002 in augite of 4389, of similar horizon and almost identical composition to 4385A.

KEY TO TABLES I AND II.

1 Augite from gabbro-picrite, 4526.
1A Bronzite from gabbro-picrite, 4526. Analysis obtained by subtracting 5·2 % of analysed augite (1) from analysis of contaminated sample and recalculating to 100 %.
3 Augite from lower olivine gabbro, 4392.
4 Augite from lower olivine gabbro, 4385A.
4A Pigeonite from lower olivine gabbro, 4385A.
5 Augite from middle gabbro, 4369.
6 Augite from middle gabbro, 4341.
6A Pigeonite from middle gabbro, 4341. Analysis obtained by subtracting 3·8 % of analysed augite (6) from analysis of contaminated sample and recalculating to 100 %.
7 Augite from ferrogabbro, 4430.
7A Pigeonite from ferrogabbro, 4430. Analysis obtained by subtracting 10 % of analysed augite (7) from analysis of contaminated sample and recalculating to 100 %.
8 Augite from ferrogabbro, 4306.
9 Augite from ferrogabbro, 4309.
10 Augite from ferrogabbro, 4314.

See fig. 1 for height of the rocks in a vertical succession.

Analyses 1, 1A, 3, 5, 6, 6A, 7, 7A, 8, 9, 10 by E. A. Vincent.

Analyses and separation of 4, 4A by P. E. Brown.

A few augites are slightly zoned with an irregular narrow outer rim having 2V up to 3° greater than that of the main part of the crystal. Although too sporadically developed to take into account, this will have some effect on the accuracy of a correlation between optical properties and chemical compositions.

The Na and Cr contents decrease during fractionation, the $Fe'''$ remains remarkably constant, while the Mn shows a very slight overall increase in the later stages. The K remains very low throughout the series. The Ti content hardly varies, except that in specimens 9 and 10 the charge balance requires a small amount of Ti in the (*Z*) group. This unusual condition is not related to a progressive increase during fractionation because later pyroxenes in the sequence (to be published later) contain amounts comparable with those of specimens 1 to 8. Despite the unusual distribution of Ti in these two augites the $TiO_2$ % is not abnormally high (cf. Wilkinson 1956, table II, in which the high $TiO_2$ % of 56 clinopyroxenes from alkali olivine-basalt magmas is demonstrated). The entry of Ti into the (*Z*) group is also a function of $Al_2O_3$ content, and pyroxenes with a higher $TiO_2$ content than these Skaergaard augites may not contain Ti in the (*Z*) group, provided the $Al_2O_3$ content is high enough (e.g. Hess, 1949, analyses 24 to 26).

When the compositions of coexisting augites and calcium-poor pyroxenes are considered it is seen that the augites are, in each case, relatively enriched in Al (*Z* group), $Fe'''$, Na, Ti, and Cr.

*The nature of the gradual changes in character and composition of the*

*Skaergaard pyroxenes during fractionation.* The pyroxenes that crystallized from the Skaergaard magma changed gradually in character and composition (related to Ca:Mg:Fe ratio) over a considerable range during fractionation (fig. 1). The changes resemble those summarized by Poldervaart and Hess (1951), who predicted the range and sequence of changes for pyroxenes from a single body of strongly fractionated

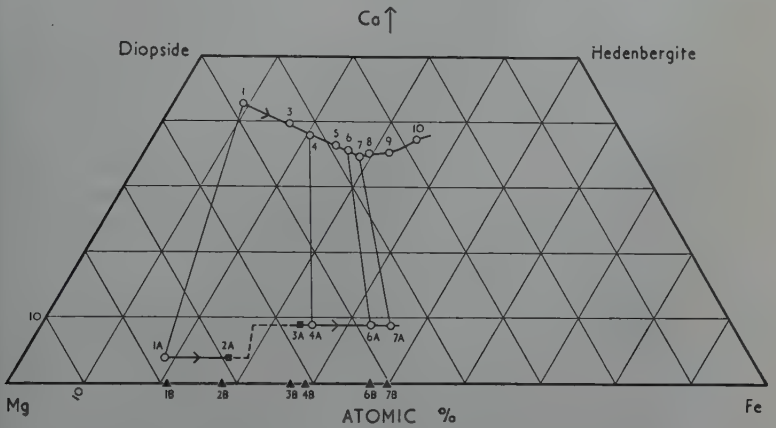


FIG. 2. Trend of crystallization of calcium-rich and calcium-poor Skaergaard pyroxenes; ○ analysed specimens (1 to 10, augite; 1A, orthopyroxene; 4A to 7A, pigeonite); ▲ composition, as Fe:Mg ratio, derived from optical properties (1F, 2B, primary orthopyroxene; 3B to 7B, orthopyroxene from pigeonite inversion); ■ composition, as Ca:Mg:Fe ratio, derived from optical properties and the assumption of standard calcium content in orthopyroxene and pigeonite.

basaltic magma by assembling evidence, at several fractionation stages, from different intrusions.

The textures of the earliest crystal accumulate, the gabbro-picrite, indicate that although olivine probably began to crystallize before pyroxene, it was soon joined by a diopsidic clinopyroxene (no. 1, fig. 2), while poikilitic plates of orthopyroxene (no. 1A, fig. 2) grew from the interprecipitate liquid. The presence of orthopyroxene rather than pigeonite at this stage indicates crystallization of the calcium-poor phase below the clinopyroxene–orthopyroxene inversion temperature curve (cf. Hess, 1941, fig. 9), while the presence of inverted pigeonite in the chilled margin indicates crystallization of this pyroxene phase above the inversion curve, the subsequent inversion to orthopyroxene taking place at sub-solidus temperatures.

In order to represent this relationship a diagram including both solidus

and liquidus curves, in addition to the inversion curve, is necessary (fig. 5; construction explained in Appendix, p. 541). The gabbro-picrite contains orthopyroxene (*B*) as the calcium-poor phase, while the chilled magma (EG 4507) contains pigeonite (*D*), now inverted. If the magma at the commencement of pyroxene crystallization is represented by

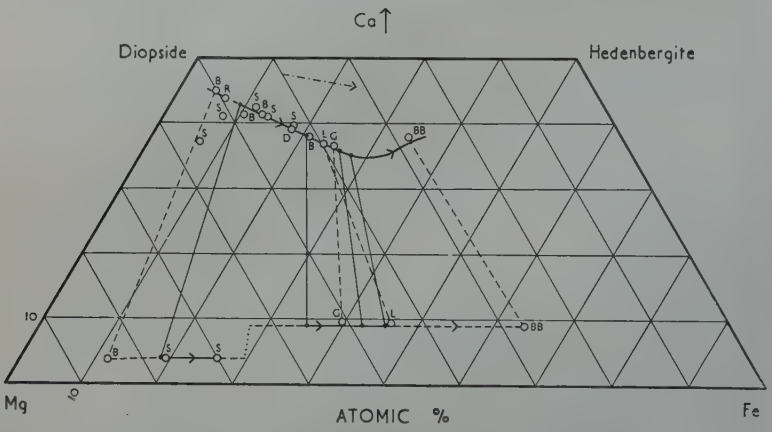


FIG. 3. Pyroxenes from well-described, slowly cooled, tholeiitic-basalt magmas plotted in relation to the Skaergaard trends. Apart from two augites from the Stillwater complex the plot indicates a well-defined general trend of crystallization, both for calcium-rich and calcium-poor pyroxenes. The tie-lines between analysed pairs of pyroxenes from the same rock are shown. ———— Skaergaard intrusion (• analysed co-existing pairs); – – – – other intrusions; • • • • probable inversion interval for plutonic pyroxenes (cf. Kuno and Nagashima, 1952, p. 1001, for volcanic pyroxenes); – • – • → general trend of augites from alkali-basalt magmas (Wilkinson, 1956). B = Bushveld, D = Duluth, G = Goose Creek, L = Lambertville, S = Stillwater (Hess, 1949 and 1952); BB = Beaver Bay (Muir, 1954); R = Rhum (Brown, 1956).

point *C* in fig. 5, chilling with supercooling of the liquid will result in the crystallization of pigeonite at point *D*. Further cooling will result in inversion to orthopyroxene. With slow cooling of this magma, on the other hand, pyroxenes (*B*) representing the solid phase in equilibrium with liquid *C* at this temperature will separate, and in view of their composition will crystallize as orthorhombic pyroxene. Pyroxenes *B* and *D* bear a relationship similar to that of intratelluric pyroxene phenocrysts to groundmass pyroxenes of a porphyritic lava (*P*1, *G*1, ..., fig. 5).

The perpendicular-felspar rock, which crystallized as part of the marginal border group, but later than the gabbro-picrite, also contains

augite and orthopyroxene, the latter (no. 2A, fig. 2) lying between *B* and *P*1 (fig. 5) in composition. The last important rock type to crystallize in the marginal border group is the wavy-pyroxene rock, which contains rare inverted pigeonite of composition close to that of *D* (fig. 5).

The lower olivine gabbros, of which 4392 (fig. 1) is an example, contain both augite (no. 3, fig. 2) and rare inverted pigeonite, in each case as poikilitic plates enwrapping olivine and plagioclase. Easily recognizable primary precipitate crystals of augite and pigeonite are not found until 250 m. above the base of the exposed layered series, and it is not easy to predict the character of the pyroxenes in the hidden layered series. By analogy with other intrusions (e.g. Hess, 1949) it might be expected that after the deposition of the gabbro-picrite a series of clinopyroxenes would crystallize between augites 1 and 3 (fig. 2), in equilibrium at first with orthopyroxenes (such as 2A) and later with pigeonites. The hidden layered series, in all probability, contains the clue as to the position at which a pigeonite, rather than an orthopyroxene, begins to crystallize in equilibrium with augite. In view of the lack of evidence for this position in the Skaergaard intrusion, the transition from orthopyroxene to pigeonite has been placed (fig. 2) at the stage defined by Kuno and Nagashima (1952, fig. 2).

For the first 250 m. of the lower olivine gabbros it is not uncommon to see orthopyroxene free from coarse exsolution lamellae forming narrow extensions to the variety rich in blebs and lamellae, thought to be inverted pigeonite. As the trend of fractionation is from orthopyroxene to pigeonite this relationship is unexpected. If the observed relationship were due to growth of the orthopyroxenes from the late residual liquid after the temperature had dropped below the inversion temperature, the composition of the orthopyroxene ought to be more ferriferous than the host orthopyroxene of the inverted pigeonite. In fact the two are identical in composition, and the relationship may possibly be explained by assuming that the whole grain (core plus extension) was originally pigeonite, and that exsolution began at the centre, the exsolved material from the rim migrating there and leaving the extension free from exsolution lamellae. The texture shown in pl. XVII, fig. 7, would be difficult to explain on any other hypothesis.

At the 600-m. level augite and pigeonite co-exist as a primary precipitate, and both have been analysed from 4385A (fig. 2, nos. 4 and 4A). The pyroxenes throughout the lower olivine gabbros vary little in composition, considering the thickness of gabbro involved. By comparing the change in composition of pyroxenes 1 to 3 with that of pyroxenes 3

to 5, then, assuming a similar rate of fractionation, some estimate of the great thickness of hidden layered series can be obtained.

At 800 m. olivine ceased to crystallize, and the olivine-free middle gabbro series begins. Two typical rocks of this group, 4369 and 4341, still contain augite and pigeonite as a primary precipitate, and the four minerals have been analysed. The analyses show that the disappearance of olivine does not produce a sharp change in the trend-line (fig. 2), as suggested by Muir (1951, fig. 1). The rate of fractionation, as illustrated by the change in pyroxene composition with height in the intrusion, is seen to be increasing markedly. The habits of the augite and pigeonite have changed slowly through the lower olivine gabbro and the middle gabbro horizons. In rocks such as 4369 the discrete, primary-precipitate character of the pigeonite is more easy to detect than at lower horizons, possibly owing to there being less material added to these grains, in the form of irregular extensions, from the interprecipitate liquid. The pigeonite and augite tend to occur together in aggregates of four to six grains. In 4341 and higher in the succession these aggregates of pyroxene grains have become the most distinctive textural feature, the pigeonites being even more uniform in size and shape than in 4369 (fig. 4). The clusters of pyroxenes usually consist of at least twelve (often twenty) grains of augite and pigeonite. Though closely packed they are rarely intergrown. A few of the grains of pigeonite, in 4341, show only partial inversion to orthopyroxene.

Olivine is found as a primary precipitate in 4429 (1570 m.) and after 770 m. of middle gabbros this marks the beginning of the ferro-gabbros in the layered series. From 20 m. above this horizon ferrogabbro 4430 was collected and found to contain, as well as olivine, augite and pigeonite with the same habit and proportions as in 4341, except that the close packing of the two pyroxenes has become even more impressive. In the rocks from this horizon the contact between adjacent augites and the pigeonites is frequently marked by intergrowth. The large patches of pyroxene are only resolved into their component grains under crossed nicols, the texture being reminiscent of that found in the pyroxenes low in the purple band and attributed by Wager and Deer (1939, p. 111) to the inversion of wollastonite. Although the augites are mainly pale brown at these horizons in the large clusters they are pale-coloured where, at the centres of the clusters, several are in contact. The pale-coloured part of each grain has a 2V which is 5° to 7° higher than the brown part, while associated with it are a few discrete grains of orthopyroxene, hornblende, and chlorite. It looks as though, with lowering temperatures

and increasing volatiles in the interstitial liquid between the grains of each cluster, the orthopyroxene component was completely exsolved from the augites, leaving the latter more calcic. The two pyroxenes from 4430 (brown augite and pigeonite) were separated with difficulty and analysed; the results show no marked change in direction of the trend-line of the augites and ferroaugites with the renewed precipitation of

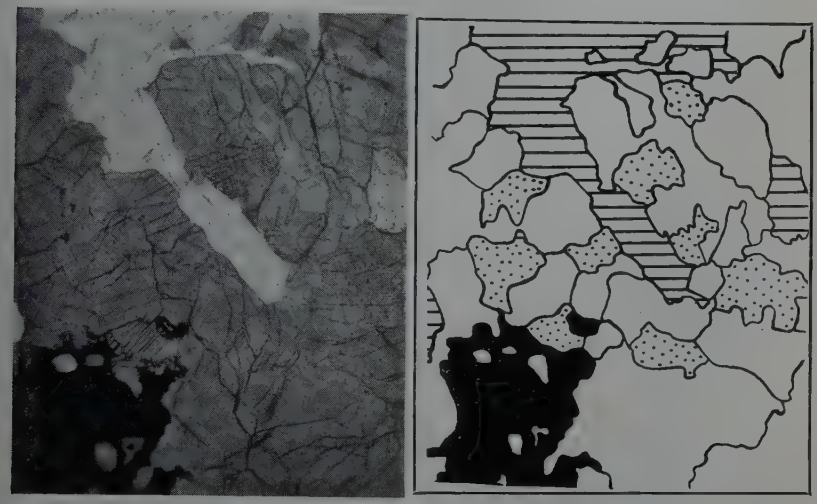

Fig. 4A (left). Photomicrograph of middle gabbro (4341) showing typical closely-packed aggregate of discrete crystals of augite and inverted pigeonite, found to be increasingly common as the limit of two-pyroxene crystallization is approached. Ordinary light. × 18.

Fig. 4B (right). Tracing of fig. 4A to distinguish between pigeonite (stippled) and augite (clear), and between individual crystals of augite (olivine reaction rims are, together with iron ore, black).

olivine as a primary phase. A suitably orientated grain of uninverted pigeonite from 4432 (30 m. above 4430) had $2V+16°$.

One or two small grains of pigeonite were seen in thin sections of 4306 to 4309, 150 m. above 4430, but it was impossible to separate them for analysis. This horizon (1740 to 1840 m.) has therefore been designated the highest at which two pyroxenes are found, although the analysis of the pigeonite from 4430 (150 m. below) is the closest available estimate of the composition of the last calcium-poor pyroxene to crystallize. From simple extrapolation it is unlikely, however, that the Fe content (as a percentage of Ca+Mg+Fe) of the last pigeonite will exceed $Fe_{55}$.

It is not practicable to state the horizon at which the limit of the two-pyroxene field[1] is reached more precisely, because it is not clear whether the odd grains of pigeonite in rocks 4306 to 4309 were crystallizing in equilibrium with augite, or were held in suspension rather longer than the last main batch.

The cessation of pigeonite crystallization, somewhere between 4306 and 4309 (analyses 8 and 9, fig. 2), implies a passage of the magma from the field of two-pyroxene to that of one-pyroxene crystallization. The compositions of these two augites, which fall on each side of the field limit, prove that there is no marked compositional break at the limit, but a gradual change in the direction of the fractionation trend towards calcium enrichment. Of particular significance is the fact that the disappearance of the calcium-poor pyroxene phase is not accompanied by the crystallization of a single pyroxene with calcium content intermediate between the calcium-rich and calcium-poor phases. The augites and ferroaugites from 4306 and 4309 (1740 to 1840 m.) each contain 35 % Ca of total Ca+Mg+Fe and illustrate clearly that for the Skaergaard series this is the maximum replacement of the larger Ca by the smaller Mg and Fe ions.

Augites from 4309 and 4314 (nos. 9 and 10, fig. 2) are almost uniform in character, being deep brown in colour and almost free from exsolution lamellae, apart from the schiller-structure (p. 528) noted in the augites from rocks 4306 to 4310. The only exception to the uniformity is the presence of fingers of pale-coloured augite intergrown with the brown augite in narrow zones at the contact with iron ores. The pale augite is optically discontinuous with the brown variety, and has a 2V 6° to 10° greater than the latter. The textures suggest that it has formed by reaction between interstitial liquid and iron ore (the iron-rich varieties having higher optic angles in this range), but it is surprising that the reaction product has not grown as an optically continuous zone to the brown augite, but is intergrown in a fashion that suggests a structural break between the two varieties.

*The limit of the two-pyroxene field.* Three hypotheses have been advanced by previous investigators to explain why, in the later stages of fractionation of a basaltic magma, the calcium-poor pyroxene ceases to crystallize. There may be reaction of the calcium-poor pyroxene with the liquid to form a fayalitic olivine (Poldervaart and Hess, 1951, p. 479);

[1] The term 'two-pyroxene boundary' was used by Hess (1941) to define this limit, but by Tsuboi (1932) to define the binary cotectic. The term 'limit of the two-pyroxene field' is used in this account to avoid this ambiguity.

the binary cotectic relationship between calcium-rich and calcium-poor pyroxene may at this boundary cease to exist, being replaced by a solid-solution with a minimum (Hess, 1941, and Tsuboi, 1932); or the minimum of the liquidus may migrate towards one of the limbs of the solvus until it passes beyond the limit of intersection with the solvus, when either a lime-rich or a lime-poor pyroxene will crystallize (Muir, 1954, p. 384 and fig. 4).

Both augites and pigeonites have now been analysed from the horizons in the Skaergaard intrusion just before, during, and after the stage at which olivine failed to crystallize as a primary precipitate phase. It is now clear that at these stages there was no marked change in the composition of the pyroxenes, and it can be assumed that there is no simple, sympathetic relationship between the crystallization of olivine and of calcium-poor pyroxene.

If, during iron enrichment, the slope of the crest of the solvus exceeds the slope of the liquidus minimum, then a temperature might be reached when the solidus of the solid-solution series no longer intersects the solvus and one pyroxene would crystallize instead of two. In order to apply this hypothesis it is necessary to know the slopes of both the liquidus minimum and the crest of the solvus from the diopside-clinoenstatite boundary to the hedenbergite-ferrosilite boundary, and even then the effect of other constituents, particularly volatiles, in the magma would have to be considered. The experimental work of Bowen (1914) and of Bowen, Schairer, and Posnjak (1933) has provided an estimate of the slope of the solid-solution minimum, from about 1400° C. for diopside-clinoenstatite to about 950° C. for hedenbergite-ferrosilite. The crest of the solvus for diopside-clinoenstatite has been shown to be at 1380° C. by Atlas (1952, fig. 4), but nothing is known of the temperature of the crest for the hedenbergite-ferrosilite series. Kuno (1955, fig. 1) assumes that the temperature of the crest must lie below the hedenbergite-ferrosilite minimum because members of the hedenbergite-ferrosilite solid-solution are found in the later fractions of the Skaergaard intrusion. However, these pyroxenes are magnesium-bearing and are part of the series crystallized in the one-pyroxene field. Kuno's assumption is therefore only tenable if one is prepared to accept the second hypothesis under consideration, i.e. that in the one-pyroxene field the solid-solution series minimum is at a higher temperature than the crest of the solvus, and it would not be logical to use his assumption to support this hypothesis.

The crest of the solvus lies only very slightly below the solidus for the

system diopside-clinoenstatite, and it is generally believed that the addition of other constituents would lower the solidus to a temperature at which it is intersected by the solvus, so that two pyroxenes would then exist in cotectic equilibrium. During iron enrichment these conditions would continue to prevail, but should the slope of the crest of the solvus exceed that of the solid-solution minimum, there would be a change in composition of the two pyroxene phases such that the calcium-rich phase would become poorer, and the calcium-poor phase richer, in calcium. The type of change would depend upon the slopes of each limb of the solvus, but there would be a tendency towards ultimate convergence at the crest of the solvus (cf. Barth, 1952, fig. 30). If the solvus were a dome-shaped surface with steep sides, the two converging trend-lines on the Ca:Mg:Fe diagram would be convex towards the diopside-hedenbergite and clinoenstatite-ferrosilite joins respectively.

In the Skaergaard case the augite trend is concave towards the diopside-hedenbergite join, the calcium-poor pyroxene trend is parallel to the clinoenstatite-ferrosilite join, and there is no sign of convergence of these trends. None of this evidence supports the simple conception of a domed solvus dipping more steeply towards the hedenbergite-ferrosilite join than does the crystallization surface, until instead of intersecting this surface it dips beneath it, at the limit of two-pyroxene crystallization. The general conception of a crystallization surface with a gentler slope than the two-pyroxene to one-pyroxene 'transition surface' drawn by Tsuboi (1949, fig. 6) would require the production of a single pyroxene at one side of the intersection of these surfaces, equal to the average composition of the two pyroxenes at the other side of the intersection. Until this can be shown to happen, the specific trend-lines of each pyroxene in the two-pyroxene field and the peculiarly calcic composition of the pyroxene in the one-pyroxene field must be explained ultimately by reference to the structure of the pyroxenes and the effect of other components, particularly the olivines, on their equilibrium relationships.

The augites plotted in fig. 2 show no change in calcium content at the limit of two-pyroxene crystallization, which can be drawn somewhere between nos. 8 and 9 (each containing 35 % Ca of total Ca+Mg+Fe). In the hypothetical pyroxene equilibrium diagrams in which the augite in the one-pyroxene field is depicted as crystallizing at a liquidus minimum, and that in the two-pyroxene field on the calcic limb of a solvus, the only explanation for the Skaergaard pyroxene relationships shown in fig. 2 must require this minimum to be in practically the same

position (with respect to Ca:(Mg+Fe) ratio) when it intersects the solvus as when it leaves it. When basaltic magmas equivalent in composition to the earlier Skaergaard liquids crystallize to give one pyroxene, such as the sub-calcic augites, there is evidence for a liquidus minimum close to the line Ca:(Mg+Fe) = 25:75 (Kuno, 1955, figs. 2 and 7). This suggests that, during the fractionation of the Skaergaard magma, the minimum of the liquidus curves joining calcium-rich and calcium-poor pyroxenes in equilibrium moved towards the calcic component. The trace of this minimum on the Ca:Mg:Fe diagram (the 'two-pyroxene boundary' of Tsuboi, 1932, and the 'cotectic' of Hess, 1941) would show a change from Ca 25 to Ca 35. This evidence for migration of the liquidus minimum supports Muir's hypothesis that the cessation of pigeonite crystallization might be attributed to a migration of this type rather than to the fall of the solvus crest below the liquidus minimum.

*Sub-solidus exsolution and inversion.* Certain patches and lamellae of one pyroxene in another, once thought to be inclusions or replacement textures, have been attributed by Hess (1941) and by Poldervaart and Hess (1951) to exsolution in the solid state. These workers showed that particular exsolution textures in the pyroxenes could be linked with various stages of fractionation of a basaltic magma. Similar textures are present in the pyroxenes of the Skaergaard intrusion, and were described briefly by Wager and Deer, some being attributed to exsolution (1939, pp. 81 and 83). Detailed investigation of these textures has now shown that they can be closely related to the cooling history of the Skaergaard intrusion.

Exsolution textures in augites may be lamellae of orthopyroxene or pigeonite (usually inverted to orthopyroxene). Owing to their narrowness it is impossible to tell which they have been, but from Buerger's work (Hess and Poldervaart, 1951, p. 481) it seems likely that exsolution lamellae of orthorhombic in monoclinic pyroxene (and vice versa) will be ‖ (100) while exsolution lamellae of monoclinic in monoclinic pyroxene will be ‖ (001). If this is so then it ought to be possible to distinguish between the exsolution lamellae of orthopyroxene and pigeonite in augite purely on the basis of orientation. One would expect, however, that the type of pyroxene exsolved from the augite would generally be the same as that present as a separate mineral in the same rock.

In the Skaergaard augites the exsolution lamellae are very thin (about 0·003 mm. and totalling about 5 % of each grain) and their only recognizable optical property is a low birefringence; they are therefore probably orthopyroxene, but some may have developed through

pigeonite inversion. The calcium-rich augites of the gabbro-picrite (no. 1, fig. 2) are free from exsolution lamellae, but other rocks from the border group containing orthopyroxene in addition to augite (e.g. perpendicular-felspar rock, no. 2A, fig. 2) show exsolution lamellae of orthopyroxene || (100) in the augite. The augites of the wavy-pyroxene rock and lower members of the lower olivine gabbros (e.g. 4390 to 4392) contain lamellae parallel to both (100) and (001). Continuing the fractionation sequence, the augites in the layered series, up to those ferrogabbros in which the calcium-poor pyroxene phase ceases to crystallize, contain lamellae || (001), presumably of inverted pigeonite. In the ferroaugites of the remaining ferrogabbros, no exsolution lamellae can be seen, although in those from the lower levels represented by nos. 8 and 9 (fig. 2) there is an interesting schillerization due to the presence of a few extremely thin exsolution lamellae || (001) (Wager and Deer, 1939, p. 81). The schiller is only detected by rotating in a plane normal to the plane of the lamellae, when distinctive interference colours in ordinary light (probably produced through a diffraction process) are seen at positions $3\frac{1}{2}^\circ$ at each side of the plane of the lamellae. There is thus a continuous and gradual change in the character of the exsolution lamellae in the augites which, as shown below, can be related to the gradual change in character of the calcium-poor pyroxene.

The orthopyroxenes in the gabbro-picrite (no. 1A, fig. 2) and the perpendicular-felspar rock (no. 2A, fig. 2) contain the type of fine-scale augite lamellae || (100) figured by Hess and Phillips (1938, fig. 2) while the wavy-pyroxene rock and lower members of the lower olivine gabbros (4390 to 4392) contain orthopyroxenes with these lamellae, forming rims and irregular extensions to orthopyroxenes rich in blebs and broad lamellae (pl. XVI, fig. 4). In some sections there is a strong suggestion that this association is due to exsolution in pigeonite beginning in the centre, to which material exsolved from the outer fringes is added, so that when inversion takes place the orthopyroxene at the margins is free from the broader lamellae (pl. XVII, fig. 7). Moreover, the fine lamellae || (100) in the orthopyroxenes of the earlier perpendicular-felspar rock die out towards the margins. However, the presence of lamellae parallel to both (001) and (100) of the augite at this horizon suggests that both orthopyroxene and pigeonite may have been in equilibrium with augite at approximately this temperature, although if there is any order of crystallization implied by the textures of the calcium-poor phase one would have expected the inverted pigeonite to rim the orthopyroxene.

The prevalent calcium-poor pyroxene of the layered series is a pigeonite, which has usually inverted on cooling to an orthopyroxene. It is classed as a pigeonite because of its calcium-content (9 % Ca of total Ca+Mg+Fe; see Poldervaart and Hess, 1951, p. 482) and, in the rare cases where it has not inverted, by its low positive 2V (16°). The presence of 9 % calcium is proven by chemical analysis of three examples, and supported by measurement of the proportion of exsolution lamellae of augite (usually 20 %) in orientated grains. Poldervaart and Hess (1951, p. 482) have suggested that most lamellae exsolved from pigeonite are ‖ (001) and that upon inversion these lamellae as well as the simple (100) twin plane are preserved in the host orthopyroxene, the grain retaining the 'herringbone twin' structure characteristic of monoclinic rather than orthorhombic minerals. This was verified in Skaergaard examples by measurement of the angle (001):(100), for the $\beta$ angle in pigeonite has been determined from X-ray spectrograms (Kuno and Hess, 1953) and is approximately $71\frac{1}{2}°$. In certain cases it was possible to use this method as a further check on the Skaergaard inverted pigeonites, but, as will be shown below, the occasional lack of lamellae parallel to (001), the scarcity of preserved twin planes, and the frequent failure of the orthopyroxene to retain the *b* and *c* crystallographic axes of the parent pigeonite on inversion meant that this method was of limited value.

Although pigeonite occurs in the inverted form throughout a great thickness of the layered series, reference to fig. 5 will indicate that there is likely to be a great deal of variation in the conditions under which the exsolution of augite and inversion to orthopyroxene takes place. From the point at which the crystallization curve passes above the inversion curve, falling temperature and iron enrichment widen the gap between the two curves. This means, assuming a fairly constant rate of cooling, a progressive increase in the period available for exsolution prior to inversion and therefore an increase in the opportunity for ordered arrangement of the exsolved augite within the pigeonite structure before the latter inverts to the orthorhombic form. This is borne out by the Skaergaard inverted pigeonites, for in the lower olivine gabbros they contain exsolved augite as irregular blebs thrown out of the orthopyroxene which probably formed before they could be arranged as lamellae parallel to distinct structural planes in the pigeonite (i.e. not due to rapid cooling only, as suggested by Poldervaart and Hess, 1951, p. 482). Upward in the sequence lamellae develop in place of the blebs, at first incomplete and irregular (pl. XVII, fig. 6), but finally (in the middle gabbros) becoming regular, fully traversing each grain (pl. XVII, fig. 8).

Most of the broader lamellae exsolved from pigeonite are about 0·01 mm. thick and 0·04 mm. apart, in contrast to the fine-scale lamellae of the host orthopyroxene, less than 0·001 mm. thick. Despite the variation in pigeonite exsolution textures now to be considered, a generalized diagram (fig. 6) can be used to show the orientation and general character of the exsolution lamellae in the ideal case where the *b*- and *c*-axes of pigeonite are retained, on inversion, by the orthopyroxene.

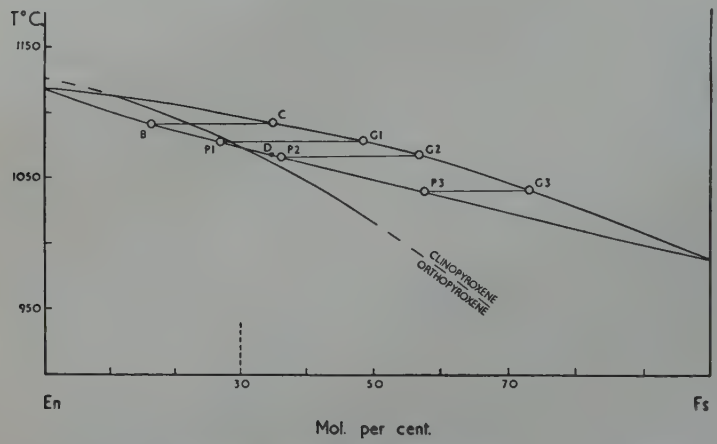


Fig. 5. Possible relationship between the crystallization curve of calcium-poor pyroxenes and the inversion curve (see Appendix). D = pigeonite of chilled marginal gabbro (4507), Skaergaard intrusion; B = bronzite of gabbro-picrite (4526), Skaergaard intrusion, crystallized at temperature (C); P1, G1, . . . = coexisting phenocryst and groundmass pyroxenes of Japanese lavas (Kuno, 1950).

In the chilled margin the inverted pigeonite (now orthopyroxene, $Fe_{37}$, through exsolution of augite) contains fine lamellae ∥ (001) and (100) and irregular patchy plates ∥ (010). In the lower rocks of the lower olivine gabbros, e.g. 4392, the inverted pigeonite (now orthopyroxene, $Fe_{37}$, no. 3A, fig. 2) contains no lamellae ∦ (001), but large blebs ∥ (010), short broad lamellae ∥ (100), and, rarely, the better-known fine-scale lamellae ∥ (100) occur in the host orthopyroxene (pl. XVI, fig. 4). The blebs in a single grain of orthopyroxene are in optical continuity with one another, but the optical orientation of sets of blebs, in relation to that of their host orthopyroxene, is extremely variable from grain to grain and shows no order. Also in a single grain the optical orientation of the augite in the blebs is different from that in the augite of the broader (100) plates. The 'blebs' are really small plates and in sections

|| (010) frequently show elongation || (100), though they rarely extend beyond 20 % of the width of the host mineral. In pigeonites from higher rocks of the lower olivine gabbros, such as 4385A (now orthopyroxenes, $Fe_{39}$, no. 4A, fig. 2), lamellae begin to develop || (001). However, these lamellae rarely extend more than half the width of the grain and are occasionally bleb-like when viewed in sections || (001) (pl. XVI, fig. 2). Leading from the lamellae, as seen in (010) sections, are narrow lamellae || (100), but these do not resemble the narrow fine-scale lamellae seen in orthopyroxenes of the marginal border group and common in bronzites of the Bushveld and Stillwater intrusions. They are short, merely linking adjacent (001) lamellae (cf. Wager and Deer, 1939, p. 83), whereas those in some of the lower inverted pigeonites are parallel and can be joined at each side of the (001) lamellae. This suggests that the shorter (100) lamellae were exsolved from the pigeonite rather than from the orthopyroxene subsequent to inversion, although both types may be present (pl. XVI, fig. 4). Abundant opaque ore inclusions distinguish inverted pigeonite from augite in ordinary light and are probably released upon inversion to orthopyroxene (hence their lack of orientation). The pigeonite contains less Fe‴ than the augite (table II), while this textural evidence suggests that the orthopyroxene contains even less Fe‴ than the pigeonite.

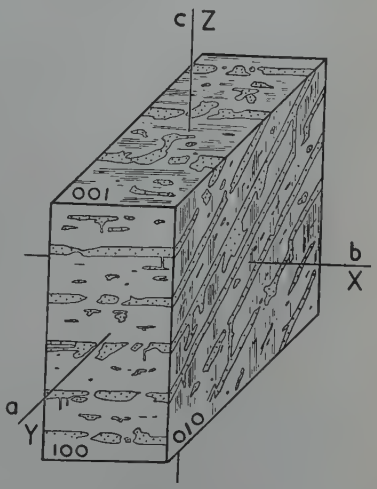


Fig. 6. An inverted pigeonite with the common exsolution lamellae of augite (stippled and fine lines) now in orthopyroxene. The broad lamellae (0·01 mm. thick and 0·04 mm. apart) are parallel to (001) and, though less common and complete, parallel to (100) and (010) of the original pigeonite. The more regular, narrow lamellae (0·001 mm. thick) are parallel to (100) of the host orthopyroxene. The example drawn is a generalized case in which the *b* and *c* crystallographic axes of the pigeonite are retained, upon inversion, by the orthopyroxene, and in which the degree of exsolution is extreme. The crystallographic and optic directions shown apply to the orthopyroxene host.

In the middle gabbros and lower ferrogabbros the exsolution lamellae in the inverted pigeonites are broad, well developed, and fully traverse each grain. Between each pair of lamellae is a string of tiny blebs that

appear to be exsolved augite, in insufficient quantity to form lamellae but spread along the (001) plane (pl. XVII, fig. 8). There are also abundant fine-scale lamellae || (100), which together with the (001) lamellae and blebs make the determination of optic axial angle, refractive index, and unit-cell dimensions of the host orthopyroxene difficult. The compositions of the host orthopyroxenes (4B, 6B, 7B, of fig. 2) of the inverted pigeonites indicate that the exsolved augite is more ferriferous in composition than the augite existing as a separate phase in the same rock.

Poldervaart and Hess (1951, p. 482 and fig. 7) have observed that 'in the great majority of cases of inversion of pigeonite to orthopyroxene, the orthopyroxene will develop in such an orientation that it retains the *b* and *c* crystallographic axes of the parent-pigeonite'. In exceptional cases, they remark, a rotation of *c* through 45° has been recorded. In the case of the Skaergaard inverted pigeonites the reverse is true, for it is rare to find the orthopyroxene host retaining either *b*- or *c*-axes of the parent pigeonite. It is clear from textural evidence that augite and pigeonite, when adjacent, crystallized so as to share the three major crystallographic axes. This is shown by the optical continuity between augite plates exsolved from pigeonite and adjacent augite crystals, and even more convincingly in the relationship illustrated by pl. XVI, fig. 2: a twinned augite has been poikilitically enclosed by pigeonite, the latter crystallographically continuous to the extent of reproducing the twinned structure; the pigeonite has subsequently exsolved augite lamellae (bleb-like in this basal section), which have in turn crystallized in continuity with the twinned pigeonite (finally inverted). The final result superficially suggests that the central twinned augite has exerted a complex influence on the growth of the two sets of blebs, but this is not directly true, for the role of pigeonite must be included in the process. However, when the augite blebs in the inverted pigeonite from rocks such as 4392 are considered (p. 530), it is clear that the relationship between the orientations of host orthopyroxene and augite blebs varies from one grain of inverted pigeonite to the next. If the augite retains the crystallographic orientation of the pigeonite (and there is plenty of evidence of the type cited above to support this suggestion) then the host orthopyroxene cannot be retaining the *b*- and *c*-axes of the parent pigeonite, otherwise the *b*- and *c*-axes of host orthopyroxene and exsolved augite would also correspond.

Further evidence on this point was obtained when a stereographic plot was made of the *a*-, *b*-, and *c*-axes of the host orthopyroxene and

the pole of the broad exsolution plates from a number of inverted pigeonites at representative horizons within the Skaergaard intrusion. From this it had been hoped, initially, to record the planes in the parent pigeonite along which exsolution developed prior to inversion. Several poles of exsolution lamellae fell on a point in the stereogram represented by $\beta$ 71½° (approx.), provided that the *b*- and *c*- axes in pigeonite and orthopyroxene are assumed to be shared, and as these poles correspond to the pole of (001) in pigeonite it is likely that the axes are, in fact, shared. However, the poles of the broad lamellae from other grains fell in random positions on the plot and showed no concentrations. This is interpreted as implying that the lamellae represent neither random inclusions nor various important crystallographic planes within the pigeonite, but that they were parallel to (001) of the parent pigeonite, and that upon inversion the orthopyroxene has become randomly orientated so as to retain neither the *b*- nor the *c*-axes of the parent pigeonite. If this is true then it is impossible to tell which plane of a parent pigeonite is represented by a particular set of exsolution lamellae, merely by relating these lamellae to the optic axial plane of the host orthopyroxene. However, it can be done by using the relict (100) twin plane in conjunction with lamellae, if the former is preserved. A grain examined in this way (pl. XVII, fig. 9) shows the (100) twin plane and (001) exsolution lamellae as relict structures of the parent pigeonite, as proven by a measurement of $\beta$ (orientated on the universal stage). Yet in the same grain can be seen fine-scale augite lamellae parallel to the optic axial plane, (100), of the host orthopyroxene that are far from parallel to the (100) twin plane of the parent pigeonite. Rotation about both *b*- and *c*-axes is involved in this inversion. Further evidence is brought by the numerous cases, especially at the middle gabbro horizon, in which a single crystal of pigeonite has inverted to two or more crystals of orthopyroxene, optically discontinuous with one another (pl. XVI, fig. 3). Even if one of these crystals retained the *b*- and *c*-axes of the parent pigeonite the other(s) could not. Measurement of one such inverted pigeonite from the top of the lower olivine gabbros (4378) showed that from one orthopyroxene to the next $\gamma$ was rotated through 100° about a pole (*hk*0) at an angle of 32° from *a* and 68° from *b*. Although it was not possible to obtain more measurements of this type, the one example proves that even if one orthopyroxene retained *b* and *c* of the parent pigeonite, the other shows rotation about both *b*- and *c*-axes. Together with the rest of the evidence given, it seems most likely that upon inversion the retention of *b*- and *c*-axes, or rotation with reference to one or both, is a random process.

The proportion of grains of inverted pigeonite that show rotation rather than retention of axes on inversion increases with iron content and is most marked in the middle gabbros (pigeonites now orthopyroxenes, $Fe_{47-50}$). Bowen and Schairer (1935, p. 164 and fig. 8) investigated synthetically the inversion relationships between monoclinic and orthorhombic pyroxenes, although they could only do this in the direction orthorhombic to monoclinic, on heating. In doing so they pointed out (1935, p. 169) that although in the more magnesian members there is a tendency towards the retention of the prism zone, 'In general, a single crystal or crystal fragment of orthorhombic pyroxene is transformed into an aggregate of several grains of monoclinic pyroxene of random orientation with respect to each other and to the original orthorhombic substance.' In reverse, this is what has happened to the Skaergaard pigeonites on inversion, those with an intermediate composition showing the phenomenon more markedly than the more magnesian members. Bowen and Schairer (1935, p. 167) cite further experimental evidence in support of this fact, for while the members approaching the two ends of the series are transformed readily, the intermediate members behave much more sluggishly. It is possible that this sluggishness is because of the inability of the intermediate members to grow, upon inversion, with the orientation of the parent mineral. Moreover, the presence of rare grains of uninverted pigeonite and partially inverted pigeonite amongst these intermediate members alone is probably due to the sluggishness of inversion at a stage when an appreciable interval separates the temperatures of crystallization and inversion (fig. 5). The inversion curve for the intermediate and ferriferous pigeonites is, in fact, likely to fall to temperatures at which processes involving significant rearrangement of the pyroxene structure will become increasingly difficult at the rate of cooling of fairly high-level, small intrusions.

*Optical properties in relation to chemical composition.* The most reliable method at present of determining the Ca:Mg:Fe ratio of a calcic clinopyroxene from the optical properties is to determine $2V_\gamma$ by direct rotation between optic axes and $\beta$ refractive index on (100) parting tablets, using techniques and determinative curves similar to those given by Hess (1949). For the analysed Skaergaard augites these techniques were used and only $2V_\gamma$ and $\beta$ refractive index were determined as these are the significant diagnostic optical properties.

In comparing the optical properties of an augite with the composition it is necessary to bear in mind the effect on the optics of factors other

than the Ca:Mg:Fe ratio, chief of which are the degree of exsolution of calcium-poor pyroxene (which mainly affects 2V) and the amount of minor constituents such as Al and Ti (which affects both 2V and refractive index).

Through exsolution of orthopyroxene or pigeonite the optic axial angle measured will be that of the host augite and will not correspond to the augite represented by the bulk composition. The discrepancy between 2V of augite before and after exsolution of calcium-poor pyroxene will vary with the amount and composition of the exsolved material. The amount will be controlled by the rate of cooling of the rock below the temperature of augite crystallization and the initial composition of the augite (exsolution will cease when, or perhaps a little before, the host augite attains the composition of diopside-hedenbergite). The composition of the exsolved material may be either orthopyroxene or pigeonite, but if a calcium-poor pyroxene ceases to form as a crystal phase in equilibrium with the magma (as in the case of most of the Skaergaard ferrogabbros) then it is unlikely that there will be exsolution of this phase from the augites.

Variable 2V in a single grain, often classed as 'zoning' (i.e. variation chiefly in Fe:Mg ratio), is more likely to be a function of irregular Ca distribution and may be due to exsolution being variable in extent throughout the grain.

If use is to be made of the correlation between optical properties and chemical composition of pyroxenes, it is essential that the composition and quantity of the exsolved phase be estimated and taken into account in compiling determinative tables and curves. In the case of the Skaergaard pyroxenes there are no exsolution lamellae in the diopsidic augite of the gabbro-picrite (because of its calcic composition) and in the ferroaugites of most of the ferrogabbros (because of the instability of pigeonite). In the other analysed augites the exsolution lamellae are of inverted pigeonite (see p. 528) amounting to approximately 5 % of each crystal. The composition of the exsolved phase is assumed to be that of the inverted pigeonite present as a separate phase in the same rock, and although this is only an approximation it is the most likely assumption. Using the compositions given in table I a close approximation to the composition of the host augite is obtained (table III) and these are the compositions used in compiling fig. 7. Ultimately it should be possible to derive the composition of the host augite in terms of Ca, Mg, and Fe from unit-cell dimensions (providing the unit-cell determinative curves are initially constructed using augites free from exsolution lamellae,

possibly homogenized by heating), and relate this composition to the optical properties of the host augite. However, the calcium-poor pyroxene also contains smaller amounts of Al, Fe‴, Ti, Cr, and Na than the augite (table II and p. 518) and when more is known about the effect of these constituents on the optical properties of augites the composition of the host augite must be more accurately determined.

When the compositions of the Skaergaard augites have been corrected for exsolution and plotted on Hess's curves (1949, pl. I) they correspond to a 2V about 7° in excess of that observed, whereas when plotted uncorrected for exsolution the 2V is about 4° in excess of that observed.

TABLE III. Composition of analysed augites (atomic %) recalculated to give approximate composition of augite free from 5 % exsolution lamellae of pigeonite. (Specimen numbers refer to the analyses of table I.)

| | 3. | 4. | 5. | 6. | 7. | 8. | 9. |
|---|---|---|---|---|---|---|---|
| Ca | 41 | 39 | 38 | 37 | 36 | 36 | 36 |
| Mg | 42·5 | 41 | 39 | 37·5 | 37 | 35 | 32 |
| Fe | 16·5 | 20 | 23 | 25·5 | 27 | 29 | 32 |

This suggests that certain parts of Hess's curves correspond more closely to the composition of host plus lamellae than to host, and that a better estimate of composition is obtained if 3° is added to the 2V observed (cf. Brown, 1956, pp. 25 and 51) rather than subtracted as suggested by Hess (1949, p. 636). Moreover, some of the augites used by Hess may contain more or less than 5 % exsolved pigeonite, and until further details are available on the composition and quantity of exsolved material in each case, comparisons must be tentative.

The remaining discrepancy of 4° between the observed 2V and that calculated from Hess's curves can best be explained by a brief consideration of the effect on the optics of cations other than Ca, Mg, and Fe. The effect of minor constituent cations on the optical properties of augites was appreciated by Hess (1949, p. 633) but Segnit (1953) was the first to determine the effect of Ti, Al, and Fe‴ on the optical properties of a clinopyroxene, in this case synthetic diopside; he found that Al has little effect on the refractive index but increases 2V; Ti and Fe‴ increase both refractive index and 2V. An important point noted by Hori (1954, p. 73), however, is that the effect of a cation on optical properties is dependent upon its lattice site, and that Al, Ti, and Fe‴ in tetrahedral coordination decrease the refractive index and increase 2V, whereas in octahedral positions they have the opposite effect (marked in the case of Ti). The Skaergaard augites contain average amounts of $Al_2O_3$ (*ca.* 2·5 %)

and $Fe_2O_3$ (*ca.* 1·5 %) but contain almost 1 % $TiO_2$ (average 0·4 %, see Hess, 1949, p. 643). In nearly every case this excess Ti is accommodated in the octahedral position (table II), which would account for the 2V being lower than that of augites of otherwise similar composition, even after exsolution has been taken into account.

When the curves for the $\beta$ refractive index of the Skaergaard augites are considered, it is seen that for specific Ca:Mg:Fe values they read

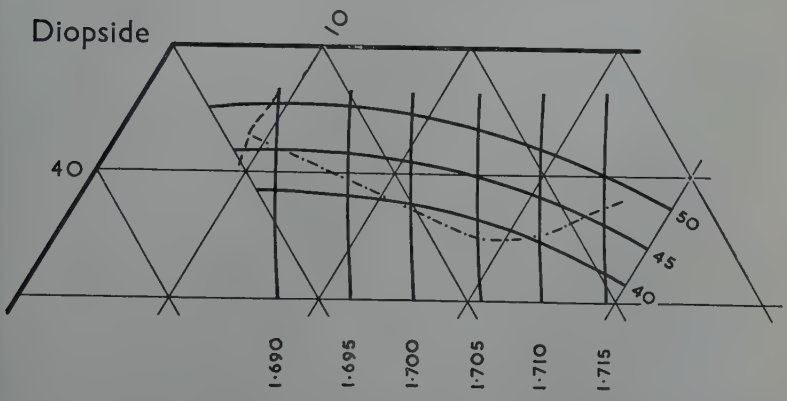


Fig. 7. Relationship between optical properties and chemical compositions of the Skaergaard augites. Composition corrected, where necessary, for exsolution (see table III). ⌒ optic axial angle; ( $\beta$ refractive index; – · – · – crystallization trend-line; – – – position of the 1·690 $\beta$ curve for chromiferous augites.

0·005 higher than those of Hess (1949, pl. I). The higher value for the Skaergaard augites might also be explained by the presence of Ti in the octahedral position, in view of Hori's hypothesis. In fact, when augite analyses nos. 28 to 33 of Hess (1949) are examined they are found to resemble the Skaergaard augites in many respects, particularly in both $TiO_2$ content (all Ti being in the octahedral position) and in the fact that their observed $\beta$ refractive indices are usually 0·005 higher than those calculated from the curves. The effect of Cr on the refractive indices has been estimated by Hess (1949, pl. I) and an allowance has been made for this constituent in fig. 7.

In view of the problems involved in dealing with so many variable factors, the simple Ca:Mg:Fe diagram is inadequate as a means of representing the optical properties of augites. Fresh curves have been drawn on such a diagram for the Skaergaard augites, chiefly to indicate how their value is limited to the estimation, from optical properties, of

the composition of the unanalysed members of a series of augites in a fractionated series, providing the nature of the sub-solidus exsolution textures is understood and the distribution of minor cations is fairly constant throughout the series. To apply to these curves the optical properties of augites crystallizing from magmas of different composition and cooling history from the Skaergaard magma, in order to estimate their composition, is bound to produce anomalous results.

The ferroaugites free from exsolution lamellae will be described in a future paper, and fresh curves will be drawn for this region. Muir (1951, fig. 4) has drawn curves (2V and $\beta$) for the ferroaugite region but these do not correspond with his recorded compositions and optical properties (1951, table II), while the trend of augite–ferroaugite crystallization towards hedenbergite is also based upon an erroneous application of observed optical properties to these curves.

The compositions of the orthopyroxenes, including those formed by inversion, were determined by measurement of $2V_{\alpha}$ and $\gamma$, using Hess's curves (1952, fig. 2).

*Conclusions.* Two pyroxenes, a calcium-rich and a calcium-poor variety, crystallized from the Skaergaard magma before fractionation began, and continued to crystallize together during fractionation until the latest stages, represented by the upper 900 m. of the exposed layered series, when the calcium-poor variety ceased to crystallize (fig. 1).

The calcium-rich variety is an augite, which changed composition with fractionation, at first by the replacement of Ca and Mg by Fe″, the slope of the trend-line being such that for (approximately) every seven Fe″ atoms gained, three Ca and four Mg atoms were lost; the loss of Ca reached a limit when Ca:(Mg+Fe) equalled 35:65, the compositions of the augites from the following 250 m. of rock changing through replacement of Mg by Fe″, without any change in the Ca percentage of 35; above (and partly within) this zone, augite crystallized as the only pyroxene and now changed composition by the replacement of Mg by both Ca and Fe″ (fig. 2).

The earliest calcium-poor pyroxene to crystallize through fractionation was an orthopyroxene, which changed composition through the replacement of Mg by Fe″. Later a pigeonite crystallized instead of orthopyroxene and also changed composition, during cooling of the Skaergaard magma, through the replacement of Mg by Fe″, the Ca content remaining constant at 9 % of Ca+Mg+Fe. The changeover from orthopyroxene to pigeonite crystallization took place between Mg:Fe =

72:28 and 63:37 (hidden layered series), while the cessation of pigeonite crystallization occurred near the composition Mg:Fe = 45:55 (fig. 2). The limit of two-pyroxene crystallization is thought to be reached when the liquidus minimum for the pyroxene system has migrated to the calcium-rich limb of the solvus, i.e. from about Ca 25 to Ca 35 in the Ca:Mg:Fe diagram.

The trend of crystallization of both calcium-rich and calcium-poor pyroxenes from the Skaergaard is, in the early and middle stages, similar to the less complete trends followed by the pyroxenes from other layered basic intrusions of the Bushveld–Stillwater type. If, however, the pyroxenes of the Skaergaard gabbro-picrite represent the earliest pyroxene fractions, their composition suggests the Skaergaard magma was cooler, or further advanced along the tholeiitic-basalt fractionation trend, than the Bushveld, Stillwater, and Rhum magmas (fig. 3).

The compositions of the inverted pigeonite of the chilled marginal gabbro and the orthopyroxene of the early-accumulate gabbro-picrite are believed to be related in the same way as the groundmass and intratelluric phenocryst pyroxenes of lavas. They are used to construct a diagram that explains the relationship between the liquidus and solidus cooling curves and the monoclinic to orthorhombic inversion curves of calcium-poor pyroxenes. The diagram, as constructed, indicates supercooling of at least 20° C. at the chilled margin, and crystallization of most of the Skaergaard intrusion within a temperature range of 50° C. (fig. 4).

Both calcium-rich and calcium-poor pyroxenes contain sub-solidus exsolution textures, the orientation and thickness of which can be related to the composition of the host pyroxene so accurately that it is possible to estimate the horizon from which a specimen was collected, purely on the basis of these textures. The majority of the pigeonites have inverted to orthopyroxene, but before and after inversion augite lamellae were exsolved from the crystals. These lamellae, beginning as blebs, become progressively more ordered and abundant with height in the layered series, and this is related to the progressive increase in the temperature interval between crystallization and inversion. At the same time it is believed that the inversion of pigeonite to orthopyroxene became progressively more difficult with height in the layered series, because the *b* and *c* crystallographic axes of the pigeonite are not always retained by the orthopyroxene on inversion, the proportion of grains showing non-retention of axes increasing with height in the series; in the few hundred metres before it ceased to crystallize altogether pigeonite

has failed to invert, at first only partially in each grain, but ultimately the whole grain remains as pigeonite.

In the past the presence of uninverted pigeonite and of 'blebby' inverted pigeonite have been attributed to quick cooling of the magma. The fact that these two phenomena occur at quite separate horizons in the Skaergaard intrusion and can be traced through gradual changes into the other varieties attributed to slow cooling, together with the more evident geological relationships, rule out the quick-cooling hypothesis. The rate of cooling must have been relatively constant, but the temperature interval, and therefore the time interval, between crystallization and inversion curves increased as cooling proceeded. Thus the time for ordered and plentiful exsolution would slowly increase while the time for inversion would slowly decrease (fig. 5).

It is evident that the degree of inversion of the pigeonitic pyroxenes, and possibly the high-transitional-low temperature form of the associated plagioclase felspars (cf. Muir, 1955) must, in general, be correlated with the composition of the minerals as well as with their cooling history.

The chemical analyses of the pyroxenes show that elements other than Ca, Mg, and Fe″ change in amount during fractionation. Of particular interest is the progressive decrease in Al, the evidence that Ti is not so abundant as indicated by previous investigators, and the enrichment of the calcium-rich pyroxene, relative to the calcium-poor pyroxene in the same rock, in Al, Fe‴, Ti, Na, and Cr.

Fresh optics curves are drawn for the Skaergaard clinopyroxenes in the range investigated, but these must be used with caution in view of the effect on the optics of exsolution, of cations other than Ca, Mg, and Fe″, and of the lattice site occupied by these cations in the pyroxene structure.

*Acknowledgements.* The material used in this investigation was collected during the East Greenland Geological Expedition, 1953, led by Prof. L. R. Wager and Prof. W. A. Deer, of which the author was a member. The leaders thank the Royal Society and the Percy Sladen trustees for generous financial assistance.

The author wishes to thank Prof. Wager for much help with the planning and final presentation of the work, and interpretation of some of the results. In particular he was concerned with the examination of primary crystallization textures, and the recognition of the significance of inverted pigeonite in the chilled marginal gabbro.

Thanks are also expressed to Prof. H. H. Hess of Princeton University for useful discussion and facilities granted for part of this study, and to Prof. Deer for making available the two analyses by Dr. P. E. Brown. A Fellowship from the Commonwealth Fund of New York, for study at Princeton, is gratefully acknowledged.

## *Appendix.*

In constructing fig. 5 reference was made to a similar one for a pigeonitic rock series drawn by Kuno (1950, fig. 24, p. 997) and later modified by Kuno and Nagashima (1952, fig. 1) in which phenocrysts from lavas were plotted on the solidus and groundmass pyroxenes on the liquidus. Kuno's diagram could not be used directly, however, because of several assumptions made in constructing his diagram which were not easily explained: no temperatures were recorded by Kuno on the ordinate; the slope of the inversion curve, attributed to Bowen and Schairer (1935), is adapted to the results obtained by Kuno without explanation (more evident in Kuno and Nagashima's diagram, where temperatures are stipulated); the diagram is complicated by a large inversion interval, despite Bowen and Schairer's statement (1935, p. 170) that the inversion interval of temperature is 'vanishingly small' and Kuno and Nagashima's evidence (1952, fig. 2) that the inversion interval of composition (as a function of En : Fs ratio) is negligible; the solidus is assumed to approach the liquidus when the groundmass pyroxene crystallizes, in order to explain the changeover from hypersthene to pigeonite. The two critical pyroxenes illustrating the Skaergaard case (p. 520) cannot therefore be plotted on this diagram and a new one was constructed to illustrate this particular case.

The three examples given by Kuno (fig. 24) were plotted (1, 2, 3), with the aid of the ordinate temperature scale by Kuno and Nagashima (1952, fig. 1), together with the inverted pigeonite from the Skaergaard chilled marginal gabbro (c) and the orthopyroxene from the Skaergaard early-accumulate gabbro-picrite (b). Each set fell on a smooth liquidus and solidus line, from which it was assumed that no difference in the relationship between solidus and liquidus existed for plutonic and volcanic rocks. In selecting an appropriate temperature of crystallization for the Skaergaard pyroxenes, reference was made to the results of experiments by Yoder and Tilley (1956, p. 100), who heated Kilauean tholeiitic basalt at 5000 bars water pressure; at 1090° C. pyroxene disappeared. In the absence of more precise figures it is assumed that pyroxenes began to crystallize from the Skaergaard magma at approximately this temperature. If the curves are applicable, the development of pigeonite, subsequently inverted, in the chilled marginal gabbro indicates supercooling of the order of 20° C. Moreover the crystallization of a calcium-poor pyroxene of composition approximately $En_{45}Fs_{55}$ (reduced to Ca-free proportions) at a level of 1900 m. suggests that most of the Skaergaard intrusion (i.e. border group + hidden layered series + $\frac{2}{3}$ exposed layered series) crystallized within a temperature range of about 50° C.

In the construction of this type of diagram, applied to natural magmas, it is not practical to retain, without slight modification, the clinopyroxene-orthopyroxene inversion curve determined by Bowen and Schairer for the simple dry system. It seems most likely that under natural conditions, in the presence of fluxes, inversion takes place at lower temperatures. The curve is therefore dropped and the shape changed slightly in order to intersect the solidus at $Fs_{30}$, where the changeover from orthopyroxene to pigeonite crystallization was observed to take place in lavas (Kuno and Nagashima, 1952). The precise point of intersection will vary according to the temperatures and compositions of the magmas, some extreme cases having been described by Muir (1954), but from fig. 5 it is clear that only very slight adjustment of the curves is necessary in order to bring the intersection to $Fs_{40}$, when the conditions of crystallization of pyroxenes from several basalts, rather than from gabbros, are represented.

*References.*

Atlas (L.), 1952. Journ. Geol., Chicago, vol. 60, p. 125 [M.A. **12**–80].
Barth (T. F. W.), 1952. Theoretical Petrology. 1st edn., p. 110. John Wiley and Sons, New York.
Bowen (N. L.), 1914. Amer. Journ. Sci., ser. 4, vol. 38, p. 207.
—— and Schairer (J. F.), 1935. Ibid., ser. 5, vol. 29, p. 151 [M.A. **6**–352].
——, Schairer (J. F.), and Posnjak (E.), 1933. Ibid., vol. 26, p. 193 [M.A. **5**–454].
Brown (G. M.), 1956. Phil. Trans. Roy. Soc., ser. B, vol. 240, p. 1.
Brown (P. E.), 1955. Ferromagnesian Minerals of the Skaergaard Intrusion, East Greenland. Ph.D. thesis (unpublished), University of Manchester.
Hess (H. H.), 1941. Amer. Min., vol. 26, pp. 515, 573 [M.A. **8**–233].
—— 1949. Ibid., vol. 34, p. 621 [M.A. **11**–15].
—— 1952. Amer. Journ. Sci., Bowen vol., p. 173 [M.A. **12**–97].
—— and Phillips (A. H.), 1938. Amer. Min., vol. 23, p. 450 [M.A. **7**–180].
Hori (F.), 1954. Sci. Papers College Gen. Education, Univ. Tokyo, vol. 4, no. 1, p. 71.
Kuno (H.), 1955. Amer. Min., vol. 40, p. 70.
—— and Hess (H. H.), 1953. Amer. Journ. Sci., vol. 251, p. 741 [M.A. **12**–334].
—— and Nagashima (K.), 1952. Amer. Min., vol. 37, p. 1000 [M.A. **12**–138].
Muir (I. D.), 1951. Min. Mag., vol. 29, p. 690.
—— 1954. Ibid., vol. 30, p. 376.
—— 1955. Ibid., vol. 30, p. 545.
Poldervaart (A.) and Hess (H. H.), 1951. Journ. Geol., Chicago, vol. 59, p. 472 [M.A. **11**–290].
Segnit (E. R.), 1953. Min. Mag., vol. 30, p. 218.
Tsuboi (S.), 1932. Japan. Journ. Geol. Geogr., vol. 10, p. 67 [M.A. **5**–219].
—— 1949. Proc. Japan. Acad., vol. 25, no. 1, p. 34.
Wager (L. R.) and Deer (W. A.), 1939. Medd. Grønland, vol. 105, no. 4, p. 1 [M.A. **11**–32].
Wilkinson (J. F. G.), 1956. Amer. Min., vol. 41, p. 724.
Yoder (H. S.) and Tilley (C. E.), 1956. Program 1956 Annual Meetings, Geol. Soc. Amer., p. 100.

## Explanation of Plates XVI and XVII.

(Specimen numbers refer to rocks in the Oxford University East Greenland Collection.)

### Plate XVI.

Fig. 1. Inverted pigeonite approximately || (010). Augite has been exsolved as broad, irregular plates || (010) (in optical continuity with augite crystal in bottom right-hand corner), long lamellae || (001), and short lamellae || (100). Orthopyroxene host at extinction. Crossed nicols. ×70. (E.G. 4454. Height 1050 m.)

Fig. 2. Twinned crystal of augite poikilitically enclosed by pigeonite. The pigeonite has grown in structural continuity with the augite, reproducing the twinned structure. The pigeonite has then exsolved blebs of augite, each set being in structural continuity with that part of the pigeonite twin from which they were exsolved. Finally, inversion of pigeonite to orthopyroxene has destroyed evidence of the twin structure in the poikilitic host mineral (shown at extinction). Crossed nicols. ×24. (E.G. 5062. Height 300 m.)

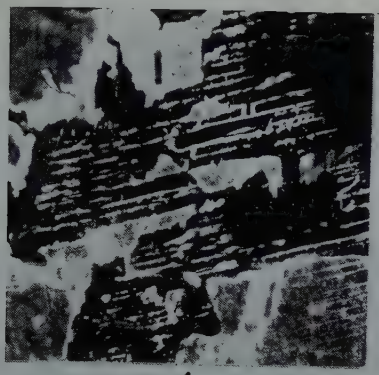

1

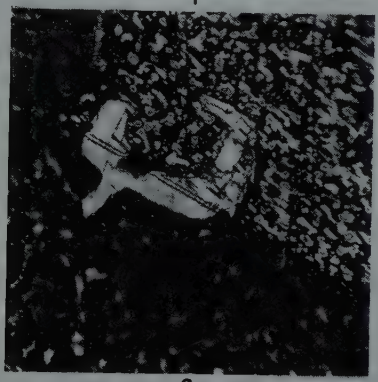

2

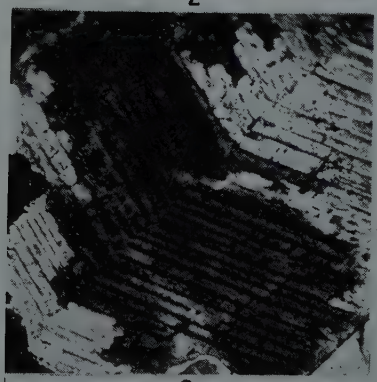

3

4

5

G. M. Brown: Pyroxenes

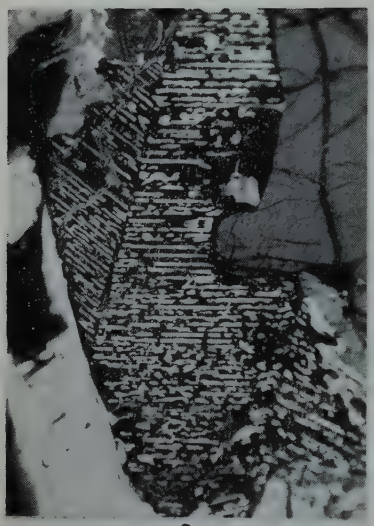

6

7

8

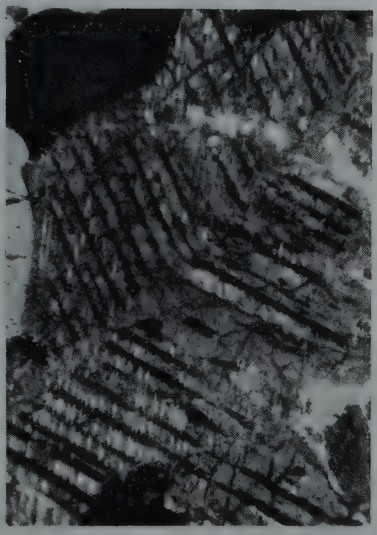

9

G. M. BROWN: PYROXENES

Fig. 3. Inverted pigeonite approximately || (010). One twinned crystal has inverted to two crystals of orthopyroxene, one of which is at extinction. Crossed nicols. ×62. (E.G. 4378 B.)

Fig. 4. Inverted pigeonite, section approximately || (010). Augite has been exsolved from the pigeonite, prior to inversion, as blebs || (010) and short thick lamellae || (100), and from the orthopyroxene host, subsequent to inversion, as very fine-scale lamellae || (100). Crossed nicols. ×52. (E.G. 4392.)

Fig. 5. Inverted pigeonite approximately || (010). Broad lamellae are || (001) of the original pigeonite, while the fine lamellae running from top to base of picture are || (100) of the host orthopyroxene (shown at extinction). The angle between the two sets of lamellae proves that the (100) planes of pigeonite and orthopyroxene do not coincide. The irregular exsolution running approximately left–right typifies the more complex patterns to be found. Crossed nicols. ×100. (E.G. 4385 B.)

## Plate XVII.

Fig. 6. Inverted pigeonite approximately || (010). Augite has been exsolved || (001) of a pigeonite twinned on (100). Small fine lamellae can be seen joining some of the broad (001) lamellae. Orthopyroxene host at extinction. Crossed nicols. ×26. (E.G. 4386.)

Fig. 7. Inverted pigeonite interstitial to olivine, augite, and plagioclase. Augite has been exsolved first from the centre, material migrating there from the margins. The symmetrical arrangement of orthopyroxene (shown at extinction) free from exsolved augite at each margin indicates that the orthopyroxene has not grown as a later rim to the pigeonite. Crossed nicols. ×105. (E.G. 4391 B.)

Fig. 8. Inverted pigeonite as distinct primary precipitate crystals in the middle gabbros. The exsolved augite lamellae || (001) are well developed, while between them are stringers of augite blebs, indicating a high degree of augite exsolution prior to inversion. Orthopyroxene host at extinction. Crossed nicols. ×78. (E.G. 4369.)

Fig. 9. Inverted pigeonite approximately || (010). The original (100) twin plane of the pigeonite is well defined by the herringbone texture (cf. Pl. XVII, fig. 6), but this does not correspond with the (100) plane of the host orthopyroxene, defined by the lamellae running from top to base of the picture. Crossed nicols. ×90. (E.G. 4378 B. Height 800 m.)

# *Measurement and distribution of zircons in some granitic rocks of magmatic origin.*

By Leonard H. Larsen, Ph.D., M.A.,

Dept. of Geology and Geography, University of Cincinnati, Ohio, U.S.A.

and

Arie Poldervaart, D.Sc., Ph.D., F.G.S.,

Dept. of Geology, Columbia University, New York, U.S.A.

[Taken as read 6 June 1957.]

*Summary.* Morphological characters of zircons in concentrates have been studied by measurement of length along the *c*-axis and breadth along the $a_1$- or $a_2$-axis of 200 doubly terminated crystals for each sample. The sample is represented graphically by a line fitted mathematically to a scatter plot of the measurements. This line, the *reduced major axis*, is visualized as a growth trend, and samples are described and compared statistically.

From a careful study of zircons in a tonalite it is concluded that zircon crystallized over a short range before crystallization of the main constituent minerals.

The distribution of zircon in a batholith of magmatic origin has also been studied. The batholith grades from a core of granodiorite to a mantle of tonalite, but the zircons are uniform throughout. Small bodies of granodiorite and quartz monzonite have sharp contacts against the main batholithic rocks, and zircon samples from these intrusives differ from one another and from those of the batholith. It is concluded that the batholith represents a single intrusion which differentiated after emplacement, and that the later intrusives each crystallized under different conditions.

MORPHOLOGICAL characters of zircons in rocks have been studied for some fifty years, and results of these investigations have been applied to various petrogenetic problems. The work on zircons in igneous rocks has been reviewed by J. C. Reed,[1] G. Hoppe,[2] and A. Poldervaart.[3] These reviews show the need for more rigid control in laboratory techniques and for better means of comparison of zircon data obtained from different rocks. The present study is an attempt to improve graphic methods of representing zircon data, to test laboratory procedures used in preparing zircon concentrates, to determine the

[1] Amer. Min., 1937, vol. 22, p. 73 [M.A. 7–188].
[2] Geologica, 1951, Reihe 9, 114 pp. [M.A. 12–32].
[3] Amer. Jour. Sci., 1956, vol. 254, p. 521.

distribution of zircons in the mineral fabric of a tonalite, and to determine the distribution of zircons in a magmatic pluton.

This investigation is restricted to calc-alkaline rocks of magmatic origin. That zircon has crystallized before the main constituent minerals in such rocks is indicated by earlier work,[1] and established anew in the present study. The dimensions of each zircon crystal have been determined by measurement of length along the $c$-axis and of breadth along the $a_1$- or $a_2$-axis. It is assumed that dimensions along the $a_1$-axis equal those along the $a_2$-axis, a relationship which has been verified repeatedly for zircons in these rocks. Only doubly terminated crystals have been measured. Elongation is defined as the ratio of length to breadth ($l/b$), and size as their geometric mean ($\sqrt{lb}$).

Fundamental ideas in these studies are based on the concept of early formation and short range of crystallization of zircon in calc-alkaline rocks of magmatic origin. The sizes and elongations of a sample of self-nucleated, free-growing crystals depend on their physico-chemical environment: specifically, on such factors as chemical composition, rate of undercooling, viscosity of melt, and surface tension of crystals against melt.[2] Physico-chemical conditions may be expected to be nearly uniform throughout a magmatic pluton shortly after its emplacement and before the crystallization of the main constituent minerals, and this environmental uniformity is likely to be reflected in a uniformity of zircon samples from all parts of the intrusive (except perhaps from chilled borders). Major changes in environment during zircon crystallization are unlikely in view of the short range of crystallization of this mineral. Shortly after the onset of crystallization there is probably a wide range of elongations among small zircon crystals; growth results in wide ranges of both size and elongation, but competition between free-growing crystals ultimately produces relatively narrow ranges of preferred sizes and elongations. Zircons in a slowly cooled calc-alkaline rock of magmatic origin may therefore be expected to show simple monomodal frequency distributions (normal or skewed) of size and elongation. Although there are probably larger and smaller crystals present in the rock than are recovered in the zircon concentrate, their proportions are generally small and the zircons of the rock are to a close approximation represented by the concentrate.

If validated by the results, these ideas suggest numerous applications

[1] A. Poldervaart, loc. cit., p. 546.

[2] W. Eitel, The Physical Chemistry of the Silicates, 1954, Chicago Univ. Press, p. 569.

of zircon studies to petrogenetic problems. Physico-chemical conditions are probably not the same in two separate intrusions, even if they are almost contemporaneous and of similar magma type, and once crystallized, zircons are not likely to show the effects of subsequent magmatic differentiation. Thus zircon studies may be used to distinguish connected from disconnected intrusives, to trace differentiates of the same magma, and to separate them from differentiates of other magmas. They might also be used to advantage in establishing mixing of magmas,[1] or to test immiscibility in magmas.[2] The particular value of these studies is that they provide 'tracers' to the earliest magmatic conditions. In H. H. Read's[3] Granite Series, autochthonous granites are distinguished from parautochthonous and intrusive granites; the latter may be magmatic or migmatitic. In migmatitic intrusives the initial presence of residual solid phases and a partial melt may be reflected in the distribution of two or more distinct types of zircons throughout the body. Such a pluton is now being investigated by these methods.

## *Procedures.*

*Methods of graphic representation.* The problem of graphic representation of length and breadth measurements has not been solved satisfactorily in earlier work. F. Smithson[4] has defined a sample field of zircons by plotting lengths and breadths as points on a scatter diagram; he also employed frequency curves of length, breadth, elongation ($l/b$), or size ($\sqrt{lb}$) constructed from histogram data using a moving average method. Subsequent workers have adopted these methods of representing their data.

In preparing scatter diagrams of length–breadth measurements of doubly terminated zircons separated from granitic rocks of magmatic origin, the authors have found that each sample field shows a linear distribution or trend, which can be generalized by a straight line. Taking advantage of existing procedures we have made extensive use of a line fitted mathematically to each scatter plot, and have further characterized each sample by appropriate statistical measures. At least four different lines can be fitted mathematically to such a scatter diagram;[5] regression of length on breadth, regression of breadth on length, a line

[1] For example, E. S. Larsen *et al.*, Amer. Min., 1938, vol. 23, p. 255 [M.A. **7**–178].

[2] N. Holgate, Jour. Geol., Chicago, 1954, vol. 62, p. 439 [M.A. **12**–537].

[3] Trans. Geol. Soc. South Africa, 1951, vol. 54, Annex, 27 pp.; Geol. Soc. Amer., Spec. Paper 62, 1955, p. 409.

[4] Geol. Mag., 1939, vol. 76, p. 351.

[5] J. Imbrie, Bull. Amer. Mus. Nat. Hist., 1956, vol. 108, art. 2, p. 230.

called the major axis, and a line called the reduced major axis. Of these we have chosen the reduced major axis as best representing the data. Regression methods are not as suitable because a regression line, being designed to indicate the most probable value of one variable for a given value of the other, does not exhibit the relation of the two variables in an unbiased manner. The major axis would really be the optimum estimate, since the errors in length and breadth (when both are expressed in mm.) will be the same; but the difference from the reduced major axis is likely to be far less than the variation imported from preparative techniques, etc., and the reduced major axis for a bivariate population is far easier to compute. The writers believe that the reduced major axis of a scatter plot of length and breadth measurements comes nearest to an expression of a trend of zircon growth in a particular environment. A dynamic concept is thus introduced.

The theory of the reduced major axis as a fitted line has been developed by K. A. Kermack and J. B. S. Haldane[1] and has been used by palaeontologists to describe growth trends of invertebrate fossils. Imbrie has given a lucid exposition of the method and the calculations involved in its use. The authors have found the method excellent when applied to zircons in calc-alkaline rocks of magmatic origin, though certain aspects of zircons in other types of rocks are better illustrated by frequency curves or contoured scatter diagrams. For the sake of brevity the abbreviation RMA is used in this paper for the *reduced major axis of a scatter plot of length and breadth measurements of a zircon sample.*

Kermack and Haldane and Imbrie have treated their data logarithmically because organic growth trends are usually curved on arithmetic plots. Various tests on data for zircons indicate an approximately linear variation of length and breadth on scatter diagrams with arithmetic coordinates; logarithmic transformations are therefore not essential. In such cases it is the choice of sample properties to be illustrated that largely determines arithmetic or logarithmic treatment of data. The writers have used the former treatment because it shows the variation of length and breadth of crystals more directly than logarithmic treatment, and because the RMA is employed in this study as a graphic means for comparison of samples.

Computations necessary for the RMA can be conveniently performed on a correlation form of the type developed by P. S. Burnham.[2] The necessary statistics are: number of crystals measured, $N$; mean length,

[1] Biometrika, 1950, vol. 37, p. 30.

[2] J. Imbrie, loc. cit., p. 244.

$\bar{x}$; mean breadth, $\bar{y}$; standard deviation of length,[1] $s_x$; standard deviation of breadth, $s_y$; coefficient of correlation, $r$; and coefficient of relative dispersion about the reduced major axis, *Dd*. The fitted line is drawn through the plotted point $(\bar{x}, \bar{y})$ at a slope $a = s_y/s_x$ with standard error, $\hat{\sigma}_a$. These statistics are defined as follows:

Mean of $x$, $\bar{x} = \Sigma(x)/N$, expresses the central value of the $x$ observations. Mean of $y$, $\bar{y}$, is determined analogously.

Standard deviation of $x$, $s_x = \sqrt{\{\Sigma(x-\bar{x})^2/N\}}$, is a measure of absolute variation within the sample. Standard deviation of $y$, $s_y$, is determined analogously.

Correlation coefficient, $r = \Sigma(x-\bar{x})(y-\bar{y})/\sqrt{\{\Sigma(x-\bar{x})^2\Sigma(y-\bar{y})^2\}}$, is a measure of closeness of the relationship between the two variables. If $r = \pm 1$, correlation is perfect; if $r = 0$, correlation is absent.

Coefficient of relative dispersion about the reduced major axis, as defined by Imbrie,[2] $Dd = 100\sqrt{\{2(1-r)(s_x^2+s_y^2)/(\bar{x}^2+\bar{y}^2)\}}$, expresses (per cent.) the relative scatter of points about the RMA.

Slope, $a = s_y/s_x$, is the tangent of the angle at which the fitted line is drawn through the point $(\bar{x}, \bar{y})$.

Standard error of slope, $\hat{\sigma}_a = a\sqrt{\{(1-r^2)/(N-2)\}}$, is a measure of the reliability of the slope of the sample as an estimate of the slope of the actual population; the smaller the value of the standard error the more reliable the estimate.

A zircon sample can thus be defined by the statistics: mean length and breadth, standard deviation of length and breadth, slope and standard error of slope of the RMA, and coefficients of correlation and relative dispersion about the RMA. In addition, a length may be assigned to each RMA as a graphic means of indicating the observed range of sizes within the sample. The writers have found this a useful graphic measure of these essential data for comparing samples even though no formal mathematical use has been made of it. In this study the end points of each RMA have been determined arbitrarily by graphically eliminating on the correlation form the extreme $2\frac{1}{2}$ % each of the smallest and largest crystals. It is felt that, by excluding these extremes of variability, the length of the RMA has greater significance as a graphic sample measure. Wherever possible 200 or more zircons have been measured to obtain a statistically large sample.

Differences between samples may be evident upon visual comparison

[1] More precisely, $s_x$ is the standard deviation (in $x$) of the sample, as distinct from the unknown $\sigma_x$, the standard deviation (in $x$) of the total population, and $\dot{\sigma}_x$, the best estimate of $\sigma_x$; $\sigma_x = s_x\{\sqrt{N}/(N-1)\}$.

[2] Loc. cit., p. 241.

of RMAs. If this is not the case, final judgement of similarity or dissimilarity should be based on objective procedures for determining significant differences. Although arithmetic frequency curves of length, size, or elongation of zircon samples are usually skewed, in large samples ($N = 200$) the lack of normality causes negligible error and statistical tests may be applied with confidence in comparing RMAs of different samples.[1]

The simple $z$-test is used here; a test based upon the assumption that the two samples being compared were drawn from the same population (null hypothesis). The test allows us to ascertain the probability that a difference as great as that observed might occur because of chance factors arising from random sampling; i.e. a conclusion concerning the reasonableness of the original assumption.

In this study the RMA represents a linear trend of zircon growth of which the essential elements are slope and position. Procedures for comparing these elements for pairs of RMAs are given below.

*Comparison of slope.* First calculate $z$ for the two slopes:

$$z = (a_1 - a_2)/\sqrt{(\hat{\sigma}^2_{a_1} + \hat{\sigma}^2_{a_2})};$$

then from a table[2] of $z$ determine the probability $P$ that the observed difference is due to chance alone. For a large sample when $z$ is numerically greater than 1·96, the probability is 0·05 or less; that is, the difference between slopes can be due to chance alone five or less times out of one hundred. This has arbitrarily been chosen here as the level of confidence at which differences are considered statistically significant; i.e. when $P$ is numerically less than 0·05 ($z > 1{\cdot}96$) differences are considered real. Further experience may necessitate revision of this level of confidence.

*Comparison of position.* If the slopes tested are significantly different no further tests are necessary. When slope differences are not significant a positional comparison can be made[3] that tests the hypothesis that, for a value $x = x_0$, the true growth trends coincide; i.e. that $y_1 - y_2 = 0$ when $x_1 = x_2 = x_0$. This test is valid only when slope differences are not statistically significant. Calculate $z$ for the two positions:

$$z = \{x_0(a_1 - a_2) + b_1 - b_2\}/\sqrt{\{\hat{\sigma}^2_{a_1}(x_0 - \bar{x}_1)^2 + \hat{\sigma}^2_{a_2}(x_0 - \bar{x}_2)^2}$$

where $x_0$ is arbitrarily chosen $\geqslant \bar{x}_1$ and $\bar{x}_2$, and $b = y$-intercept

[1] Prof. Howard Levene, Columbia University, 1956, personal communication.

[2] Values of $z$ are tabulated in most statistical texts. If $N$ is large (e.g. 200) $z$ may be regarded as equivalent to $t$, and $t$ tables may be used instead.

[3] J. Imbrie, loc. cit., p. 237.

calculated from the form $y = ax+b$. As before, if $z$ is numerically greater than 1·96, the difference in position is taken to be significant.

*Comparison of joint means.* If desired, the positional differences between means of length and breadth may be tested using the following formulae in which $x$ and $y$ are interchangeable. Calculate the standard error of the mean, $\hat{\sigma}_{\bar{x}}$ or $\hat{\sigma}_{\bar{y}}$, for the two samples: $\hat{\sigma}_{\bar{x}} = \hat{\sigma}_x/\sqrt{(N)}$. Next, calculate $z$ for the two sample means: $z = (\bar{x}_1 - \bar{x}_2)/\sqrt{(\hat{\sigma}^2_{\bar{x}_1} + \hat{\sigma}^2_{\bar{x}_2})}$. As before, if $z$ is numerically greater than 1·96, the difference in position of the means is taken to be significant.

*Preparation and measurement of zircon samples.* Procedures followed in this laboratory have been described by A. Poldervaart.[1] The following study was conducted to test and improve these methods.

Three samples of hand-specimen size were taken from a large block of friable, coarse-grained tonalite (LL–13–W) from the Kaniksu batholith, Idaho–Washington. One sample was treated for four days on a steambath with HF and $H_2SO_4$ (1:1) with repeated renewal of the acid mixture. This only partly dissolved the rock. The residue was washed, separated on bromoform, and the total heavy residue (about 500 zircons) mounted on a single slide. The second sample was crushed in a disk-grinder at a coarse setting, such that two-thirds of the crushed sample did not pass through a 20-mesh U.S. Standard sieve (0·84 mm. opening). The third sample was crushed at the finest setting of the grinder; all the crushed material passed through a 60-mesh U.S. Standard sieve (0·25 mm. opening). The crushed samples were individually separated with bromoform, followed by removal of magnetic minerals with a Frantz isodynamic separator, and the residues were further purified by settling with bromoform, followed by settling with Clerici solution. The concentrates were reduced in size by a cone-and-quarter technique suggested by C. O. Hutton.[2] Portions of about 2000 to 3000 zircons each were mounted on single slides, two portions being taken for each concentrate. Concentrates of practically pure zircon were obtained. Recovery was smallest from the sample treated with acid, while about four times as much zircon was obtained from the finely crushed sample as from the coarsely crushed sample.

Two hundred doubly terminated crystals were measured for each mount at a high magnification (×270), using an ocular micrometer. Only those zircons visible in the microscope field at equally spaced intervals along equally spaced traverses distributed over the entire slide

[1] Amer. Jour. Sci., 1955, vol. 253, p. 435.
[2] Bull. Geol. Soc. Amer., 1950, vol. 61, p. 643.

were measured. A Chayes point counter was used for this purpose, and the measurements were made a second time for a single slide of each concentrate obtained from the crushed samples.

The results of these measurements are shown in fig. 1 and table I. The

TABLE I. Statistical parameters of zircon samples for tonalite LL-13-W. (Under *Sample* read HF as acid separation, CC as coarse crush, and FC as fine crush; CC–1(1) as coarse crush, first slide, first measurement, CC–1(2) as coarse crush, first slide, second measurement, and CC–2 as coarse crush, second slide. Column B is the number of singly terminated, apparently broken zircons counted during measurement of each sample.)

| *Sample* | B | $a$ | $\hat{\sigma}_a$ | $\bar{x}$(mm.) | $\bar{y}$(mm.) | $s_x$ (mm.) | $s_y$ (mm.) | $r$ | $Dd$ |
|---|---|---|---|---|---|---|---|---|---|
| HF | 48 | 0·4183 | 0·0268 | 0·1140 | 0·0427 | 0·0455 | 0·0190 | 0·7139 | 29·9 |
| CC–1(1) | 64 | 0·3730 | 0·0245 | 0·1076 | 0·0379 | 0·0376 | 0·0140 | 0·6445 | 28·9 |
| CC–1(2) | 49 | 0·3701 | 0·0216 | 0·1099 | 0·0387 | 0·0335 | 0·0124 | 0·5629 | 29·7 |
| CC–2 | 72 | 0·4034 | 0·0245 | 0·1081 | 0·0406 | 0·0383 | 0·0154 | 0·6261 | 30·9 |
| FC–1(1) | 56 | 0·4139 | 0·0267 | 0·1026 | 0·0357 | 0·0280 | 0·0116 | 0·4385 | 27·3 |
| FC–1(2) | 55 | 0·3940 | 0·0256 | 0·1030 | 0·0365 | 0·0321 | 0·0127 | 0·5258 | 30·8 |
| FC–2 | 58 | 0·3595 | 0·0238 | 0·1155 | 0·0419 | 0·0373 | 0·0134 | 0·5836 | 29·4 |

differences between the joint means and the slopes of RMAs resulting from two measurements of the same slides are near the limit of accuracy for measuring single crystals; the differences between joint means and slopes of RMAs resulting from cone-and-quarter techniques are as much as ten times this amount, as are the differences resulting from different zircon-liberating techniques. Some statistical comparisons are given below in which $z_a$, $z_{\bar{x}}$, and $z_{\bar{y}}$ are $z$ values calculated for slope, mean length, and mean breadth. The sample symbols are the same as in table I.

| | | | | | | | |
|---|---|---|---|---|---|---|---|
| FC–(1)—FC–1(2): | $z_a$ 0·56 | $z_{\bar{x}}$ 0·13 | $z_{\bar{y}}$ 0·20 | CC–1(1)—FC–1(1): | $z_a$ 1·23 | $z_{\bar{x}}$ 0·54 | $z_{\bar{y}}$ 1·71 |
| CC–1(1)—CC–1(2): | 0·10 | 0·64 | 0·62 | HF—CC–1(2): | 1·62 | 1·02 | 2·48 |
| FC–1(1)—FC–2: | 1·63 | 3·98 | 4·91 | HF—FC–1(1): | 0·13 | 3·08 | 4·41 |
| CC–1(1)—CC–2: | 1·01 | 0·13 | 1·80 | HF—FC–2: | 2·02 | 0·36 | 0·47 |

These tests indicate the magnitudes of error attributable to statistical sampling errors and the liberating and sampling techniques used, and emphasize the need for rigid standardization of methods for liberating and concentrating zircons from rocks in studies of this type. Mounting the entire zircon crop on as many slides as necessary and sampling of all the slides by spaced microscope traverses is desirable for consistent results, instead of the cone-and-quarter technique of sampling concentrates.

The extent of zircon breakage during crushing has been a major cause for concern in this work, and broken crystals are present in all the

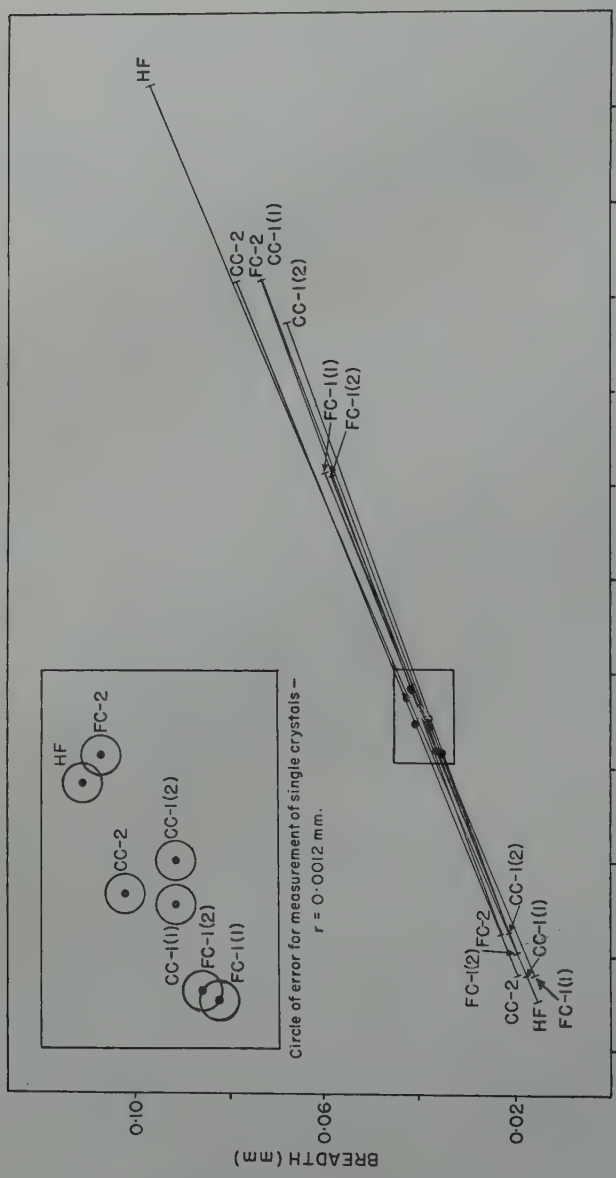


FIG. 1. RMAs for tonalite LL-13-W. For explanation of the term RMA see text.

concentrates; sometimes in relatively high proportions. It is therefore significant that in measuring 200 doubly terminated zircons liberated by acid treatment without crushing, forty-eight singly terminated, apparently broken crystals were encountered. The data in table I show no evidence of severe breakage of zircons due to crushing of rock samples, even when fine crushing is used. Apparently broken zircons in a rock may result from imperfect crystallization, or from breakage due to partial alteration and differential expansion of the main constituent minerals.

Rock crushing probably causes significant breakage among the largest zircons of high elongation, but normally such crystals are few in number. Fine crushing liberates three to four times as many zircons as coarse crushing, although the proportion of broken crystals is not significantly different in the two cases (table I). Fine crushing apparently assures more uniform results than coarse crushing by release of larger and more representative portions of the zircon sample at the expense of relatively few larger crystals. For those rare rocks having a preponderance of large zircons fine crushing should not be used.

It is also best to process all the crushed material that passes through a 60-mesh U.S. Standard sieve without removal of the fine dust by washing; separation of the finest material is facilitated by centrifuging. After removal of the magnetic minerals, final concentration of zircon crops by heavy liquids should be done without filter paper. Separations at this stage can be done in small tube-shaped vials, allowing the concentrate to settle and then floating the light minerals off; washing of the concentrates can be done in the vials, which also serve for storage until the concentrates are mounted.

### *Distribution of zircon in a tonalite.*

The early formation and the short range of crystallization of zircon in magmatic calc-alkaline rocks are critical assumptions made in applying results of zircon studies to petrogenetic problems. The work reported here was undertaken to test these assumptions. The rock used, a tonalite (LL–11–I) from the Kaniksu batholith, Idaho-Washington, was selected because in it zircon is unusually abundant, and because evidence presented by J. L. Gillson[1] indicates that the opposite of the above assumptions holds for this batholith. The chemical analysis and mode of this rock are given in table II, the mode being based on three thin sections and 2000 points obtained by traversing the sections at regularly spaced intervals

[1] Amer. Min., 1925, vol. 10, p. 187.

with a Chayes point counter. Agreement between analysis and mode is poor, and calculations from the analysis indicate about 4 % less quartz and 4 % more chlorite than are found modally; the discrepancies may be due to silica deficiency in plagioclase, presence of magnesium in the muscovite, and errors in the analysis and mode.

TABLE II. Chemical analysis and mode of tonalite LL-11-I, together with zircon and zirconium abundance in the main minerals. (1000 zircons were counted by point-counter traverses of which 82 were found athwart grain boundaries, while the remainder were included as shown below. Silicate analysis by Dr. H. B. Wiik, Helsinki, Finland. Spectrographic data by Dr. Karl Turekian, Yale University, New Haven, Connecticut, U.S.A.)

| | % | | *Mode* % | *Zircons counted* | *Relative abundance zircons (by volume)* | *Spectrographic abundance zirconium (ppm)* |
|---|---|---|---|---|---|---|
| $SiO_2$ | 65·83 | Quartz | 30·8 | 368 | 12 | < 100 |
| $TiO_2$ | 0·55 | Plagioclase | 48·3 | 312 | 6 | ≈ 100 |
| $Al_2O_3$ | 16·98 | Orthoclase | 1·7 | 29 | 16 | ≈ 100 |
| $Fe_2O_3$ | 0·64 | Hornblende | 0·6 | nil | | |
| FeO | 2·86 | Biotite | 10·0 | 166 | 18 | > 200 |
| MnO | 0·07 | Muscovite | 3·4 | 43 | 13 | > 200 |
| MgO | 1·16 | Magnetite | 0·6 | nil | n.d. | > 200 |
| CaO | 4·17 | Epidote | 3·3 | nil | — | — |
| $Na_2O$ | 3·90 | Chlorite | 0·8 | nil | — | — |
| $K_2O$ | 1·76 | Apatite | 0·5 | nil | n.d. | n.d. |
| $P_2O_5$ | 0·26 | Total | 100·0 | | | |
| $H_2O^+$ | 0·98 | | | | | |
| $H_2O^-$ | 0·07 | | | | | |
| $CO_2$ | nil | | | | | |
| Total | 99·23 | | | | | |

*Thin-section studies.* Thin-section studies of zircon are generally of limited use because of the small number of zircons present in each thin section, the minute size of the crystals, their random orientation, and the difficulties experienced in their recognition as inclusions in various host minerals. Observations regarding the shapes of zircons are unreliable when based on thin-section work.[1]

The unusual abundance of zircon in the tonalite sample is shown by the presence of 800 to 1000 zircons in a single thin section. Many of the crystals are minute, often less than 0·001 mm. in breadth. Three thin sections were traversed at equally spaced intervals, noting zircon crystals in relation to the host minerals quartz, plagioclase, orthoclase, biotite, and muscovite. Observations on 1000 zircons are included in table II

[1] A. Poldervaart, Amer. Jour. Sci., 1956, vol. 254, p. 529.

without regard to their sizes and shapes. Relative abundance of zircons in the various host minerals is calculated by dividing the number of enclosed zircons by the volume per cent. of the host mineral, and may be compared with zirconium abundance determined spectrographically for pure fractions of the main constituent minerals. Too great a reliance should not be placed either on the thin-section observations or on the spectrographic data.

Thin-section observations show, however, that zircons are enclosed in all the non-opaque minerals; magnetite was found to contain more than 200 parts per million of zirconium (like biotite and muscovite).

TABLE III. Sequence of crystallization of main minerals in tonalite LL-11-I.

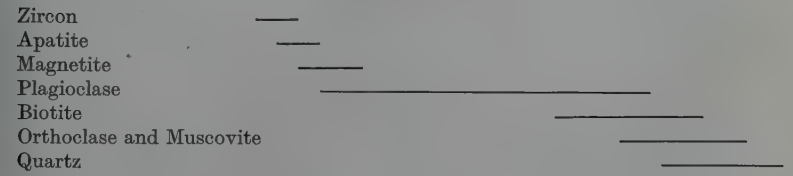


Apatite contains numerous minute zircons and occasional larger zircon crystals themselves contain minute zircons as inclusions. In addition there are zircons between crystals of the constituent minerals. In traversing the thin sections one gets the impression that zircons sometimes tend to be distributed in clusters, with proportionately large barren areas between clusters; no further work was done to confirm this impression.

The order of crystallization as determined from thin sections is shown in table III. The observations indicate that zircon was the first mineral to crystallize, but they do not warrant a conclusion concerning its range of crystallization. Evidently zircon crystals were present in the residual magmas throughout the magmatic consolidation sequence.

The distribution of zircon crystals in the mineral fabric of a magmatic rock is the overall result of a number of factors: time and range of crystallization of zircon relative to that of other constituent minerals, nucleation and rate of seeding of nucleii of zircon in the magma, nucleation of other constituent minerals on zircon crystals, and enclosure of zircons through growth and mutual interference of other constituent minerals. It has been suggested by Poldervaart[1] that minerals such as apatite, magnetite, biotite, and muscovite may nucleate on zircon

[1] Loc. cit., p. 547.

crystals with more facility than do felspars or quartz. Present observations tend to support this, but more detailed studies are required fully to ascertain the distribution of zircon crystals in a rock.

*Studies of concentrates.* The tonalite was crushed approximately to grain size, and pure fractions of quartz, plagioclase, orthoclase, biotite, muscovite, magnetite, and apatite were separated. Zircon was separated from apatite by solution of apatite in hot concentrated HCl, while the other mineral fractions were carefully crushed and processed with heavy liquids and a Frantz magnetic separator. Zircons in each concentrate were measured with results given in fig. 2 and table IV; included are data for a sample of the tonalite processed in its entirety.

TABLE IV. Statistical parameters of zircon samples for tonalite LL-11-I and its main constituent minerals, together with comparisons of RMA slopes of the constituent minerals with that of the tonalite.

| *Sample* | *N* | $a$ | $\sigma_a$ | $\bar{x}$ (mm.) | $\bar{y}$ (mm.) | $s_x$ (mm.) | $s_y$ (mm.) | $r$ | *Dd* | $z_a$ |
|---|---|---|---|---|---|---|---|---|---|---|
| Tonalite | 200 | 0·3343 | 0·0196 | 0·1017 | 0·0338 | 0·0365 | 0·0122 | 0·5572 | 33·8 | — |
| Biotite | 100 | 0·3415 | 0·0224 | 0·0986 | 0·0322 | 0·0396 | 0·0135 | 0·7575 | 28·1 | 0·241 |
| Muscovite | 100 | 0·3549 | 0·0308 | 0·0828 | 0·0293 | 0·0263 | 0·0093 | 0·5165 | 31·4 | 0·564 |
| Orthoclase | 66 | 0·3506 | 0·0316 | 0·0951 | 0·0321 | 0·0338 | 0·0118 | 0·6790 | 27·8 | 0·438 |
| Plagioclase | 100 | 0·3814 | 0·0283 | 0·0869 | 0·0283 | 0·0357 | 0·0136 | 0·6682 | 34·0 | 1·31 |
| Quartz | 50 | 0·4767 | 0·0312 | 0·0771 | 0·0270 | 0·0228 | 0·0109 | 0·8870 | 14·7 | 3·88 |
| Magnetite | 100 | 0·4216 | 0·0246 | 0·0723 | 0·0255 | 0·0293 | 0·0124 | 0·8133 | 25·4 | 2·78 |
| Apatite | 200 | 0·2873 | 0·0171 | 0·0214 | 0·0049 | 0·0113 | 0·0032 | 0·5386 | 51·3 | 1·81 |

In fig. 2 the RMA for the entire tonalite, if extended, passes nearly through the origin, indicating that the zircons are self-nucleated; i.e. they have not themselves nucleated on other minerals. The joint means of the RMAs from the different mineral fractions lie on or near the RMA of the tonalite, but the slopes do not all coincide with that of the tonalite. Statistical comparisons of these data are also shown in table IV where slopes of RMAs for the pure mineral fractions are compared with that of the rock. RMA slopes for quartz and magnetite are significantly different from the RMA slope of the tonalite, while apatite is a borderline case. RMA slopes for biotite, muscovite, orthoclase, and plagioclase are not significantly different from the RMA slope of the tonalite or from one another. Of this group of four mineral fractions the positions of muscovite and biotite differ most from one another, but a $z$-test indicates no significant difference in position between them.

Since the RMA slopes of quartz, magnetite, and apatite are significantly different from the RMA slope of the rock, statistical tests cannot be applied to test the analogous positional differences. But the positional differences are visibly not greater than that between the RMAs of

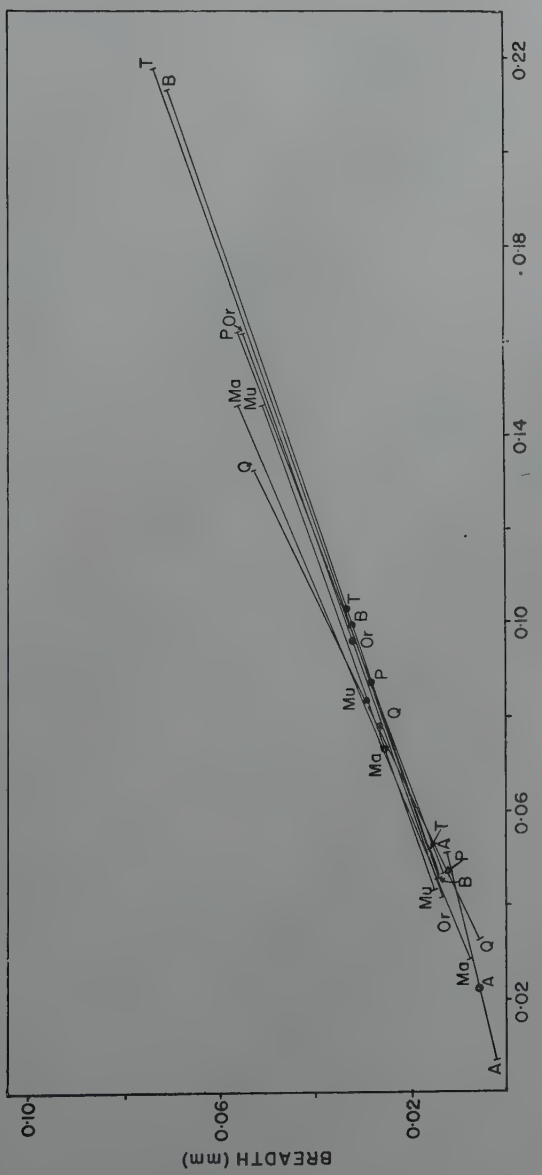


FIG. 2. RMAs for tonalite LL-11-I and its main constituent minerals.

muscovite and the rock: hence it is assumed that there are no significant positional differences between the RMAs of the mineral fractions and the RMA of the tonalite. The joint means all fall close to the RMA for the rock. There is clearly a difference in average size between samples, but not in average shape.

Differences in RMA slopes for quartz and magnetite are probably attributable to crushing. Quartz and magnetite have no well-developed cleavage, and quartz and zircon are of equivalent hardness, with magnetite not much different; crushing of quartz and magnetite is therefore likely to cause breakage, especially of elongated zircons, and most zircons, broken or unbroken, are likely to remain enclosed in the host mineral. This interpretation is fully supported by the results: although equal amounts of quartz and plagioclase were used for the preparation of the zircon concentrates, and thin-section studies indicate that these minerals enclose equivalent numbers of zircons (table II), only 50 zircons were recovered from the quartz, while 150–200 zircons were obtained from the plagioclase. Further, examination of the crushed quartz after zircon separation shows that many broken and unbroken zircons have remained enclosed in the quartz particles.

Thus it seems that the lower elongations and smaller sizes of zircons recovered from quartz and magnetite as compared with those obtained from minerals with good cleavage is an effect of crushing. It is apparent from fig. 2 that the combined effect of zircons separated from main constituent minerals with good cleavage, in which release of zircons upon crushing is high, masks that of quartz, in which release of zircons upon crushing is low. Well-developed cleavage in the main constituent minerals clearly plays an important role in the liberation of zircon without serious breakage.

Earlier it was concluded (table III) that zircon and apatite overlap in crystallization, because not only does apatite include numerous minute zircons, but a few large zircons partly enclose apatite crystals. Since zircons included in apatite are always small (fig. 2) and abundant it appears that the zircon population was still immature and actively growing at the onset of apatite crystallization, and further, that apatite may have nucleated on minute zircons. Magnetite began to crystallize after apatite and before plagioclase, but the mean size of the zircons contained in magnetite (fig. 2) indicates that the zircon population was nearly or quite full-grown. Hence it is concluded that zircon was the earliest mineral to crystallize, and that its range of crystallization was brief.

*Distribution of zircon in a batholith.*

The Bald Mountain batholith, Oregon, provides an ideal example of the uniformity of zircons throughout a magmatic pluton, and also yields examples of the lack of uniformity of zircons in different magmatic bodies. W. H. Taubeneck[1] has made an unusually detailed study of the batholith and his field and laboratory observations leave no doubt that it is a magmatic intrusive. The main phases are a mantle of tonalite

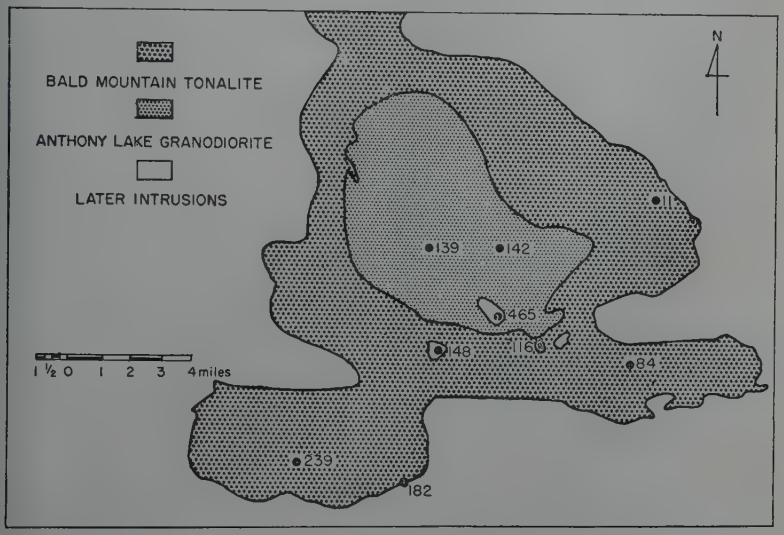


Fig. 3. Sketch-map of Bald Mountain batholith, Oregon.

that grades continuously into a core of granodiorite. Fig. 3 is a sketch-map in which a boundary between core and mantle has been arbitrarily drawn at a modal content of K-felspar of about 6 %. Small intrusives of granodiorite and quartz monzonite are found within the batholith and have sharp contacts against the main batholithic rocks.

Zircons from six main batholithic rocks (4 tonalites and 2 granodiorites) and from each of three later intrusives were separated and measured by Taubeneck. The samples are geographically widely separated (max. 15 miles; fig. 3), differ in altitude by as much as 2000 feet, and differ in petrographic type. The authors have calculated RMAs for these samples, and the results are shown in fig. 4 and table V.

Fig. 4 shows that the RMAs for the six main batholithic rocks are

[1] Bull. Geol. Soc. Amer., 1957, vol. 68, p. 181.

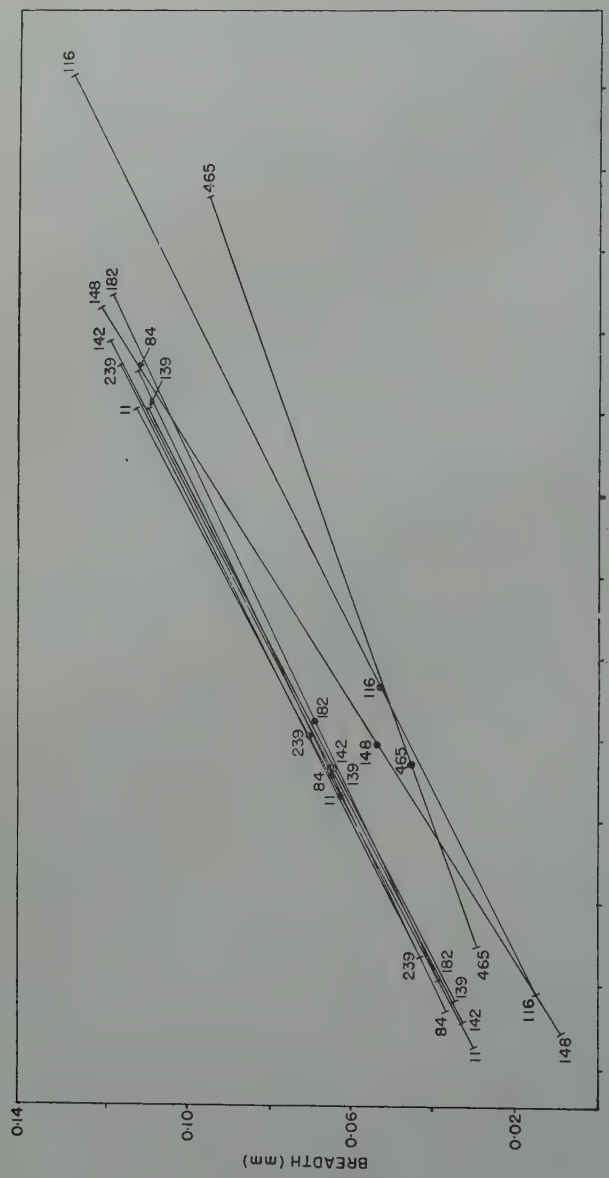


FIG. 4. RMAs for rocks of Bald Mountain batholith, Oregon.

similar, while the RMAs for the three later intrusives are different. Of the six similar RMAs, samples 11 and 182 differ most in slope, but a test of slopes shows this difference to be insignificant ($z_a = 1{\cdot}88$). A positional test between samples 11 and 182 also shows no significant difference ($z_p = 0{\cdot}83$). All the main batholithic samples may therefore be considered to have been drawn from a single population of zircons, and a mean growth trend may be calculated to represent this population (MGT; table V).

TABLE V. Statistical parameters of zircon samples for rocks of Bald Mountain batholith, Oregon. (300 zircons were measured in each sample. Samples 11, 84, 182, and 239 are tonalites and 139 and 142 are granodiorites, all from the main batholithic series; the mean growth trend for these six samples is given against *MGT*. Samples 116 and 148 are later granodiorite intrusives, and sample 465 is a late quartz monzonite intrusive.)

| *Sample* | $a$ | $\sigma_a$ | $\bar{x}$ (mm.) | $\bar{y}$ (mm.) | $s_x$ (mm.) | $s_y$ (mm.) | $r$ | $Dd$ |
|---|---|---|---|---|---|---|---|---|
| 11 | 0·5332 | 0·0214 | 0·1059 | 0·0625 | 0·0388 | 0·0207 | 0·7187 | 26·8 |
| 84 | 0·4954 | 0·0205 | 0·1109 | 0·0640 | 0·0414 | 0·0203 | 0·6984 | 27·8 |
| 182 | 0·4793 | 0·0191 | 0·1242 | 0·0690 | 0·0434 | 0·0208 | 0·7233 | 24·8 |
| 239 | 0·5098 | 0·0159 | 0·1202 | 0·0702 | 0·0382 | 0·0195 | 0·8403 | 17·4 |
| 139 | 0·5230 | 0·0224 | 0·1128 | 0·0640 | 0·0406 | 0·0213 | 0·6704 | 28·7 |
| 142 | 0·5188 | 0·0192 | 0·1129 | 0·0646 | 0·0433 | 0·0230 | 0·7672 | 26·2 |
| *MGT* | *0·5097* | *0·0199* | *0·1145* | *0·0657* | *0·0411* | *0·0209* | *0·7364* | *25·3* |
| 116 | 0·5070 | 0·0244 | 0·1326 | 0·0528 | 0·0562 | 0·0285 | 0·5529 | 41·8 |
| 148 | 0·6401 | 0·0233 | 0·1184 | 0·0535 | 0·0506 | 0·0234 | 0·7768 | 28·7 |
| 465 | 0·3567 | 0·0179 | 0·1139 | 0·0451 | 0·0464 | 0·0165 | 0·4937 | 40·4 |

Although zircon shapes are not significantly different in these samples, fig. 4 shows considerable variation in size of zircon crystals. The smallest and largest joint means of zircons are from the tonalite mantle, while the two granodiorites from the core have zircons of intermediate sizes. There is no complete assurance that these size differences are real and not due to variations resulting from laboratory procedures in separation, sampling, and measurement of the crystals, but, assuming that the differences are real, the following explanation may account for the observed size variation: G. C. Kennedy[1] has argued that water concentrations are likely to vary over short distances near the margins of a batholith; higher water concentrations are likely to promote growth of zircon crystals through lowering of the viscosity of the magma, while lower water concentrations probably have the opposite effect; hence considerable variations in size of zircons may be expected in the marginal portions of the batholith, while in the central portions variations in size of zircons from one rock sample to the next are likely to be negligible.

[1] Geol. Soc. Amer., Spec. Paper 62, 1955, p. 489.

It is evident from fig. 4 that each of the three later intrusives has zircons of a different character. Tests of RMA slope difference give the following results: 116–148, $z_a$ 3·93; 116–465, $z_a$ 4·97; 148–465, $z_a$ 9·63. Of this group only sample 116 is similar in RMA slope to the mean growth trend of the main batholithic rocks. A positional comparison yields a $z_p$ value of 9·88, showing the difference to be significant. These results emphasize not only that zircons from the same magmatic intrusive are alike, but also that zircons from different magmatic bodies are different.

It is concluded from these observations that the Bald Mountain batholith was formed by a single magmatic intrusion. After this had crystallized there were three further pulses of magmatic activity which formed separate bodies within the batholith. The three later intrusions are not differentiates of the same magma that produced the main batholith, but are distinct from that magma and represent three disconnected magmas that cooled individually. If one accepts the concept of large magmatic reservoirs at depth that are maintained for several hundreds, perhaps thousands, of years, it is still possible to argue that the main batholithic magma and the three later magmas may all have originated at different times from the same reservoir; the authors admit but do not favour this possibility.

*Discussion.*

For some time, students of petrogenetic problems connected with calc-alkaline plutons have felt the need for a method that might yield clues to early conditions in these bodies. Recognition that there are granites and granites and the development of the concept of a Granite Series by H. H. Read[1] have accentuated this need. Several workers in this field have turned to studies of the morphological characters of zircons in these rocks as a possible source of information on early conditions in granitic plutons. Much of the earlier work on zircons has been of a reconnaissance nature; it has served to crystallize fundamental ideas in this work and has opened the way toward more detailed and specific studies, while at the same time certain conclusions have emerged that are of importance to the application of these studies to petrogenesis.

Basic assumptions in this type of work are: that the morphological characters of zircons are controlled by the physico-chemical environment in which they crystallized; that zircon crystallizes so early and its range

[1] Trans. Geol. Soc. South Africa, 1951, vol. 54, Annex; and Geol. Soc. Amer., Spec. Paper 62, 1955, p. 409.

of crystallization is so short that normally there is no appreciable change in environment during its crystallization; that similar environments produce similar zircons, while different environments produce significantly different zircons; that although growth results in a wide range of sizes and habits of zircons, competition between crystals growing in the same environment will produce a relatively narrow range of favoured sizes and habits, which will be of high frequency and can thus be used to characterize the sample; finally, that the narrow range of preferred sizes and habits are normally included in the zircons concentrated from a rock, and these zircon samples are therefore representative of the zircon population in the rock (effects of possible procedural bias can be reduced by use of bivariate rather than univariate analyses).[1]

These assumptions are largely warranted by earlier zircon studies and are further confirmed in this paper. The earlier work also shows clearly that these assumptions do not all apply to all igneous rocks; the physico-chemical environment may change rapidly during the final stages of magmatic consolidation, and zircon is frequently of late crystallization in basaltic and in sodic peralkaline rocks.[2] Environment may change rapidly even during the earliest stages of crystallization, for example in volcanic centres or in the flat roof zones of batholiths emplaced high in the crust. We do not know whether zircon samples would be similar or dissimilar in different parts of such intrusives; these are examples yet to be studied. According to H. H. Read[3] and others, intrusive granitic plutons may be migmatitic or magmatic; if they are migmatitic, zircons in these rocks are likely to be of more than one type, reflecting their crystallization from the partial melt, as well as their crystallization in the residual solid phases. Zircons of autochthonous and parautochthonous members of the Granite Series should also be studied.

Studies of the morphological characters of zircons can be focused on the habits or on the dimensions of crystals. Y. Karakida[4] has published an excellent study of zircon habits in two granitic plutons. The authors have chosen to study dimensions of crystals because this best suits the purpose of this restricted investigation and is more easily expressed numerically and controlled statistically. In different cases, other methods of zircon study may be more suitable; for example, the development of outgrowths and overgrowths on zircons of autochthonous granites[5] is

[1] J. Imbrie, loc. cit., p. 223.
[2] A. Poldervaart, loc. cit., p. 522.
[3] Loc. cit., 1951, p. 21.
[4] Jour. Geol. Soc. Japan, 1954, vol. 60, p. 517.
[5] F. D. Eckelmann and A. Poldervaart, Bull. Geol. Soc. Amer., 1955, vol. 66, p. 947.

best studied in zircon samples from series of rocks by counts of crystals that do and do not show these features than by measurement of lengths and breadths of crystals only.

In this study, unusual precautions have been taken in the separation, sampling, and measurement of zircons. Such a procedure is proper since this is a pilot study; it is also necessitated by the high sensitivity of the method of the reduced major axis and by rigid statistical comparisons made between RMAs of different samples. The method of the reduced major axis is not a panacea, but if care is taken in laboratory procedures it offers an elegant and rigidly controlled means of expressing and comparing the data. As a method of bivariate analysis it also involves a dynamic concept of relative growth and focuses on growth pattern, rather than static morphological characters. For reconnaissance types of zircon studies, visual comparison of elongation, length, and breadth frequency curves, or of contoured scatter diagrams, probably remains the easiest method of approach. For more detailed studies of specific rocks it will be necessary to augment comparison of RMAs with other means of graphic representation (frequency curves and contoured scatter diagrams) and other data (tabulated counts and observations) to bring out and trace specific morphological characters of zircons.

*Acknowledgements.* Prof. John Imbrie and Prof. Howard Levene, both of Columbia University, gave expert counsel on statistical method and theory. Dr. William H. Taubeneck, of Oregon State College, generously made his data on the Bald Mountain batholith (Oregon) available for this study. Dr. Karl Turekian, of Yale University, did the spectrographic work on zirconium.

Parts of this work were financed by the Kemp Memorial Fund and the Eugene Higgins Fund; this assistance is gratefully acknowledged.

# *The paragenesis of garnet in charnockite, enderbite, and related granulites*

(With Plate XVIII.)

By R. A. Howie, M.A., Ph.D., F.G.S.
Geology Dept., University of Manchester
and
A. P. Subramaniam, A.M., M.Sc., Ph.D., F.G.S.
Geological Survey of India.

[Read 24 January 1957.]

*Summary.* The presence of garnet in acid rocks of the charnockite series south of Madras is reported. Petrographic descriptions of garnetiferous enderbites and related pyroxene-granulites, khondalites, and leptynites are accompanied by new chemical analyses of 6 rocks, 8 garnets, and 5 orthopyroxenes from the type area near Madras, and from Ceylon, Varberg, and Uganda. The garnets show a considerably higher FeO/MgO ratio than the coexisting orthopyroxenes and the host rocks. The presence or absence of garnet appears to be related to the bulk chemistry of the rocks. Basic garnetiferous granulites associated with these rocks are considered to represent an unstable mineral assemblage and may be genetically unrelated to the acid types. Attention is drawn to the prevalence of enderbitic rocks in the type area.

In his memoir on the charnockite series of India Holland (1900) defined charnockite as 'a quartz–felspar–hypersthene–iron ore rock in the charnockite series', the latter being a name used to express the fact that he grouped together in the one petrographic province a number of petrological types which he considered to be genetically related to charnockite and to one another. Holland made no mention of garnet in his list of characteristic constituents or in the detailed petrography of charnockite although he briefly described the occurrence of garnet in some basic rocks of the series and in garnetiferous leptynite (light-coloured acidic granulite). The purpose of this paper is to record and emphasize the occurrence of garnet in the rocks of the type area south of Madras and to describe the mineralogy of these garnet-bearing charnockites and related rock types.

In general to avoid ambiguity the nomenclature of Holland will be used, but without any petrogenetic significance. In particular the name charnockite is confined to the normal dark orthopyroxene-bearing acid

member of the series. Tilley (1936) has suggested the name enderbite for acid rocks of this series in which plagioclase is the predominant felspar rather than microcline or orthoclase, and in this restricted sense many of the garnetiferous rocks here described are enderbites rather than charnockites, although both felspars are present.

After the appearance of Holland's memoir very little work was done on the type area for forty years, although Washington (1916) published petrographic descriptions and analyses of a suite of rocks from the Madras charnockite series, none of which contained garnet. Rajagopalan (1946 and 1947), working on material from St. Thomas's Mount, Madras, again does not report any garnet in rocks of the series ranging from 49 to 75 % in $SiO_2$ content. Although Muthuswami (1953) described a basic garnetiferous diopside granulite from Pallavaram, in the various 'norites' of the district garnet is reported to be absent: an area marked 'garnetiferous charnockite' is, however, indicated on the sketch-map of the country south-east of Pallavaram. Naidu (1955) states that 'garnet occurs in the basic, intermediate, and acid charnockites', but in the 42 modal analyses presented the only acid rocks with garnet do not contain any orthopyroxene: similarly Narayanan *et al.* (1955), who re-examined the Pallavaram area, describe leptynite grading into garnetiferous charnockite at Cheri Hill: but the mode of their 'acid charnockite' shows no orthopyroxene to be present. Leelananda Rao (1955) described garnetiferous khondalites and leptynites from Pachaimalai, 2 miles south-west of Pallavaram, but reported that basic, intermediate, and acid members of the charnockite series bear no garnets.

In a recent chemical and mineralogical study by one of the present authors, working largely on material supplied by the Geological Survey of India, no garnets were found other than in the leptynite (Howie, 1955). Although various authors have described garnetiferous intermediate and acid members of the series from elsewhere in India and from other pre-Cambrian areas, the garnetiferous rocks of the Madras district have thus been largely overlooked.

One of us (A. P. S.) has recently had the opportunity to map and investigate the field relationships in the area of St. Thomas' Mount and Pallavaram, where numerous quarries have been opened in the last few years, and it is now apparent that garnetiferous charnockite or enderbite is of fairly common occurrence: indeed an examination of the paratype, the tombstone of Job Charnock in St. John's Churchyard, Calcutta, reveals that it itself contains easily discernible red garnets. Basic granulites containing garnet as well as orthopyroxene are abundant in

the Madras area. The garnet-bearing leptynites and the khondalites (garnet–quartz–sillimanite rocks) will also be briefly considered as they are of importance in discussing the possible origin and relationship of the charnockites. Only brief details of the field occurrence of these garnetiferous rocks are given here, as the field and petrogenetic relationships in the type area will be discussed in a separate communication by one of us (A. P. S.).

*Field occurrence and petrography.*

For convenience of description the rocks may be divided into six groups: the acid garnetiferous charnockites or enderbites, the dark acid garnetiferous granulites without orthopyroxene, the rocks of intermediate composition, the basic garnetiferous 'norites', the light-coloured garnetiferous leptynites, and the sillimanite-bearing khondalites. The constant textural feature is the even-grained granular character of the constituents: the rocks are remarkably fresh and the orthopyroxene when it occurs is strongly pleochroic.

*The garnetiferous enderbites.* Rock Ch 113 from west of Hasanapuram quarry to the south of Pallavaram is typical of this group and has the almost greasy lustre and dark bluish-grey colour characteristic of charnockite, with grains of red garnet occasionally visible. In thin section the potash felspar is strongly perthitic with a slightly shadowy extinction: the refractive indices $\alpha$ 1·523, $\gamma$ 1·530 (both $\pm$ 0·001) indicate a composition of $Or_{55}$ ($\pm$ 7 % Or). The quartz shows evidence of strain, each grain consisting of several optically related individuals all showing wavy extinction, while the plagioclase is antiperthitic with the irregular blebs of potash felspar regularly oriented in the crystals: its composition from optics is $An_{30}$. The orthopyroxene occurs in ragged and embayed grains but is relatively fresh (pl. XVIII, fig. 1); it is strongly pleochroic. The pink garnet forms large masses of indeterminate shape with many quartzo-felspathic and iron ore inclusions: a small amount of iron ore is found, both magnetite and ilmenite being present; other accessories include a little reddish-brown biotite and rounded grains of zircon.

Specimen 56 from Pallavaram is rather coarser than the previous rock, and has a more olive-brown colour. In this rock it was noticed that on a freshly sliced surface the quartz was light greyish blue and the felspar yellow, although after a few months the colour gradually changed to the usual overall olive-brown hue. In thin section the mineralogy is rather similar to Ch 113 but the large grains of microperthite show a more noticeable undulatory extinction together with the faint suggestion

of cross-hatching typical of incipient microclinization: the quartz contains some minute hair-like inclusions. The garnet and orthopyroxene tend to be roughly associated in clumps.

*Acid garnetiferous granulites without orthopyroxene.* Ch 219 from Tattan Kunnu quarry, between the two rifle ranges south of Minambakkam railway station, has the typical dark appearance in hand specimen with blue quartz and greenish-blue felspars together with rounded grains of red garnet and in the field forms a marginal facies of the normal non-garnetiferous charnockite. In thin section orthopyroxene is virtually absent though one grain was found in one of the 20 sections examined: it may therefore be classed as a garnetiferous granulite without orthopyroxene. Specimen Ch 44 is a fairly coarse alaskitic rock from the south-east face of knoll 150, west of Ottaiyambakkam, 8 miles south of Pallavaram, and is light-coloured but with parallel streaks of bluish-grey quartz and deep-brown garnets throughout the rock: its mineralogy is similar to Ch 219. Rock Ch 58 is a similar type found as a band in pyroxene granulites and khondalitic rocks in a knoll a mile south of Umamanchori, 3 miles south-east of Vandalur railway station: its strongly perthitic potash felspar has refractive indices $\alpha$ 1·522, $\gamma$ 1·526 indicating a composition of $Or_{65}$ ($\pm$ 7 % Or).

*Garnetiferous pyroxene granulites of intermediate composition.* No garnetiferous rocks of this type are reported from the Madras area; specimen S.347 is the rock described by Groves (1935, p. 164) as a quartz–hypersthene–diorite, from Mt. Wati (Ote), West Nile District, Uganda, falling in the intermediate division of the Uganda charnockite series. It is a fairly coarse-grained rock with plagioclase of composition $An_{32}$ as the dominant light mineral: the quartz has undulose extinction and a few dusty inclusions, while the potash felspar is a microperthitic orthoclase. The dark minerals consist of approximately equal amounts of ferrohypersthene, greenish-yellow hornblende, sheaves and laths of brown biotite, and pink grains of garnet clouded with inclusions; the garnet generally occurs in association with iron ore and biotite and contains inclusions of biotite and quartz. The modal analysis of this rock as given in table I differs from that given by Groves (1935, p. 166) for material from the same hand specimen, the variation being accounted for by the inclusion of biotite in the new mode and also by the splitting up of the felspar into its components, which was facilitated by the sodium cobaltinitrite staining technique for potassium felspar (Chayes, 1952).

Rock V.2 from Fästningsberget, Varberg, Sweden, is from the rock mass described as 'intermediate charnockite' by Quensel (1951, pp.

247–51). It is a medium grained yellowish-brown rock, with traces of dark minerals in bands between the olive-green felspars. Strongly antiperthitic plagioclase of composition $An_{25-28}$ is accompanied by almost non-perthitic intermediate microcline and lesser amounts of quartz. Moderately pleochroic iron-rich orthopyroxene (table VI) is the most abundant dark mineral and occurs with hornblende, clinopyroxene, ilmenite, and magnetite, together with minor zircon and fluor-apatite.

Specimen 68671 from the roadside at 21/5 culvert, Hatton, Ceylon (cf. Adams, 1929, p. 470), is a typical dark pyroxene granulite, with a few red garnets visible in hand specimen. Under the microscope quartz and antiperthite (sodic andesine) are abundant and are accompanied by moderately pleochroic ferrohypersthene and hornblende, weakly pleochroic augite, pink garnet, and lesser amounts of iron ore and apatite.

*Basic garnetiferous granulites.* Rock Ch 199 is a basic two-pyroxene granulite or garnetiferous 'norite' from Paravatta Hill, Pallavaram, and is a medium-grained dark rock showing occasional patches of red garnet and greenish-yellow felspar. In thin section the plagioclase is clear and fresh, the $\alpha$ index 1·565 $\pm$ 0·001 indicating a composition in the range $An_{65-70}$. Light green weakly pleochroic augite showing salite structure is the commoner pyroxene and has $\alpha$ 1·705, $\beta$ 1·714, $\gamma$ 1·735 (all $\pm$ 0·001), $2V_\gamma$ 49°$\pm$1°, absorption $\alpha < \beta < \gamma$: the less abundant ferrohypersthene (table VI) is only weakly pleochroic ($\alpha$ pale pink, $\beta$ yellowish pink, $\gamma$ light green). A yellowish-brown hornblende occurs in embayed grains often intimately associated with the pyroxenes: it is strongly pleochroic with $\alpha$ pale yellow, $\beta$ pale brown, $\gamma$ deep brown and has $\alpha$ 1·670, $\beta$ 1·685, $\gamma$ 1·693 (all $\pm$0·001). Garnet occurs in large pink grains of irregular outline poikiloblastically enclosing the other dark minerals (pl. XVIII, figs. 3 and 4) and sometimes also plagioclase: iron ore and reddish biotite are the accessories.

Specimen Ch 200 occurs as lenses and thin layers in the garnetiferous pyroxene granulite (Ch 199) and is light-coloured, with garnets and green pyroxene appearing in a carbonate base. The pyroxene is in the hedenbergite range $\alpha$ 1·714, $\gamma$ 1·744 (both $\pm$0.001), $2V_\gamma$ 60°$\pm$1°, $\gamma$: [001] 44°$\pm$1°, absorption $\alpha < \beta < \gamma$, and in thin section other minerals visible are garnet, sphene, calcite, apatite, plagioclase ($An_{75-90}$), and scapolite: the latter has $\epsilon$ 1·561, $\omega$ 1·596 ($\pm$0·001) indicating a composition of $Me_{80-85}$.

Specimen V.1 from Högahalla quarry, Träslövsläge, Varberg, is described as a 'basic charnockite' by Quensel (1951, pp. 239–46), and is a massive fine-grained dark rock with a granular texture. The felspar

is a moderately antiperthitic andesine, the composition of the plagioclase phase from optics being $An_{35}$, the most common composition in the charnockite series. The dark minerals include a green pleochroic clinopyroxene, strongly pleochroic hypersthene, pink garnet with inclusions of quartz and felspar, yellowish to green-brown hornblende, brown biotite, magnetite, and ilmenite; a few grains of apatite also occur.

*Garnetiferous leptynite.* Rock 3708 (G.S.I. 9·665), the garnetiferous leptynite from Pallavaram, has already been described by Holland (1900, p. 173, pl. XV) and by Howie (1955). In hand specimen it is greyish white in colour sprinkled with red garnets. In thin section strained quartz crystals can be seen to occur among small grains of microcline microperthite ($Or_{80\cdot7}Ab_{17\cdot9}An_{1\cdot4}$): orthopyroxene is absent, pink anhedral garnets being the main ferro-magnesian mineral; small amounts of both ilmenite and magnetite are also present. Holland considered this rock to represent a dynamically metamorphosed charnockite.

*Khondalites.* Specimen Ch 119 is a khondalite from the northern end of Pachaimalai hill 360, south-west of Chromepet railway station: it is buff-coloured and schistose with abundant brownish garnet and visible aggregates of sillimanite. In thin section quartz is seen to form more than half the rock, occurring in large grains with undulose extinction, hair-like inclusions, and sutured margins: the potash felspar is a microperthite. Garnet occurs as subhedral crystals and ragged grains occasionally forming 'atolls': inclusions of quartz, plagioclase, ores, green spinel, biotite, and sillimanite may be seen. Elsewhere the sillimanite forms elongated prisms with a preferred orientation and is closely associated with the garnets: green spinel is also found bordering the garnets.

Ch 121 is a recrystallized khondalite from a small knoll south of Oddapalaiyam, one mile south-west of Pallavaram railway station: it represents a recrystallized facies of the normal khondalite and occurs near typical charnockite. The rock is medium-grained and greyish with rose-coloured garnet porphyroblasts and in thin section shows a mosaic of granulated quartz and subordinate perthite in which irregular grains of garnet are scattered. The felspar shows incipient cross-hatching and its refractive indices $\alpha$ 1·521, $\gamma$ 1·525 indicate a composition of $Or_{80}$ ($\pm 7$ % Or): a small amount of plagioclase ($An_{25}$) sometimes rims the larger perthite plates. Sillimanite occurs as prismatic crystals, and other minerals include brown biotite, iron ores, and a minor amount of iron-rich amphibole.

*The chemistry of the rocks.*

Analyses of seven of the Madras rocks together with those of the Uganda and Varberg rocks are given in table I, where the C.I.P.W. norms and volume percentage modes are also listed. Modal analyses were carried out by the point-counting method, 15 000 points being determined for specimens Ch 113 and 219 which were rather variable in mineral composition, while 4 000 to 5 000 points were determined on the remaining rocks.

The garnetiferous enderbites are relatively poor in silica compared with normal charnockites, while alumina is fairly high, bringing in appreciable amounts of corundum to the norm. The enderbitic nature of these rocks is not very pronounced as the potash values remain above 2 %. The $Fe_2O_3/FeO$ ratio is low, being less than 0·3 compared with an average value of 0·88 for 546 granites (Goldschmidt, 1954, p. 37); indeed this value is low throughout these Indian rocks, suggesting high temperature metamorphism (Goldschmidt, loc. cit.), or a magma deficient in water, allowing the reduction of ferric iron to ferrous iron to take place. In the basic garnetiferous pyroxene-granulite (Ch 199), although $SiO_2$ is low, both the FeO/MgO ratio and the CaO content are rather high. The khondalitic rocks (Ch 119 and 121) are both very high in $SiO_2$ with more than 50 % modal quartz, the greater alkali content of Ch 121 being reflected in the development of a considerable amount of potash felspar. Ch 119 is richer in FeO and also has a higher FeO/MgO ratio, and, as will be seen later, its garnet has a higher FeO/MgO ratio than that from Ch 121. The Uganda intermediate rock S.347 is rather similar chemically to V.2 from Varberg, and both could be compared with intermediate non-garnetiferous rocks from the Madras charnockite series (Howie, 1955): the $Fe_2O_3/FeO$ ratio is particularly low in the Uganda rock. The basic granulite from Varberg (V.1) resembles chemically the Madras rock of this type (Ch 199), the greater amount of $K_2O$ in the Varberg specimen being reflected in the noticeably antiperthitic plagioclase. In general all these rocks are rather high in alumina, and the iron oxides are also high with ferrous oxide greatly in excess of ferric oxide. Total alkalis are found in normal amounts in the charnockitic rocks, although they are low in the khondalites and leptynite. Soda is almost always in excess of potash in the orthopyroxene granulites.

*Mineralogy.*

The garnets and orthopyroxenes were initially concentrated to above 90 % purity with the aid of an isodynamic separator and final purification

TABLE I. Chemical analyses, CIPW norms, and modes of garnetiferous enderbites, pyroxene-granulites, and associated rocks.

| | 56. | Ch 113. | Ch 219. | Ch 199. | Ch 121. | Ch 119. | 3708. | S.347. | V.2. | V.1. |
|---|---|---|---|---|---|---|---|---|---|---|
| $SiO_2$ | 64·18 | 65·95 | 67·49 | 47·71 | 81·08 | 75·88 | 77·93 | 60·45 | 60·12 | 45·00 |
| $TiO_2$ | 1·12 | 0·99 | 0·54 | 0·97 | 0·52 | 0·58 | 0·31 | 1·50 | 0·95 | 2·40 |
| $Al_2O_3$ | 16·40 | 15·27 | 16·13 | 15·57 | 9·88 | 11·03 | 10·65 | 17·56 | 16·63 | 16·62 |
| $Fe_2O_3$ | 0·95 | 1·12 | 1·14 | 2·31 | 0·57 | 2·46 | 0·99 | 0·62 | 2·19 | 6·05 |
| FeO | 5·21 | 4·86 | 4·47 | 10·85 | 2·33 | 6·27 | 2·50 | 5·77 | 4·79 | 8·97 |
| MnO | 0·07 | 0·22 | 0·12 | 0·38 | 0·00 | 0·11 | 0·04 | 0·10 | 0·10 | 0·31 |
| MgO | 2·41 | 2·70 | 1·60 | 7·24 | 1·16 | 1·51 | 0·18 | 1·60 | 0·82 | 7·24 |
| CaO | 3·26 | 2·95 | 3·44 | 11·52 | 0·42 | 0·18 | 0·40 | 4·72 | 3·75 | 9·50 |
| $Na_2O$ | 3·64 | 3·74 | 3·13 | 2·07 | 1·26 | 0·59 | 2·19 | 3·75 | 4·73 | 2·76 |
| $K_2O$ | 2·52 | 2·06 | 1·47 | 0·42 | 2·22 | 0·11 | 4·54 | 2·45 | 4·25 | 0·96 |
| $H_2O+$ | 0·14 | 0·25 | 0·27 | 1·11 | 0·49 | 0·85 | 0·08 | 0·75 | 0·25 | 0·16 |
| $H_2O-$ | 0·28 | 0·20 | 0·40 | 0·07 | 0·14 | 0·17 | 0·16 | 0·53 | — | 0·06 |
| $P_2O_5$ | 0·08 | tr. | 0·04 | 0·12 | 0·03 | 0·03 | tr. | 0·31 | 0·77 | 0·00 |
| Total | 100·26 | 100·31 | 100·24 | 100·34 | 100·10 | 99·77 | 99·97 | 100·36 | 99·56 | 100·03 |
| | | | | *C.I.P.W. Norms.* | | | | | | |
| Q | 19·74 | 22·92 | 30·97 | — | 61·68 | 65·28 | 45·48 | 13·88 | 7·26 | — |
| or | 14·85 | 12·23 | 8·67 | 2·25 | 12·79 | 0·56 | 26·69 | 15·01 | 25·02 | 5·59 |
| ab | 30·79 | 31·44 | 26·46 | 17·82 | 10·48 | 5·24 | 18·34 | 31·44 | 39·82 | 22·25 |
| an | 15·71 | 14·73 | 16·76 | 31·97 | 1·95 | 1·11 | 1·95 | 21·78 | 11·68 | 30·07 |
| C | 1·92 | 1·53 | 3·24 | — | 4·79 | 9·38 | 1·43 | 0·64 | — | (ne)·70 |
| di | — | — | — | 21·00 | — | — | — | — | 1·89 | 13·67 |
| hy | 13·05 | 13·53 | 10·60 | 8·89 | 5·80 | 12·38 | 4·28 | 11·66 | 6·68 | — |
| ol | — | — | — | 12·89 | — | — | — | — | — | 14·20 |
| mt | 1·37 | 1·62 | 1·64 | 3·25 | 0·93 | 3·71 | 1·39 | 0·93 | 3·25 | 8·77 |
| il | 2·14 | 1·98 | 1·03 | 1·98 | 0·91 | 1·22 | 0·61 | 2·89 | 1·82 | 4·56 |
| ap | 0·19 | — | 0·10 | 0·29 | 0·07 | 0·07 | — | 0·67 | 1·68 | — |
| | | | | *Modes (vol. %).* | | | | | | |
| Quartz | 20·6 | 23·8 | 39·4 | — | 52·9 | 53·7 | 53·4 | 14·3 | 14·7 | — |
| K-felspar | 20·8 | 16·3 | 16·8 | — | 24·3 | 7·4 | 40·5 | 21·3 | 23·4 | — |
| Plagioclase | 40·2 | 32·2 | 25·5 | 37·5 | — | — | 2·1 | 43·6 | 41·0 | 34·8 |
| Orthopyroxene | 9·7 | 12·3 | — | 6·4 | — | — | — | 3·9 | 6·8 | 9·1 |
| Clinopyroxene | — | tr. | — | 24·8 | — | — | — | 1·9 | 3·2 | 25·5 |
| Garnet | 5·8 | 12·6 | 16·1 | 8·6 | 13·5 | 27·6 | 2·9 | 4·0 | 2·8 | 13·2 |
| Hornblende | — | — | — | 20·0 | — | — | — | 4·3 | 3·0 | 7·5 |
| Biotite | 0·9 | 1·0 | 1·1 | — | 4·6 | — | — | 4·0 | — | 4·6 |
| Sillimanite | — | — | — | — | 4·2 | 8·9 | — | — | — | — |
| Apatite & Zircon | 0·3 | 0·7 | 0·3 | — | — | — | — | 0·4 | 0·9 | 0·1 |
| Ores | 1·7 | 1·1 | 1·1 | 2·7 | 0·5 | 0·6 | 1·1 | 2·3 | 4·2 | 5·2 |
| Green Spinel | — | — | — | — | — | 1·8 | — | — | — | — |
| *D* | 2·66 | 2·84 | 2·77 | 3·10 | 2·77 | 2·87 | 2·67 | 2·74 | 2·77 | 3·19 |

56 Garnetiferous enderbite, Pallavaram. Anal. R. A. Howie.

Ch 113 Garnetiferous enderbite, west of Hasanapuram quarry, south of Pallavaram, Madras. Anal: T. Katsura, Tokyo. ($K_2O$, $Na_2O$, $H_2O+$, and $H_2O-$ by R. A. Howie.)

Ch 219 Garnetiferous granulite, Tattan Kunnu quarry, between the two rifle ranges, south of Minambakkam Railway station. Anal. R. A. Howie.

Ch 199 Basic granulite ('norite'), summit of Paravatta Hill, south of Mosque Hill, Pallavaram. Anal. T. Katsura, Tokyo.

Ch 121 Recrystallized khondalite, near contact with charnockite, south of Oddapalaiyam. Anal. T. Katsura, Tokyo.

Ch 119 Khondalite, northern end of Pachaimalai hill 360. Anal. T. Katsura, Tokyo.

3708 Garnetiferous leptynite (G.S.I. 9·665, Holland, 1900, p. 173), Pallavaram. Anal. R. A. Howie (Howie, 1955).

S. 347 'Quartz–hypersthene–diorite', Mt. Wati (Ote), West Nile district, Uganda. (Anal. also shows $ZrO_2$ 0·01, BaO 0·18, S 0·09.) Anal. A. W. Groves (Groves, 1935).

V.2 'Intermediate charnockite', Fästningsberget, Varberg, Sweden (with BaO 0·21). Anal. R. Mauzelius (Quensel, 1951).

V.1 'Basic charnockite', Högahalla quarry, Träslövsläge, Varberg. Anal. N. Sahlbom (Quensel, 1951).

was accomplished by use of Clerici's solution. The garnets in many cases had to be ground to pass a 300-mesh sieve to release quartz or sillimanite inclusions. Refractive indices were measured in sodium light with an estimated accuracy of $\pm 0{\cdot}001$ for the orthopyroxenes and $\pm 0{\cdot}004$ for the garnets. Normal analytical techniques were used, special care being taken over the determination of FeO and MnO. For the estimation of ferrous iron in the garnets samples that had been particularly finely ground were taken, and using the normal Pratt method the acid attack was continued for up to 25 minutes, the operation being repeated until consistent results were obtained. Susceptibility to attack varied, some garnets going into solution relatively easily: but in the analysis of the garnet from the recrystallized khondalite (Ch 121) the FeO determination was repeated eight times before consistent values resulted. In the estimation of MnO, MnO was looked for in both the calcium and magnesium precipitates as well as in the $R_2O_3$ portion.

The cell sizes of the garnets were measured using a 9-cm. diameter powder camera with Mn-filtered Fe-$K\alpha$ radiation; the accuracy is estimated to be $\pm 0{\cdot}002$ Å. Specific gravities were determined in a pycnometer, the final reading being taken after several preliminary checks over 24 hours to eliminate trapped air bubbles: the accuracy is probably better than $\pm 0{\cdot}03$. In tables II and III the calculated physical properties are also given, using the values for synthetic end-member garnets (Skinner, 1956). The agreement for cell size and refractive index is generally fair, but the correlation for specific gravity is poor except in the two cases where more than about 2 g. of the purified mineral powder was used (3708 and S.347): otherwise the observed values are low with respect to the theoretical values, part of the reason being the small amount of material used for the determination and its more than usually fine grain size. The refractive indices and cell sizes of unanalysed garnets are given in table IV. The trace-element contents of the nine analysed garnets have been determined by Dr. S. R. Nockolds and Mr. R. S. Allen: their results are given in table V.

*The garnets.* In all the rocks the garnet is well crystallized in subhedral grains, faintly pink in thin section, fresh in appearance and often containing a few pools of quartz and occasionally felspar and biotite, or, in khondalite, inclusions of green spinel and sillimanite. In all the garnets now examined the dominant 'molecule' is almandine, though an analysis by Groves (1935) of a garnet from 'dynamo-metamorphosed charnockite' showed a very high proportion of pyrope (table III, G.79). Analyses of Madras garnets are presented in table II: their structural

TABLE II. Chemical analyses and physical properties of Madras garnets.

| | Ch 113. | Ch 219. | Ch 199. | Ch 121. | Ch 119. | 3708. | J.1. |
|---|---|---|---|---|---|---|---|
| $SiO_2$ | 38·02 | 38·35 | 37·65 | 39·21 | 38·51 | 37·20 | 36·20 |
| $TiO_2$ | 0·03 | 0·08 | 0·04 | 0·11 | 0·03 | 0·07 | 1·04 |
| $Al_2O_3$ | 21·02 | 21·10 | 20·87 | 22·42 | 22·10 | 21·75 | 26·26 |
| $Fe_2O_3$ | 1·98 | 1·50 | 1·87 | 0·85 | 0·93 | 0·71 | 0·88 |
| FeO | 28·12 | 28·48 | 27·65 | 25·20 | 27·92 | 33·30 | 26·46 |
| MnO | 0·64 | 0·71 | 1·10 | 0·32 | 0·15 | 0·74 | 0·42 |
| MgO | 7·87 | 7·93 | 3·74 | 11·38 | 9·50 | 4·82 | 5·60 |
| CaO | 2·25 | 2·04 | 7·16 | 0·77 | 0·81 | 1·58 | 2·42 |
| $Na_2O$ | 0·11 | 0·01 | 0·09 | tr. | 0·04 | n.d. | 0·06 |
| $K_2O$ | 0·01 | 0·04 | 0·02 | 0·04 | 0·00 | n.d. | 0·41 |
| $H_2O+$ | n.d. | n.d. | n.d. | 0·02 | 0·04 | n.d. | 0·18 |
| $H_2O-$ | 0·09 | 0·02 | 0·02 | 0·03 | 0·05 | 0·09 | 0·01 |
| Total | 100·14 | 100·26 | 100·21 | 100·35 | 100·08 | 100·26 | 100·01 |
| *Percentage composition in terms of garnet end-member molecules* | | | | | | | |
| Almandine | 65·3 | 66·0 | 64·5 | 58·5 | 64·9 | 77·6 | 66·3 |
| Andradite | 6·6 | 4·8 | 5·7 | 2·7 | 2·6 | 2·5 | — |
| Grossular | 0·3 | 1·2 | 14·6 | — | — | 2·0 | 7·8 |
| Pyrope | 26·3 | 26·4 | 12·7 | 38·0 | 32·1 | 16·3 | 25·0 |
| Spessartine | 1·5 | 1·6 | 2·5 | 0·8 | 0·4 | 1·6 | 0·9 |
| *Observed physical properties* | | | | | | | |
| $n$ | 1·796 | 1·800 | 1·800 | 1·788 | 1·794 | 1·806 | 1·795 |
| $a$(Å.) | 11·528 | 11·529 | 11·594 | 11·507 | 11·509 | 11·541 | |
| $D$ | 3·99 | 4·02 | 4·01 | 3·99 | 4·02 | 4·17 | 4·14 |
| *Calculated physical properties using values for synthetic end-members* | | | | | | | |
| $n$ | 1·801 | 1·801 | 1·804 | 1·786 | 1·795 | 1·810 | 1·792 |
| $a$(Å.) | 11·544 | 11·541 | 11·600 | 11·526 | 11·507 | 11·538 | |
| $D$ | 4·09 | 4·09 | 4·09 | 4·02 | 4·04 | 4·17 | 4·08 |

Ch 113 Garnet from garnetiferous enderbite.
Ch 219 Garnet from garnetiferous granulite.
Ch 199 Garnet from basic orthopyroxene granulite.
Ch 121 Garnet from recrystallized khondalite.
Ch 119 Garnet from khondalite.
3708 Garnet from garnetiferous leptynite (Howie, 1955, table VI).
J.1 Garnet from 'leptite' (Naidu, 1955). Anal. H. Schwander. (Anal. includes 0·07 $P_2O_5$.)

All are from Pallavaram type area: for detailed localities see table I. Anal. except for J.1, R. A. Howie.

formulae on the basis of 12 oxygen ions (table VII) show that in general they conform fairly closely with the theoretical ratio of 3:2:3 for the $R''$, $R'''$, and $z$ groups in the garnet series, although the $R'''$ group is always very slightly greater than 2, probably indicating that the ferric iron has been overestimated.

TABLE III. Chemical analyses and physical properties of granulite garnets from outside India.

| | S.347. | G.79. | V.1. | V.2. | A. | 9. | 13. |
|---|---|---|---|---|---|---|---|
| $SiO_2$ | 38·10 | 39·55 | 37·85 | 37·33 | 36·70 | 36·35 | 37·19 |
| $TiO_2$ | 0·19 | 0·21 | 0·03 | 0·02 | 0·00 | 1·72 | 0·38 |
| $Al_2O_3$ | 20·76 | 17·67 | 21·06 | 20·96 | 16·58 | 22·97 | 21·02 |
| $Fe_2O_3$ | 1·56 | 7·39 | 1·40 | 0·68 | 12·72 | — | 1·28 |
| FeO | 28·54 | 17·93 | 26·79 | 30·58 | 20·70 | 24·72 | 28·61 |
| MnO | 1·32 | 0·46 | 0·86 | 2·19 | 3·00 | 0·64 | 0·93 |
| MgO | 3·12 | 14·66 | 4·94 | 1·25 | 2·73 | 11·80 | 3·08 |
| CaO | 6·70 | 2·07 | 7·20 | 7·05 | 7·00 | 1·87 | 7·41 |
| $Na_2O$ | n.d. | n.d. | 0·03 | 0·03 | 0·03 | — | 0·02 |
| $K_2O$ | n.d. | n.d. | 0·00 | 0·00 | 0·11 | — | 0·09 |
| $H_2O+$ | n.d. | n.d. | n.d. | n.d. | 0·68 | — | 0·16 |
| $H_2O-$ | 0·03 | n.d. | 0·03 | 0·03 | 0·00 | — | 0·00 |
| Total | 100·32 | 99·94 | 100·19 | 100·12 | 100·25 | 100·07 | 100·17 |
| *Percentage composition in terms of garnet end-member molecules* | | | | | | | |
| Almandine | 67·1 | 42·3 | 61·7 | 71·3 | | 55·6 | 67·0 |
| Andradite | 6·2 | 6·6 | 4·5 | 2·0 | | — | 4·1 |
| Grossular | 12·8 | — | 15·4 | 17·3 | | 4·8 | 16·4 |
| Pyrope | 10·7 | 50·0 | 16·4 | 4·2 | | 38·2 | 10·5 |
| Spessartine | 3·2 | 1·0 | 2·0 | 5·2 | | 1·4 | 2·0 |
| *Observed physical properties* | | | | | | | |
| $n$ | 1·805 | | 1·794 | 1·808 | (1·808) | 1·76 | |
| $a$(Å.) | 11·597 | | 11·570 | 11·603 | | | |
| $D$ | 4·12 | | 3·98 | 4·13 | | 3·80 ± 0·04 | |
| *Calculated physical properties using values for synthetic end-members* | | | | | | | |
| $n$ | 1·803 | | 1·798 | 1·809 | | | |
| $a$(Å.) | 11·595 | | 11·591 | 11·596 | | | |
| $D$ | 4·11 | | 4·06 | 4·14 | | | |

S.347 Almandine garnet from 'Quartz-hypersthene–diorite', Uganda. Anal. R. A. Howie.

G.79 Garnet from 'dynamo-metamorphosed charnockite', Bunyoro district, Uganda (after recalculation free from 21·6 % normative quartz). Anal. A. W. Groves (1935).

V.1 Almandine garnet from 'basic charnockite', Högahalla quarry, Varberg, Sweden. Anal. R. A. Howie.

V.2 Almandine garnet from 'intermediate charnockite', Fästningsberget, Varberg. Anal. R. A. Howie.

A Garnet from 'intermediate charnockite', Fästingsberget, Varberg (Quensel, 1951). Anal. N. Sahlbom.

9 Garnet from basic hypersthene granulite, Kevuavdshi, Kevujoki, Lapland (Eskola, 1952). Anal. A. Huhma.

13 Almandine garnet from garnet–pyroxene–oligoclase granulite, one mile W. of Elizabethtown, Adirondacks (Buddington, 1952). Anal. L. C. Peck.

The garnets from the dark acid granulites (Ch 113 and 219) and that from the basic granulite (Ch 199) are rather similar in FeO and $Fe_2O_3$ content, their main compositional difference lying in the greater pyrope component of Ch 113 and 219 while Ch 199 has more grossular. In the corresponding orthopyroxenes that from Ch 113 is also richer in MgO

TABLE IV. Refractive index and cell-size of unanalysed garnets.

| | *Rock.* | *n.* | *a*(Å.). |
|---|---|---|---|
| Ch 44 | Acidic granulite, south of Pallavaram | 1·801 | 11·545 |
| Ch 58 | Acidic granulite, Pallavaram | 1·800 | 11·518 |
| 56 | Garnetiferous enderbite, Pallavaram | 1·802 | 11·520 |
| Ch 200 | Calc-granulite lens in Ch 199 | 1·790 | 11·675 |
| 68671 | Pyroxene granulite, Hatton, Ceylon | 1·798 | 11·592 |

TABLE V. Trace elements in the garnets of garnetiferous granulites (in parts per million).

| | *r*(Å.). | *s*. | V.1. | Ch 199. | V.2. | S.347. | Ch 113. | Ch 219. | 3708. | Ch 119. | Ch 121. |
|---|---|---|---|---|---|---|---|---|---|---|---|
| Ga | 0·62 | 1 | 10 | 10 | 12 | 50 | 10 | 15 | 40 | 15 | 10 |
| Cr | 0·63 | 2 | 45 | 450 | * | 25 | 450 | 450 | * | * | * |
| Li | 0·68 | 1 | 1 | * | 3 | 1 | 1 | 3 | 12 | 3 | 3 |
| Mo | 0·70 | 2 | * | * | * | * | * | * | 25 | * | * |
| Co | 0·72 | 5 | 30 | 45 | * | 15 | 30 | 30 | 5 | 5 | 5 |
| V | 0·74 | 5 | 40 | 220 | * | 65 | 140 | 220 | * | * | * |
| Zr | 0·79 | 10 | 40 | 50 | 125 | 30 | 60 | 50 | 120 | 120 | 120 |
| Sc | 0·81 | 10 | 100 | 40 | 10 | 200 | 100 | 150 | * | * | * |
| Y | 0·92 | 15 | 140 | 150 | 1000 | 60 | 1000 | 1000 | 600 | 350 | 450 |
| Pb | 1·20 | 10 | * | * | * | * | * | * | 40 | * | * |
| Ba | 1·34 | 10 | * | * | * | 20 | * | * | * | * | * |

For details and localities see foot of tables I–III.

An asterisk denotes that the element, if present, was in an amount below the limit of sensitivity (*s*). *r* = the ionic radius of the element for sixfold coordination. Ni (2), Sn (10), Sr (10), Rb (5), and La (50) below limits of sensitivity (given in brackets) in all cases. (The values for 3708 are from Howie, 1955, table VII.)

while the rock analyses show that the MgO/FeO ratio is lower in Ch 113. Thus the distribution of calcium appears to be a controlling factor: in the acid rock the CaO content of the rock is low while in Ch 199 it is higher and the CaO/MgO ratio is also higher, so that much of the MgO is taken into the high modal percentage of augite and hornblende.

The garnets from the khondalites (Ch 119 and 121) contain relatively little calcium, reflecting the composition of their parent rocks: the difference in the chemistry of the rocks is shown in the FeO/MgO ratios of the garnets, that of the garnet from the recrystallized khondalite (Ch 121) being the lower. S. V. L. N. Rao (1955) gives an analysis of a garnet from a garnetiferous gneiss (khondalite) from Vizagapatam district with 77 % almandine, and quotes another from Kondapalli with

65·7 % of the almandine molecule, while Fermor (1926) computed the composition of a khondalite garnet from Kalahandi, knowing the composition of the rock, and estimated it to be 78·8 % almandine (assuming all the iron to be in the ferrous condition). The garnet of the garnetiferous leptynite (3708) was the most iron-rich in the present investigation with 77·6 % of the almandine molecule, it being the only ferromagnesian mineral in the rock. Naidu (1955) reports a garnet from a 'leptite' at Pallavaram (table II, J.1) with 66·3 % almandine,[1] the modal composition of the rock showing almost four times as much iron ore as in 3708. Other analyses of garnets from leptynites are given by S. V. L. N. Rao (1955), showing lower iron contents, but as no details are given of the rocks themselves they will not be discussed here.

Three new analyses of garnets from orthopyroxene granulites from Uganda and Varberg are given in table III, together with earlier analyses from both these localities and from other granulite areas in Lapland and the Adirondacks. The garnet from the 'intermediate charnockite' of Groves (S.347) is again fairly rich in iron with 67 % of the almandine molecule: it has a FeO/MgO ratio greater than that of its parent rock (table I) and much greater than that of the coexisting orthopyroxene (table VI), clinopyroxene, hornblende, or biotite.[2] The garnet G.79 is much richer in MgO and is from a charnockite which Groves considered to have suffered subsequent dynamo-metamorphism, the garnet being considered to be derived directly from orthopyroxene with the setting free of the quartz, which occurs as inclusions. In the original description of this garnet (Groves, 1935, p. 160) the percentage composition is wrongly stated in terms of the end-member molecules, and has since been quoted thus elsewhere: the corrected values (Groves, 1952, personal communication) are as given in table III.

The garnets from the two Varberg rocks are again fairly rich in iron, and like the Uganda and Madras examples they have a considerably higher FeO/MgO ratio than either their parent rocks or their coexisting orthopyroxenes. That of V.2, the more acid rock, is richer in the almandine molecule, although for a rock with only 45 % $SiO_2$ the V.1 garnet with 61·7 % almandine is still very rich in iron. Analysis A (table III) is of a garnet described by Quensel (1951, p. 251) from the same mass at Fästningsberget as V.2; the essential difference is in the ferrous iron

[1] In table II Naidu's values for the standard molecules for this garnet are quoted, but on recalculation FeO and $SiO_2$ are in considerable excess.

[2] Analyses of the clinopyroxene and hornblende from this rock were given by Groves (1935); the biotite has an FeO/MgO ratio of 2·26 (Howie, unpublished data).

content: the high $Fe_2O_3$ of analysis A prohibits the recalculation into normal end-member garnet molecules, as there is insufficient CaO to form andradite. Analyses 9 and 13 are of garnets from garnetiferous pyroxene granulites from Lapland (Eskola, 1952) and from the Adirondack metagabbro area (Buddington, 1952) respectively: as before the FeO/MgO ratios of the garnets are very much greater than those of the parent rocks, and in the Lapland example greater than the FeO/MgO ratio for the orthopyroxene (Eskola, 1952, p. 152).

The trace-element contents of the nine analysed garnets are given in table V. Yttrium is almost certainly being captured by manganese rather than by calcium: in garnets V.1 and V.2, for example, the yttrium content is very much larger in V.2, while the calcium values are almost identical. Lithium is probably being concentrated with respect to magnesium: scandium is rather variable, and although nickel is not present in appreciable amounts cobalt does occur and is probably camouflaged by iron. Chromium and vanadium are noticeably low in those garnets low in ferric iron. In general the garnets from the three light-coloured acidic granulites, 3708, Ch 119, and Ch 121, can be seen to have a different trace-element assemblage. On the other hand the garnets from Ch 113 and Ch 219 have an almost identical major and trace-element composition, and although both rocks have a dark aspect in hand specimen only Ch 113 carries appreciable orthopyroxene.

*The orthopyroxenes.* The analyses and properties of five orthopyroxenes from garnetiferous charnockites and pyroxene granulites are given in table VI, and their structural formulae on the basis of 12 oxygen atoms are shown in table VII. They range from 50·5 to 25·2 % enstatite, the most magnesian being from the most acid rock, the Madras garnetiferous enderbite Ch 113. The content of alumina is moderate except in Ch 113, where it rises to 4·08 %, perhaps an expression of the aluminous nature of the parent rock which has over 1·5% normative corundum: this amount of alumina, however, is not much greater than that found in orthopyroxenes of non-garnetiferous rocks of the charnockite series (Howie, 1955, p. 754), and greater amounts are known from orthopyroxenes of other basic granulites (Eskola, 1952, p. 152, and Howie, unpublished data). The MnO content of the orthopyroxenes is always just less than half that of the coexisting garnets and is greatest in the most iron-rich orthopyroxene, the eulite from the Varberg garnetiferous pyroxene-granulite V.2. The optical properties of the orthopyroxene from the same rock mass as V.1 indicate a composition of 52 % enstatite (Quensel, 1951, p. 241); those for orthopyroxene from

an 'intermediate charnockite' give a composition of 25 % enstatite, which compares well with the analytical result for V.2 orthopyroxene (26 % En). From analysis, the orthopyroxene coexisting with garnet 9 from Lapland has 62 % enstatite (Eskola, 1952). All the orthopyroxenes are very distinctly pleochroic, that from Ch 113 having the strongest

TABLE VI. Chemical analyses and physical properties of orthopyroxenes from garnetiferous granulites.

| | Ch 113. | Ch 199. | 68671. | S.347. | V.2. |
|---|---|---|---|---|---|
| $SiO_2$ | 50·05 | 49·28 | 49·73 | 49·48 | 47·33 |
| $TiO_2$ | 0·30 | 0·17 | 0·11 | 0·13 | 0·29 |
| $Al_2O_3$ | 4·08 | 2·09 | 1·96 | 1·77 | 1·37 |
| $Fe_2O_3$ | 0·68 | 0·98 | 1·72 | 1·84 | 1·09 |
| FeO | 27·50 | 32·01 | 29·64 | 31·56 | 39·41 |
| MnO | 0·27 | 0·47 | 0·53 | 0·49 | 0·94 |
| MgO | 16·51 | 13·32 | 14·66 | 14·25 | 8·02 |
| CaO | 0·46 | 1·38 | 1·24 | 0·80 | 1·25 |
| $Na_2O$ | 0·09 | 0·06 | 0·10 | 0·01 | 0·05 |
| $K_2O$ | 0·03 | 0·01 | 0·01 | tr. | 0·01 |
| $H_2O+$ | 0·02 | n.d. | 0·04 | 0·02 | 0·07 |
| $H_2O-$ | 0·11 | 0·04 | 0·11 | 0·04 | 0·23 |
| Total | 100·10 | 99·81 | 99·85 | 100·39 | 100·06 |
| | | *Atomic percentages.* | | | |
| Fe | 48·5 | 56·6 | 53·4 | 54·2 | 72·0 |
| Mg | 50·5 | 40·5 | 44·1 | 44·1 | 25·2 |
| Ca | 1·0 | 2·9 | 2·6 | 1·7 | 2·8 |
| $\gamma$ | 1·728 | 1·734 | 1·732 | 1·733 | 1·758 |
| $2V_\alpha$ | | | 52° | 54° | 66° |
| $D$ | 3·58 | 3·62 | 3·63 | 3·60 | 3·75 |

Anal. R. A. Howie.

Ch 113 Hypersthene from garnetiferous enderbite, Pallavaram.
Ch 199 Ferrohypersthene from basic granulite ('norite'), Pallavaram.
68671 Ferrohypersthene from pyroxene granulite, Hatton, Ceylon.
S.347 Ferrohypersthene from 'quartz–hypersthene–diorite', Mt. Wati, West Nile district, Uganda.
V.2 Eulite from basic granulite ('intermediate charnockite'). Fästningsberget, Varberg.

pleochroism with $\alpha$ pinkish red, $\beta$ pink, $\gamma$ light green: thus in these granulite-facies orthopyroxenes under discussion the most strongly pleochroic also has the lowest content of both ferrous and ferric iron, contrary to the widespread but fallacious belief that the degree of pleochroism can be equated with iron content in this mineral series. The orthopyroxenes of these rocks almost invariably show straight extinction, and often have well-developed 'schiller' or microplakite inclusions of thin reddish-brown plates of unknown composition.

TABLE VII. Garnet and orthopyroxene analyses recalculated to show number of metal ions per 12(O).

| | *Garnets* | | | | | | | | *Orthopyroxenes* | | | | |
|---|---|---|---|---|---|---|---|---|---|---|---|---|---|
| | Ch 113. | Ch 219. | Ch 199. | Ch 121. | Ch 119. | S. 347. | V.1. | V.2. | Ch. 113. | Ch. 199. | 68671. | S. 347 | V.2. |
| Si | 2·968 | 2·982 | 2·978 | 2·970 | 2·974 | 3·009 | 2·978 | 3·002 | 3·835 | 3·891 | 3·890 | 3·879 | 3·898 |
| Al | 0·032 | 0·018 | 0·022 | 0·030 | 0·026 | — | 0·022 | — | 0·165 | 0·109 | 0·110 | 0·121 | 0·102 |
| Al | 1·898 | 1·918 | 1·912 | 1·972 | 1·978 | 1·934 | 1·928 | 1·981 | 0·203 | 0·091 | 0·069 | 0·041 | 0·030 |
| $Fe^{3}+$ | 0·120 | 0·088 | 0·111 | 0·048 | 0·046 | 0·085 | 0·085 | 0·038 | 0·037 | 0·057 | 0·103 | 0·108 | 0·069 |
| Ti | 0·004 | 0·005 | 0·002 | 0·006 | 0·001 | 0·012 | 0·002 | 0·003 | 0·018 | 0·009 | 0·004 | 0·008 | 0·020 |
| Mg | 0·913 | 0·920 | 0·443 | 1·286 | 1·091 | 0·371 | 0·578 | 0·148 | 1·885 | 1·565 | 1·708 | 1·674 | 0·984 |
| $Fe^{2}+$ | 1·835 | 1·853 | 1·833 | 1·598 | 1·801 | 1·886 | 1·759 | 2·059 | 1·757 | 2·109 | 1·935 | 2·059 | 2·708 |
| Mn | 0·042 | 0·047 | 0·071 | 0·020 | 0·010 | 0·090 | 0·057 | 0·150 | 0·018 | 0·033 | 0·035 | 0·033 | 0·065 |
| Na | 0·018 | 0·002 | 0·016 | — | 0·005 | — | 0·004 | 0·004 | 0·018 | 0·010 | 0·019 | 0·002 | 0·008 |
| Ca | 0·187 | 0·170 | 0·608 | 0·063 | 0·067 | 0·570 | 0·609 | 0·609 | 0·037 | 0·114 | 0·103 | 0·068 | 0·111 |
| K | 0·001 | 0·003 | 0·003 | 0·004 | — | — | — | — | 0·003 | 0·001 | 0·001 | — | 0·001 |
| *Z* | 3·00 | 3·00 | 3·00 | 3·00 | 3·00 | 3·01 | 3·00 | 3·00 | 4·00 | 4·00 | 4·00 | 4·00 | 4·00 |
| *Y* | 2·02 | 2·01 | 2·02 | 2·03 | 2·02 | 2·03 | 2·01 | 2·02 | } 3·98 | 3·99 | 3·98 | 3·99 | 4·00 |
| *X* | 2·99 | 3·00 | 2·97 | 2·97 | 2·97 | 2·92 | 3·01 | 2·97 | | | | | |

*Petrogenesis and conclusions.*

The compositions of the garnets under discussion in this paper together with the compositions of their host rocks are plotted in a ternary diagram (fig. 1) in which the molecular per cent. ratios (FeO+MnO), MgO, and CaO are represented at the corners. It can be seen that the

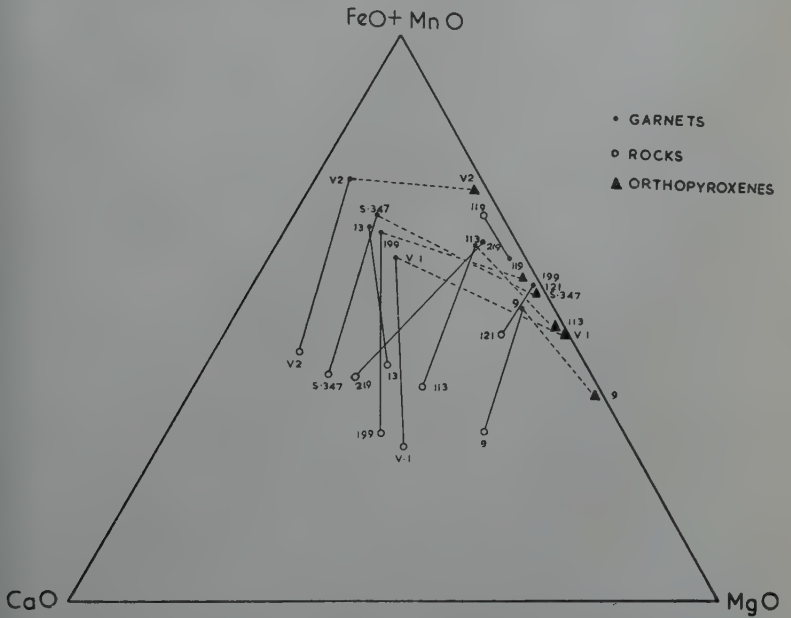


Fig. 1. (FeO+MnO), MgO, CaO molecular diagram showing the compositions of the orthopyroxenes, the garnets, and their host rocks.

(FeO+MnO)/MgO ratio in these garnets is considerably greater than in the equivalent host rocks: this relationship has previously been demonstrated by Buddington (1952) for the Adirondack gabbroic rocks, while Subramaniam (1956) has shown that a converse relationship holds good in the case of garnets in eclogites. The compositions of the coexisting orthopyroxenes are also plotted in fig. 1 and their (FeO+MnO)/MgO ratios are again seen to be considerably less than those of the garnets, being generally similar to the ratio for the host rocks. Many authors have suggested various chemical equations for the production of garnets in granulitic assemblages generally involving anorthite and spinel, corundum, or the ferromagnesian minerals (hornblende or augite or orthopyroxene). In these garnetiferous granulites, however, the (FeO+MnO)/

MgO ratio in the garnets is not only greater than that in the host rocks and the orthopyroxenes but also, as indicated by optics, greater than that in any other coexisting ferromagnesian mineral. Thus if the garnets did not form at the same time as the other minerals then their subsequent formation from pre-existing silicates must also have involved some iron-rich mineral such as magnetite or spinel, and have liberated a certain amount of silica. Evidence of the close relationship of the garnet with pyroxenes or spinel may be found in several of the rocks under discussion, although not in every section. In Ch 199, a basic pyroxene-granulite from Paravatta Hill, Pallavaram, in which both ortho- and clinopyroxenes occur together with garnet and iron ore (pl. XVIII, figs. 3 and 4), a crystal of garnet contiguous with clinopyroxene is seen enveloping magnetite. In the garnetiferous enderbites orthopyroxenes, garnets, and ore minerals are fairly closely associated (pl. XVIII, figs. 1 and 2), while in the khondalite garnet sometimes encloses green spinel. Pl. XVIII, fig. 5 is of a typically dark charnockite from the banks of the Kehelella Ela, 20 miles east-south-east of Kandy, Ceylon, with both ortho- and clinopyroxene, the latter being more abundant: here a rim of quartz can be seen between a large crystal of garnet and pyroxene. Ramanthan (1956, p. 149, sketch 4) also illustrates pyroxenes in contact with garnet, the latter containing quartz inclusions and also large grains of magnetite.

Eskola (1939) has defined the granulite facies as comprising rocks for which at basaltic bulk composition the association of hypersthene and plagioclase is typomorphic, while at granitic bulk composition quartz, felspars, and almandine-pyrope garnet occur. The garnetiferous granulites whose analyses are given here have been plotted on the appropriate ACF diagram (fig. 2), with the diopside–anorthite–orthopyroxene field extended slightly in its anorthite–orthopyroxene border to allow for the fairly considerable alumina content of the orthopyroxenes of this facies, indicated by the shaded area which covers the range 0 to 8 % $Al_2O_3$. The plots of the garnetiferous enderbites fall in the appropriate field for garnet and orthopyroxene-bearing rocks, while the non-garnetiferous charnockites plot in the anorthite–diopside–aluminous-orthopyroxene field close to the anorthite–orthopyroxene boundary (Howie, 1955, fig. 7). It has been suggested that garnet-free charnockites are unmetamorphosed igneous rocks whereas the presence of garnet in a charnockitic rock is an indication that the rock has been subjected to high-grade metamorphism. The chemical evidence given here indicates that the presence or absence of garnet in a charnockite is controlled only by the

chemical composition of the rock, the garnetiferous charnockites and enderbites being richer in $Al_2O_3+(FeO+MgO)$.

The khondalites plot well out into the alumina-rich field as would be expected from their modal sillimanite, while the leptynite and Ch 219,

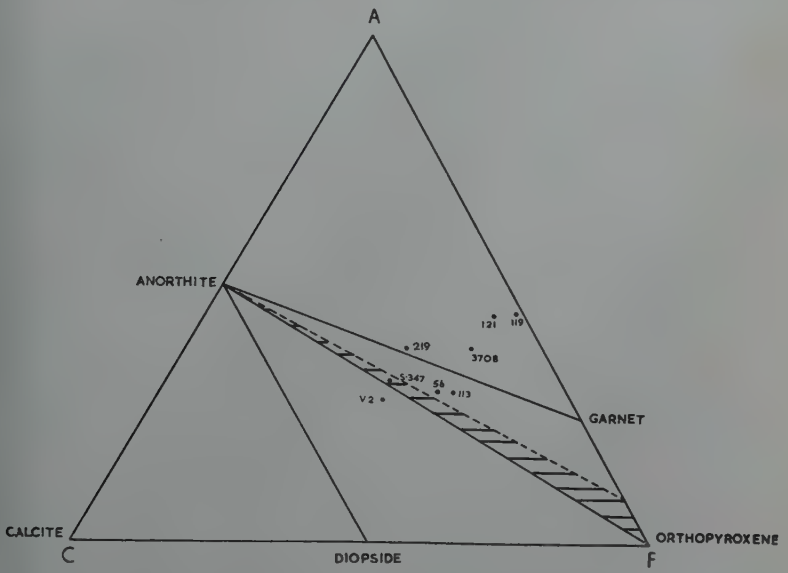


FIG. 2. ACF diagram for the garnetiferous granulites (granulite facies, with excess silica). 119, 121, 219, and 3708 are plots of garnetiferous granulites without orthopyroxene, 56 and 113 are of enderbites carrying garnet and orthopyroxene, while S.347 and V.2 are of more basic garnetiferous granulites containing both ortho- and clino-pyroxene.

the dark garnetiferous granulite without appreciable orthopyroxene, plot close to the garnet–anorthite border.

The intermediate rocks S.347 and V.2 have compositions lying in the anorthite–orthopyroxene–diopside field although both contain considerable garnet. That diopside and almandine-pyrope garnet cannot occur together in stable equilibrium in this facies is evident from the ACF diagram: thus these rocks, which contain free quartz and also both clinopyroxene and garnet in appreciable amounts (see table I), must be considered as being in a state of disequilibrium. The additional presence of hornblende in these rocks reaffirms this, as although there is evidence (Eskola, 1952) that brownish-green hornblende may exist alongside ortho- and clino-pyroxenes in the granulite facies, the assemblage

hornblende–orthopyroxene–almandine is an unstable one. Thus while in the more acid granulites and charnockites the mineralogical assemblage sillimanite–garnet–plagioclase or orthopyroxene–garnet–plagioclase is a typically stable one, in the more basic garnetiferous pyroxene granulites such as S.347 and V.2 the assemblage found is unstable.

It is not intended here to make more than a passing reference to some aspects of the petrogenesis of charnockites and associated rock types, but the new data now available may be of some significance. Holland (1900) and several later observers have considered the charnockite series as representing a genetically related group of rocks varying from basic to acid types: this conclusion is inconsistent with recent work on the field relationship, mineralogy, petrography, and chemistry of these rocks from the type area. Leaving aside the question of whether the series is an igneous one or whether it was originally igneous and has recrystallized under granulite facies conditions, if these rocks represent what was originally a differentiated igneous series derived from a common magma we should expect this to be reflected in the mineralogy of the various members of the series. In the present instance, however, for rocks around Pallavaram, the basic granulite Ch 199 carries an orthopyroxene of composition $En_{49 \cdot 5}$, while the acid garnetiferous enderbite Ch 113 has an orthopyroxene of composition $En_{50 \cdot 5}$, which is inconsistent with the accepted facts of mineral variation in a differentiation series where the basic members carry a magnesian orthopyroxene and the more acid members a progressively more iron-rich orthopyroxene. The garnets from these two rocks behave in the same way, the more basic rock having the more iron-rich garnet.

New chemical analyses of charnockitic rocks from the type area (56, Ch 113 and Ch 219) show a dominance of soda over potash, suggesting them to be akin to enderbites. The presence of enderbite in the Pallavaram area has already been indicated by Tilley (1936) and a chemical analysis is given by Howie (1955): recent field studies by one of us have, however, shown that enderbite is more prevalent in the type area than charnockite *sensu stricto*, and any theory on the petrogenesis of these rocks must be able to account for this fact. These and related problems on the type area will be discussed in a later communication.

*Acknowledgements.* The authors are grateful to Dr. S. R. Nockolds and Mr. R. S. Allen for carrying out the trace-element determinations on the analysed garnets, and to Prof. P. Quensel and the Geology Department of the Imperial College of Science and Technology for providing the specimens from Varberg and Uganda. One of us (A. P. S.) is grateful to Prof. C. E. Tilley for research facilities in the Department of Mineralogy and Petrology, to the Royal Society for the award of a

bursary enabling him to work at Cambridge, and to the Director, Geological Survey of India, for according permission to present these results. The other (R. A. H.) is grateful to Prof. W. A. Deer for his encouragement and advice and to Dr. W. S. MacKenzie for helpful criticism.

*References.*

Adams (F. D.), 1929. Canadian Journ. Research, vol. 1, pp. 425 and 467 [M.A. **4**–312].

Buddington (A. F.), 1950. Amer. Min., vol. 35, p. 659 [M.A. **11**–329].

—— 1952. Amer. Journ. Sci., Bowen vol., p. 37 [M.A. **12**–151].

Chayes (F.), 1952. Amer. Min., vol. 37, p. 337 [M.A. **12**–27].

Eskola (P.), 1939. Die Metamorphosen der Gesteine. In Barth (T. F. W.), Correns (C. W.), and Eskola (P.), Die Entstehung der Gesteine. Julius Springer, Berlin [M.A. **7**–367].

—— 1952. Amer. Journ. Sci., Bowen vol., p. 133 [M.A. **12**–152].

Fermor (L. L.), 1926. Rec. Geol. Surv. India, vol. 59, pt. 2, p. 191 [M.A. **3**–308].

Goldschmidt (V. M.), 1954. Geochemistry. Oxford (Clarendon Press) [M.A. **12**–295].

Groves (A. W.), 1935. Quart. Journ. Geol. Soc., vol. 91, p. 150.

Holland (T. H.), 1900. Mem. Geol. Surv. India, vol. 28, p. 119.

Howie (R. A.), 1955. Trans. Roy. Soc. Edin., vol. 62, p. 725 [M.A. **13**–351].

Muthuswami (T. N.), 1953. Proc. Indian Acad. Sci., vol. 37, p. 730 [M.A. **12**–272].

Naidu (P. R. J.), 1955. Schweiz. Min. Petr. Mitt., vol. 34, p. 204.

Narayanan (K.), Ramachandran (V.), and Sankaran (A. V.), 1955. Journ. Madras Univ., ser. B, vol. 25, p. 83.

Pichamuthu (C. S.), 1953. Mysore Geol. Assoc., Bangalore.

Quensel (P.), 1951. Arkiv Min. Geol., vol. 1, p. 227 [M.A. **11**–493].

Rajagopalan (C.), 1946 and 1947. Proc. Indian Acad. Sci., vol. 24, p. 315, and vol. 26, p. 237 [M.A. **10**–277].

Ramanthan (S.), 1956. Journ. Madras Univ., ser. B, vol. 26, p. 117.

Rao (N. Leelananda), 1955. Journ. Madras Univ., ser. B, vol. 25, p. 55.

Rao (S. V. L. N.), 1955. Quart. Journ. Geol. Mining Metall. Soc. India, vol. 27, p. 139.

Skinner (B. J.), 1956. Amer. Min., vol. 41, p. 428.

Subramaniam (A. P.), 1956. Bull. Geol. Soc. Amer., vol. 67, p. 317.

Tilley (C. E.), 1936. Geol. Mag., vol. 73, p. 312 [M.A. **7**–47].

Explanation of Plate XVIII. Photomicrographs of Madras and Ceylon granulites.

Fig. 1. Garnetiferous enderbite, Ch 113, Pallavaram, showing subhedral garnets (light) with small crystals of orthopyroxene (dark). ×6.

Fig. 2. Orthopyroxene–garnet–magnetite relationship in garnetiferous enderbite Ch 113. Note perthitic felspars also present. ×25.

Fig. 3. Basic pyroxene granulite Ch 199, Paravatta Hill, Pallavaram, showing granular texture. The large crystals are garnet. ×6.

Fig. 4. Pyroxene–garnet–magnetite relationship in Ch 199. Note the opaque core of magnetite and the clinopyroxene closely associated with the garnet and

magnetite. ×25 (nicols slightly moved from crossed position to distinguish between garnet and magnetite).

FIG. 5. Garnetiferous granulite, 20 miles east-south-east of Kandy, Ceylon, showing a rim of quartz in the north-west quadrant between a large crystal of garnet and crystals of ortho- and clinopyroxene: the orthopyroxene is slightly altered. ×20.

FIG. 6. Garnetiferous granulite Ch 219, Tattan Kunnu quarry, Pallavaram, showing development of myrmekite against large grains of perthite. Crossed nicols. ×25.

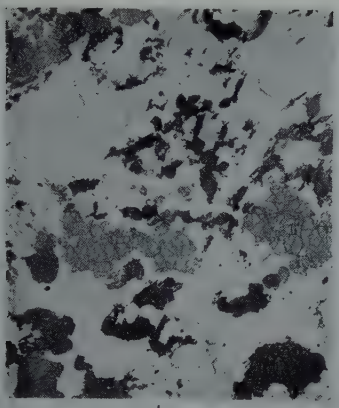

1

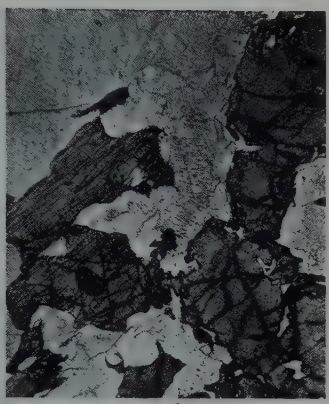

2

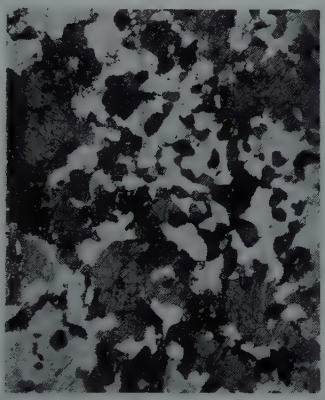

3

4

5

6

# *Isokite and triplite from Bohemia.*

By D. Jerome Fisher, Ph.D.

Dept. of Geology, University of Chicago, Illinois, U.S.A.

[Read 6 June 1957.]

*Summary.* Isokite ($CaMgPO_4F$), a new mineral homologous with sphene, was described late in 1955 from a Rhodesian carbonatite plug. A fine-grained variety is now reported from Bohemia, where it occurs as a replacement of (probably a hydrothermal alteration product of) coarse medium brown 'later' triplites. It is intimately associated with fine-grained apatite that along with quartz formed post-isokite.

SOME work on pegmatite phosphates by the writer in September 1954 yielded an X-ray powder pattern from a sample in the University of Chicago collection labelled 'triplite from Schlaggenwald, Bohemia (Foote, Philadelphia)' that could not be identified. However, from the powder-pattern data given recently with the description of the new mineral isokite (ĭ-sōk′-īt; *not* ī′-sō-kīt) by Deans and McConnell (1955), it was realized that this was probably the same as the writer's unknown. A sample of the Rhodesian isokite yielded the powder pattern given as no. 173 in fig. 1. This is substantially identical with the pattern from the unknown mineral in the Schlaggenwald triplite specimen as shown in no. 183 of fig. 1.

## *Slavkov and its triplite.*

Horni Slavkov (German name: Schlaggenwald) is in the Karlsbad Hills of north-western Bohemia about 11 km. south-south-west of Karlsbad and 20 km. north-north-east of Marienbad. The Karlsbad Hills, which are south of the Eger (Ohře) River, are underlain by granites intrusive into gneisses and schists; in fact the geology is very similar to that of the Erzgebirge north of the river. Slavkov and Krásno nad Lesy (German name: Schönfeld; 3 km. to the south-south-west of Slavkov) were the centre of the great tin-mining industry of Europe in the sixteenth century. Mining was important here as early as the twelfth to fourteenth century, but by 1870 (Groth) the mines were closed down and had caved in; nothing but a single pillar of granite was left exposed (Phillips, 1896, p. 437). Kratochvil (1943) gives 376 references for this locality, but the latest is 1934. He lists nearly 100 mineral species from Slavkov (including the phosphates apatite, pharmacolite, scorodite,

triplite, and wavellite, as well as autunite and torbernite) and gives 13 references to triplite from here, the earliest one by Glueckselig in 1854. In 1910 Lazarevič quoted Cornu as stating that the Slavkov triplite stage embraced the paragenesis (here meaning *association*): quartz, cassiterite, triplite, chalcopyrite, and molybdenite. The triplite would thus seem to occur in connexion with the tin veins, though in places these carry enough felspar so that they resemble pegmatites. In fact Cornu states that there is a felspar mine on the Mückenberg which is $5\frac{1}{2}$ km. south-west of Slavkov and $1\frac{1}{2}$ km. north-east of Lauterbach. Triplite-bearing pegmatites near Königswart and Punau in the vicinity of Marienbad have been described by Sellner (1924) and earlier writers. According to Cornu the contact metamorphic minerals from Slavkov are found in the Reinbachtal, which is only 4 km. west of Slavkov; while wollastonite and diopside, as well as manganoan siderite (oligonite), baryte, and fluorite, occur at Hub (midway between Krásno and Slavkov). No reference has been found that gives the exact locality of the triplite, and there is no indication that two generations of this mineral may be present. The Foote Mineral Company has no record to show the exact source of these triplite specimens.

Stelzner (1906, p. 932) states that a steeply-dipping gneiss block is embedded in the granite of the Lauterbach–Schönfeld–Schlaggenwald district. This block is intruded by three stock-like masses of fine-grained granite. In these the tin ores occur as stockworks of topaz-bearing greisen; they are also found in veins in the gneiss. Fiala (1947) calls this a biotitic katagneiss, and says that the Huberstock, the largest one of the three, some 570 by 180 m., which lies south of Slavkov, was the most important. The smallest one, the Klingenstock, is north-west of Krásno (Schönfeld). Between these is the Schnödenstock, 180 by 90 m., and the road from Slavkov to Krásno crosses its eastern edge. These three stocks occur along a north-east–south-west line.

In 1946 Dr. Jan Kutina collected samples of greisen from a dump on the Schnoedenstock. These carry vein-like masses of medium brown vitreous to resinous-lustred triplite up to 1·5 cm. thick forming irregular indefinite boundaries with the greisen. Brownish-pink, dull-lustred, fine-grained apatite (megascopically very similar to the isokite) is commonly present between the triplite and the greisen. Small anhedra of chalcopyrite and veinlets of quartz also occur in both the triplite and apatite. Grains of chalcopyrite and cassiterite are found in the associated greisen. Molybdenite and fluorite also occur in triplite specimens from this locality in the mineral collections of Charles University. Kutina

collected from a fresh dump; mining in this area was rejuvenated on a small scale during World War II, in the main for tungsten. On this dump were pieces of a felspar–quartz–mica pegmatite; but no triplite was found in this rock. Aplites are common in the area, and tourmaline-

TABLE I. Analyses of triplites.

| | *Slavkov.* | | | *Schoenfeld.* | *Koenigswart.*‡ | | *Punau.*§ |
|---|---|---|---|---|---|---|---|
| | *Dark.** | *Light.** | *von Kobell* (1864). | *Otto*† (1936). | *Sellner* (1924). | | |
| CaO | 3·4 | 10·0 | 2·20 | 1·80 | 6·89 | 4·90 | 8·68 |
| MnO | 27·5 | 21·5 | 30·00 | 28·48 | 31·96 | 33·40 | 22·94 |
| FeO | 29·6 | 21·9 | 26·98 | 25·80 | 24·84 | 26·50 | 16·50 |
| MgO | 0·7 | 6·0 | 3·05 | 7·20 | tr | tr | 15·54 |
| $Fe_2O_3$ | — | — | — | — | 0·17 | 1·43 | — |
| $TiO_2$ | 0·16 | 0·22 | — | — | — | — | — |
| $P_2O_5$ | — | — | 33·85 | 31·98 | 31·87 | 30·44 | 32·14 |
| F | — | — | 8·10 | 7·64 | 3·29 | 3·34 | 5·70 |
| Other | — | — | — | — | 0·64 | 0·42 | 0·90 |
| Total | | | 104·18 | 102·90 | 99·66 | 100·43 | 102·40 |
| Less O for F | | | 3·40 | 3·21 | 1·39 | 1·40 | 2·40 |
| Total | | | 100·78 | 99·69 | 98·27 | 99·03 | 100·00 |
| *D* | 3·886 | 3·828 | 3·77 | | 3·88 | | |
| $\alpha$ | 1·680 | 1·662 | 1·672‖ | 1·664 | | | |
| $\beta$ | 1·689 | 1·667 | | 1·674 | | | |
| $\gamma$ | 1·702 | 1·680 | 1·683‖ | 1·680 | | | |

* Spectrographic analyses (each constituent to ±5 % of its figure); all iron calculated as FeO.

† Otto states that this sample is from a pegmatite; Heinrich must be wrong when he says this is from Germany. The last three samples in the above table are from Bohemia, not Moravia (as stated in Hintze, Dana, and Heinrich).

‡ Density from Lazarevič (1910); analyses by W. Stanczak.

§ Recalculated from an analysis with 8·10 % insoluble. Punau (or Punnau) is 10 km. south-east of Marienbad.

‖ *n*-values for Slavkov triplite. R. Rost, Min. Abstr., 1946, vol. 9, p. 205.

bearing pegmatites are known. Fiala notes that red orthoclase–albite–quartz pegmatites are typical of the border of the greisen stocks.

The Slavkov triplites as represented by the specimens at hand contain two forms of the mineral. One is very dark brown and the other is medium or chestnut brown. The two do not occur in the same hand specimen. Both of them are thoroughly fresh. The dark material, which occurs in massive chunks and is veined by chalk-like apatite, has a light-grey (greenish tinge) streak, pitchy adamantine lustre with one indifferent cleavage. Its composition is shown in table I. The light-

TABLE II. X-ray powder data for triplite (Å.).

| *Indices.** | 1. *d.* | 1. *I.* | 2. *d.* | 2. *I.* | 3. *d.* | 3. *I.* | 4. *d.* | 4. *I.* | 5. *d.* | 5. *I.* |
|---|---|---|---|---|---|---|---|---|---|---|
| 011(?) | | | | | | | | | 5·16 | 1— |
| $\bar{2}02$, $\bar{2}11$ | 4·27 | 1 | | | | | 4·306 | 1 | 4·27 | 1 |
| 211 | 3·62 | 4 | 3·6553 | 1+ | 3·6460 | 2 | 3·659 | 5 | | 4 |
| | | | | | 3·5060 | 1/4 | | | | |
| 112 | 3·41 | 2 | 3·4304 | 2— | 3·4115 | 3 | 3·431 | 4 | | 4 |
| | | | 3·3426 | 2 | | | | | | |
| | | | 3·3067 | 2— | | | | | | |
| | | | 3·2741 | 1 | | | | | | |
| 020 | 3·23 | 6 | 3·2543 | 2 | 3·2395 | 6 | 3·257 | 7 | | 6 |
| $\bar{3}12$, $\bar{1}21$ | 3·03 | 8 | 3·0417 | 6 | 3·0291 | 7 | 3·053 | 9 | | 8 |
| 400† | 2·86 | 10 | 2·8675 | 10 | 2·8601 | 10 | 2·874 | 10 | | 10 |
| 220, $\bar{4}02$ | 2·83 | 1 | | | 2·8177 | 1/4 | 2·832 | 1/2 | | |
| $\bar{4}11$ | 2·73 | 1 | | | 2·7283 | 1 | 2·740 | 2 | | |
| 022 | 2·69 | 1 | | | 2·6789 | 1/4 | 2·691 | 1 | | |
| $\bar{2}22$ | 2·60 | 2 | 2·6057 | 1+ | 2·5920 | 1+ | 2·614 | 3 | | |
| $\bar{3}21$ | 2·53 | 1 | | | 2·5619 | 1/4 | 2·531 | 3 | | |
| 312 | | | 2·5181 | 1— | 2·5140 | 1— | 2·489 | 2 | | |
| $\bar{2}04$ | 2·471 | 1 | | | 2·4762 | 1/4 | | | | |
| 004‡ | 2·377 | 1 | | | | | 2·400 | 1/2 | | |
| $\bar{4}13$ | 2·316 | 1 | | | | | 2·340 | 1 | | |
| 321, 222, 123 | 2·290 | 1 | | | 2·2913 | 1/4 | 2·305 | 1 | | |
| 402 | 2·218 | 2 | 2·2236 | 1/4 | 2·2193 | 1— | 2·230 | 3 | | |
| 303, $\bar{5}12$, 510 | 2·179 | 1 | 2·1519 | 1/4 | 2·1439 | 1 | 2·186 | 1/2 | | |
| 420, 123, $\bar{5}03$, $\bar{4}04$ | 2·148 | 2 | | | 2·1259 | 1/4 | 2·156 | 3 | | |
| $\bar{3}23$, 501, $\bar{4}22$ | 2·108 | 3 | 2·1122 | 1— | 2·1044 | 1— | 2·120 | 4 | | |
| | 2·012 | 3 | | | 2·0099 | 1/2 | 2·024 | 4 | | |

| 1. *d.* | 1. *I.* | 2. *d.* | 2. *I.* | 3. *d.* | 3. *I.* | 4. *d.* | 4. *I.* | 5. *d.* | 5. *I.* |
|---|---|---|---|---|---|---|---|---|---|
| 1·975 | 1 | | | | | 1·979 | 1/2 | | |
| | | | | | | 1·949 | 1/2 | | |
| 1·917 | 1 | 1·9173 | 1/4 | 1·9212 | 1/4 | 1·920 | 3 | | |
| | | | | 1·9111 | 1/2 | 1·892 | 1/2 | | |
| 1·833 | 1 | 1·8341 | 1/4 | | | 1·843 | 2 | | |
| 1·825 | 1 | | | 1·8165 | 1/4 | 1·823§ | 2 | | |
| 1·815 | 1 | 1·7954 | 1/4 | 1·7853 | 1/2 | 1·800 | 2 | | |
| 1·788 | 1 | | | | | 1·776 | 1 | | |
| 1·765 | 1 | 1·7600 | 1/4 | 1·7540 | 1/4 | 1·767 | 2 | | |
| 1·744 | 1 | | | 1·7395 | 1/4 | 1·750 | 2 | | |
| 1·672 | 1 | | | | | 1·680 | 3/4 | | |
| | | | | | | 1·660 | 1/2 | | |
| 1·638 | 2 | | | | | 1·640§ | 3 | | |
| 1·627 | 2 | | | | | | | | |
| 1·600 | 2 | | | | | 1·602 | 2 | | |
| | | | | | | 1·584 | 1/2 | | |
| 1·565 | 1 | | | | | 1·566 | 2 | | |
| | | | | | | 1·541 | 2 | | |
| 1·524 | 1 | | | | | 1·523§ | 1 | | |
| 1·520 | 1 | | | | | | | | |
| 1·471 | 1 | | | | | 1·474§ | 1 | | |
| 1·453 | 3 | | | | | 1·459 | 2 | | |
| 1·435 | 1 | | | | | 1·439 | 1 | | |
| 1·414 | 1 | | | | | 1·418 | 1 | | |
| 1·394 | 1 | | | | | 1·398 | 1/2 | | |
| (8 more lines) | | | | | | (37 more lines) | | | |

1. Serra Branca, Brazil. Lindberg, Amer. Min., 1950, vol. 35, p. 72. Fe/Mn radiation.

2. Dark triplite, Slavkov. Guinier-de Wolff multiple camera (calibrated), Co-$K\alpha_1$ radiation. I have no explanation for the apparent splitting of the (020) reflection into 4 lines.

3. Light triplite, Slavkov. Same data as last.

4. Dark triplite, Slavkov. Fe/Mn radiation, 11·5 cm.-diameter camera. Spacings measured by Leon Atlas, 18 April 1949.

5. Light triplite, Slavkov. Same data as last. Given only to show presence of 5·16 line, and intensities of major lines.

* Computed graphically by the Peacock–Bloss technique (Amer. Min., 1952, vol. 37, p. 588), assuming space-group $I\,2/m$.

† Included in the range 2·85 to 2·92 are also 121, 103, 303, 013, and 213.

‡ Included in the range 2·36 to 2·42 are also 411, 501, and 213.

§ Broad and diffuse line.

*Note.* Approximate spacings for both light and dark triplite from Finland using Cu/Ni radiation with a 5·7-cm. diameter camera are given by A. Volborth, pp. 32–33.

coloured triplite occurs as small vitreous to resinous-lustred irregular anhedra embedded in fine-grained dull-lustred light-brown isokite and fine-grained light grey apatite. It has a white streak and shows no cleavage. A spectrographic analysis appears in table I. X-ray powder-diffraction data for these two triplites are given in table II. While the spacings for the light triplite are definitely consistently smaller than those for the dark triplite, any intensity differences or differences in lines present are very minor. The weak 5·16-Å. line seen in most light triplite films is absent in those made from the dark triplite.

It is probable that these triplites are of two generations. While this is not mentioned by Heinrich, it seems to be a fairly common phenomenon. Thus at the 'White Rock' (quartz core) pegmatite just north-east of Koenigswart (20 km. south-west of Slavkov and 7 km. north-west of Marienbad) Lazarevič describes two kinds of triplite: dark brown compact coarse-grained aggregates with an adamantine-oily lustre, one good cleavage and a poor one normal thereto; and light-brown, fine-grained, dull-lustred, indistinct cleavage. At Hagendorf, 40 miles south-west of Slavkov and barely across the Bavarian border, Schmid (1955, p. 353) describes two triplites; the older is chestnut brown and commonly in felspar, the younger is light brown and generally in quartz. Volborth (1954, p. 27) has an older dark brown and a younger reddish-brown triplite in the Viitaniemi (Finland) pegmatite. The isokite in the Slavkov specimens has been found only in the light brown triplite samples.

The Slavkov triplite seems to have been distributed very widely; thus many museums probably contain samples of Bohemian isokite; this was true for the Chicago Natural History Museum. At the XXth International Geological Congress Slavkov triplite (presumably with isokite) was seen in the collection of the Instituto de Geología of the Universidad Nacional de Mexico.

*Isokite.*

Isokite from the type locality (15 miles east of Isoka [pron. Ĭsōk'a] in Northern Rhodesia) occurs in the samples at hand as radiating white fibres or needles in globular masses less than a millimetre in diameter. These are sprinkled through a limonite-stained coarsely-crystalline ankeritic dolomite composing a carbonatite plug which cuts granitic and micaceous gneisses. Apatite is a principal accessory mineral. The isokite is considered to have replaced the dolomite in a late stage of metasomatic activity.

A large (2 by 5 cm.) thin section was cut from a specimen of the light-

brown Slavkov triplite which had a 15-mm. wide fissure vein of coarse green apatite across one end. A photograph of it (no analyser) appears in fig. 2. A portion of it (taken with an analysing polaroid filter) together with an explanatory 'geologic map' is shown in fig. 4, and photomicrographs of selected areas appear in fig. 3.

Neglecting the coarsely crystalline green apatite vein (analysis: Otto,

---

FIG. 1. X-ray powder diffraction photographs of minerals homologous with isokite; natural size, Fe/Mn radiation, 114·6-mm. diameter camera. 188—Durangite, Durango, Mexico. Yale Brush no. 586; 187—Sphene, Pitcairn, New York. Univ. of Chicago no. 763; 183—Isokite, Bohemia; 173—Isokite, Rhodesia; 201—Tilasite, Långban, Sweden. Riksmuseet no. 339, 650.

FIG. 2. Photomicrograph (no analyser) of large thin section from Slavkov specimen. Sides of squares of grid are 2 mm. long. Upper one-third is mainly apatite, fragment of which at upper left was broken off in grinding. The three circles indicate areas shown in more detail in fig. 3. See text for further description.

FIG. 3. Photomicrographs (crossed polars) of portions of the large thin section, as outlined by circles on fig. 2.

A1: From L4 area of fig. 2. Shows mostly a portion of a single anhedron of triplite (light grey) cut by replacement veinlets of apatite (black or dark grey). Polars not quite crossed, thus holes (fragments torn from the triplite) appear light grey. Cleavage cracks are obvious. Speckled or mottled white to grey to black areas through the triplite are the replacing isokite.

A2: Shows the portion in the circle of A1 in more detail; polars truly crossed, so holes are black. Both of these make it clear that the apatite was the last of the three minerals formed.

B1: From J9 area of fig. 2. The two isolated masses of triplite (light grey; lower left and upper right) are parts of a single anhedron. The fine-grained apatite appears dark grey to black; part of it is as two replacement veinlets, but that across the top is a portion of the large mass of such apatite along row I of fig. 4. Isokite is the most abundant mineral present.

B2: Detail from upper right circle of B1. Shows the isolated part of the triplite crystal (light grey with a dark tear-fragment spot and cleavage cracks), much fine-grained apatite, and masses of fine-grained isokite in lower left and lower right.

B3: Enlargement from lower left circle of B1. Excellent to show three masses of a single triplite anhedron (upper left, left, and below the centre) isolated from one another by isokite replacement, then cut by an apatite vein.

C1: From T4 area of fig. 2. Apatite-quartz vein on left, triplite anhedron on right, isokite between. There is everywhere a selvage of apatite separating the quartz from the isokite.

C2: Detail from portion shown by circle in C1. Triplite at top and in lower right; these constitute a small part of the large single crystal of triplite making up the lower right portion of fig. 2. Nearly all of the rest of C2 is isokite; a little apatite is found at the lower left and along the triplite cracks.

FIG. 4. Photomicrograph (crossed polars) of central portion of the large thin section, together with explanatory diagram. Here H refers to a hole in the thin section.

FIG. 1.

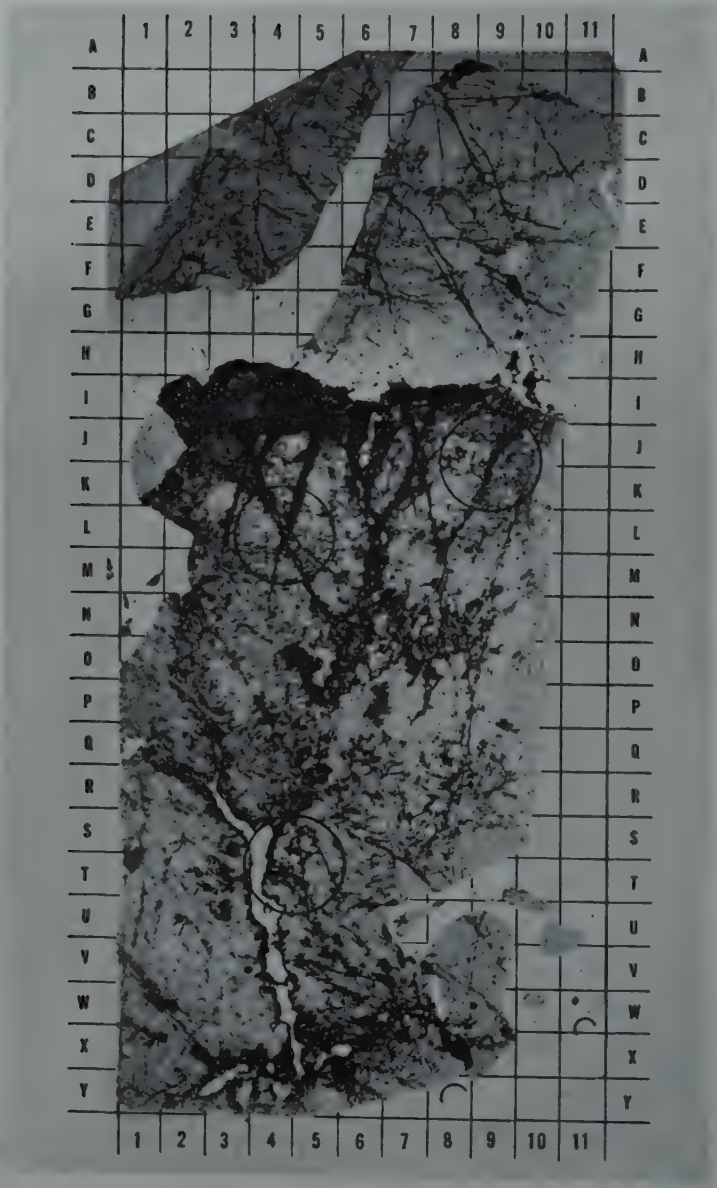


Fig. 2.

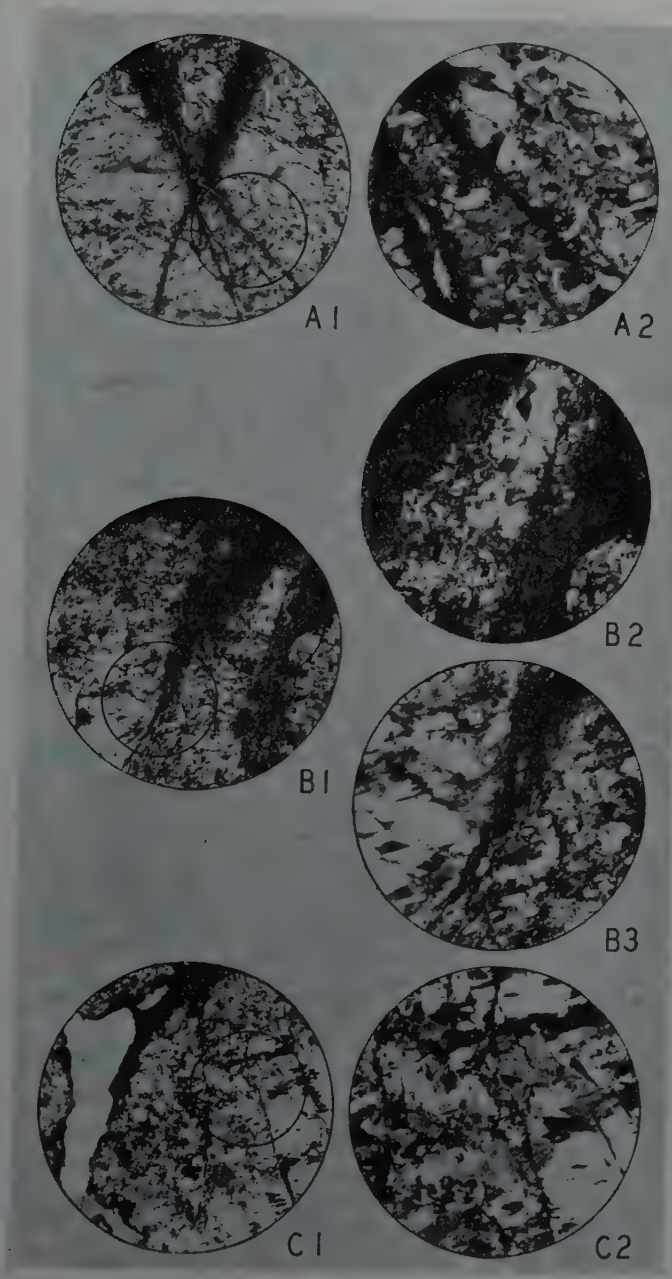


FIG. 3.

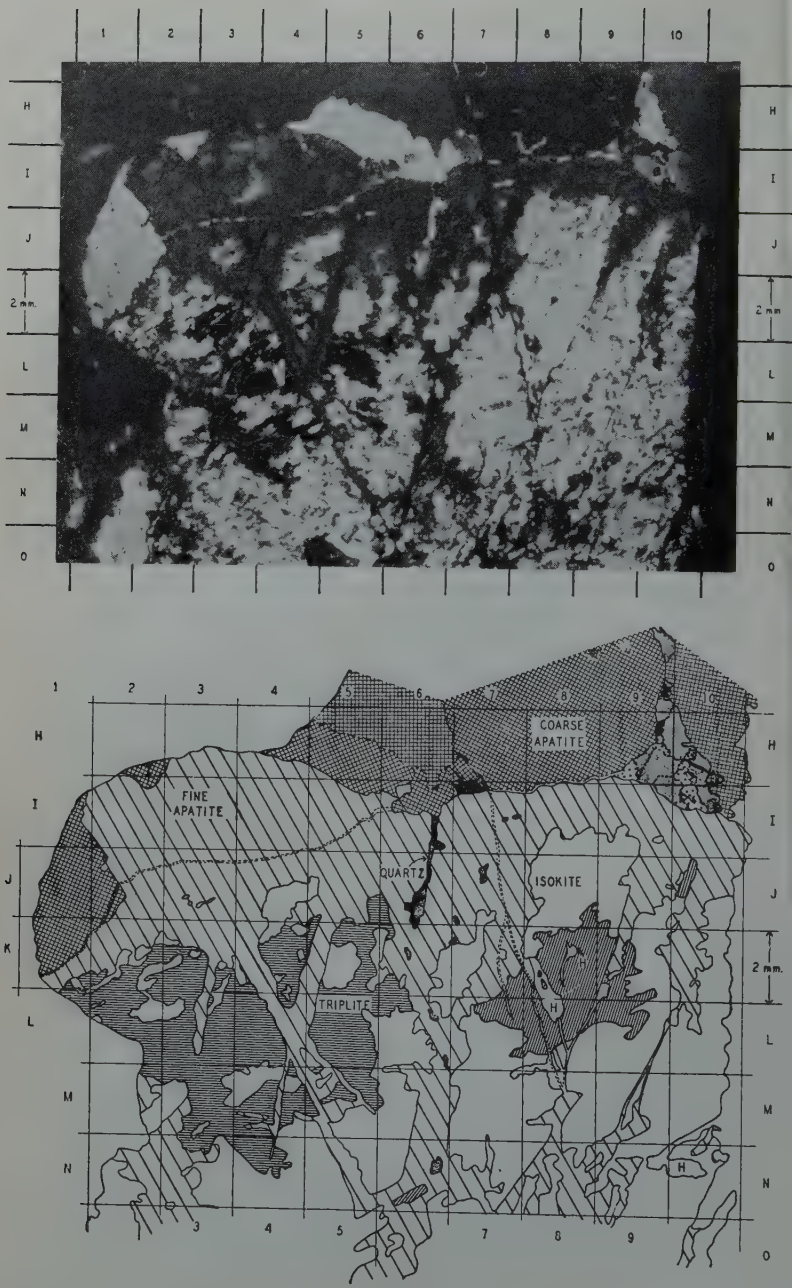
1
2
3
4
5
6
7
8
9
10
H
I
J
2 mm.
L
M
N
O
COARSE APATITE
FINE APATITE
QUARTZ
ISOKITE
TRIPLITE

FIG. 4.

1936, p. 112) across one end, this Slavkov thin section consists in the main of three large corroded triplites; by far the largest makes up the 'south-east' (map parlance) quarter of the specimen (fig. 2), but the other two in the upper half show up well in fig. 4. A quartz vein splits the lower part of the specimen along a near-vertical line; it actually extends intermittently all the way up the middle of the specimen. It is fringed with narrow borders of fine-grained apatite, outside of which is isokite; not a great part of the latter occurs to the east of the vein, but the whole south-west portion of the section is isokite, as is a central east–west band $\frac{1}{2}$ to 1 cm. in width. The isokite and triplite are differen-

TABLE III.

| | Triplite $8[(Mn,Fe,Mg,Ca)_2PO_4F]$. | Isokite $4[MgCaPO_4F]$. | Apatite $2[Ca_5(PO_4)_3F]$. |
|---|---|---|---|
| Space-group | $I\ 2/m$(♯12) | $C\ 2/c$(♯15) | $C\ 6_3/m$(♯176) |
| $a:b:c$ | 12·0:6·5:10·0 | 6·52:8·75:7·51 | 9·36:6·88 |
| $\beta$ | 105°42′ | 121°28′ | — |
| Unit-cell volume | 750 | $731 \times \frac{1}{2}$ | $696 \times 3/4$ |
| Cations per $8(PO_4)$ | 16 | 16 | $10 \times 4/3 = 13{\cdot}3$ |
| Density | 3·9 | 3·3 | 3·2 |

tiated in fig. 4 (crossed polaroids), since the former is fine-grained, and so appears speckled. The fine-grained apatite shows up well in fig. 2 (no analyser) as medium to dark grey, nearly black; it occurs near the top and along some of the straight upper veins. The courses of the latter are controlled presumably by the triplite cleavages. If this is true, the triplite was obviously once much more extensive than it is at present. The fact that the two large triplites shown in fig. 4 are broken up into very irregular corroded masses by the isokite, both of which minerals are cut by replacement veins of apatite, indicates rather clearly a sequence triplite–isokite–apatite.

Table III presents certain changes involved in the alteration of triplite to isokite; data are also given on apatite. Examination of the thin section shows that triplite was extensively altered to isokite; this would require the removal of Mn and Fe, the major cations of most triplites, with ion-for-ion replacement by Mg and Ca, with the latter two in (at least approximately) a 1:1 balance. There is little evidence from the thin section that either triplite or isokite was altered into apatite. In fact the bold veins of fine-grained apatite cutting these two minerals, and partly replacing the triplite, and probably the isokite to a much less extent, indicate strongly that apatite as such was introduced later. The quartz present as fissure-vein fillings with a selvage of fine apatite is so

closely associated with the latter that the two were probably deposited from the same solutions, though the quartz apparently formed slightly later. Locally there are very minor amounts of opaque alteration products of the phosphates.

The Slavkov isokite is very fine grained and no crystal faces were seen. Employing the universal stage double variation technique, and working with grains smaller than 100 mesh, it was found that most

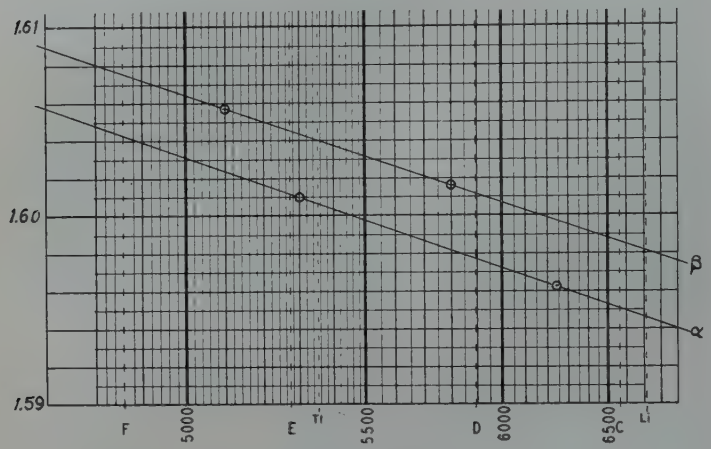


Fig. 5. Dispersion curves for $\alpha$ and $\beta$ of Slavkov isokite.

grains if not actually nearly fibrous consisted of three or more differently oriented crystals. Study of a crystal in one grain yielded the dispersion curves for $\alpha$ and $\beta$ shown in fig. 5, each line being based on but two points as indicated. These curves give for Na light $\alpha = 1{\cdot}5977$, $\beta = 1{\cdot}6012$. Since the crystal showed somewhat undulatory extinction, these results are probably about $\pm 0{\cdot}001$. The crystal was positive with $2V = 39° \pm 2°$. In several attempts no grain was found suitable for the determination of $\gamma$ by this technique. Using these values a graph indicates that $\gamma$ is about 1·629. Employing ordinary immersion techniques, the highest measured value obtained was $\gamma'$ of about 1·619 for Na light. Thus the assumed best values for Slavkov isokite for Na light are (with $2V = 39°$) $\alpha = 1{\cdot}597$, $\beta = 1{\cdot}600$, $\gamma = 1{\cdot}623$. The Rhodesian isokite was found to have $\alpha = 1{\cdot}590$, $\beta = 1{\cdot}595$, $\gamma = 1{\cdot}615$, with $2V = 51°$. No dispersion was observed in the interference figure of the Slavkov isokite. Assuming $b$ = acute bisectrix (as determined on the Rhodesian

isokite) any dispersion should be of the crossed type. This was tested against the extinction position of the trace of the optic plane for yellow and violet light. No difference greater than the probable error in readings was noted. The associated fine-grained apatite has (Na light) $\omega = 1{\cdot}633$, $\epsilon = 1{\cdot}628$, both $\pm 0{\cdot}002$.

A sample of Slavkov isokite, which unfortunately was contaminated with apatite (presumably some 35 % of the latter), subjected to spectrographic analysis showed: CaO, 40·0; MgO, 15·5; MnO, 1·5; $TiO_2$, 0·22; Fe, 1·5. The sample probably had enough triplite in it to account for the Mn and Fe.

X-ray diffraction powder data on isokite are given in table IV for three radiations. Using cobalt radiation (col. 2) with the Guinier–de Wolff multiple camera where the patterns of the Bohemian and Rhodesian isokite appear next to each other on the same film, the differences are very minor: the former lacks the 2·89 line, the latter lacks the 2·70 line, and the 2·787 line of the latter (the one whose measurements are given in col. 2) appears as a doublet on the former. Other differences are so minor as to be barely discernible. In particular there is no measureable difference in the spacing of any of the lines, showing substantial identity of unit-cell dimensions and angles; the reversal in relative intensities of the 3·18 and 3·02 lines (as compared to the values of cols. 3 and 4) is interesting. The results from the two isokites using iron radiation are given in cols. 3 and 4; here the spacings are measured much less exactly. The most pronounced distinction is the difference in relative intensities of the 2·787 line. Also the weak 1·74, 1·77, and 1·83 lines are much more apparent in the film from the Bohemian specimen, as are the 2·70 and 3·40 lines; on the other hand the weak 4·38 and 2·89 lines are apparent only in the film from the Rhodesian sample. The failure to be able to index the 2·04 line is puzzling; the ($\bar{2}21$) line should have a spacing of 2·60 rather than 2·63.

*Acknowledgements.* I am particularly indebted to Dr. Jan Kutina of Charles University (Prague), not only for the details of his mineral collecting at Slavkov and his descriptions of Slavkov specimens in the University Museum, but also for his preparation of a translation of Fiala's paper. Oiva Joensuu made the spectrographic analyses. W. F. Schmidt did the photography. Samples of the Rhodesian isokite were supplied by W. H. Bennett of the Mineral Resources Division of the British Colonial Geological Surveys through the kindness of G. E. Howling. Slavkov isokite was loaned me by H. Changnon of the Chicago Natural History Museum through the courtesy of S. K. Roy. The durangite specimen was furnished by Horace Winchell, and that of tilasite by Frans E. Wickman.

TABLE IV. X-ray powder data for isokite (Å.)

| | 1. | | 2. | | 3. | | 4. | |
|---|---|---|---|---|---|---|---|---|
| *Indices.** | *d.* | *I.* | *d.* | *I.* | *d.* | *I.* | *d.* | *I.* |
| 020 | 4·38 | w | | | | | 4·37 | 1·2 |
| 021 | 3·62 | vw | | | | | | |
| $\bar{1}12$ | 3·45 | vw | 3·4409 | 1 | | | | |
| apatite? | | | 3·4172 | ½ | 3·41 | 1− | | |
| $\bar{1}31$ | | | 3·3186 | 1− | 3·31 | ½ | | |
| 002 | | | 3·2077 | 2 | | | | |
| 111 | 3·185 | vvs | 3·1795 | 8 | 3·18 | 10 | 3·18 | 10 |
| $\bar{2}02$ | 3·023 | vvs | 3·0211 | 10 | 3·01 | 8 | 3·01 | 9 |
| ? | 2·887 | vvw | | | | | 2·89 | ½ |
| 200 | 2·784 | m | 2·7868 | 5 | 2·79 | 6† | 2·78 | 2 |
| apatite? | | | | | 2·70 | 1½ | 2·70 | ½ |
| $\bar{2}21$? | 2·630 | vvs | 2·6287 | 7 | 2·62 | 7 | 2·62 | 9 |
| 022, 130 | 2·586 | m | 2·5903 | 6 | 2·57 | 3 | 2·57 | 2+ |
| $\bar{2}22$ | 2·487 | vw | | | | | | |
| $\bar{1}32$ | 2·301 | s | 2·3026 | 4 | 2·30 | 3 | 230 | 4 |
| 112 | | | 2·2332 | 2− | 2·24 | 1 | | |
| 040, 131 | 2·222 | m† | 2·2201 | 2− | 2·22 | 2 | 2·22 | 3† |
| 003, $\bar{3}12$, $\bar{2}23$ | 2·105 | m | 2·1066 | 2 | 2·10 | 1½ | 2·10 | 2 |
| 041 | 2·069 | m | 2·0729 | 1− | 2·065 | 1 | 2·07 | 2+ |
| ? | 2·041 | m | 2·0421 | 2 | 2·035 | 1½ | 2·04 | 2 |
| $\bar{3}13$ | 1·962 | w | | | 1·96 | ½ | 1·96 | ½ |

1. Deans and McConnell, Cu-$K\alpha$ radiation, 19-cm. camera. Rhodesia.
2. Guinier–de Wolff multiple camera (calibrated), Co-$\kappa\alpha_1$ radiation.
3. Fe/Mn radiation, 11·5-cm. camera, spacings measured with Nies scale (spacings not accurate; listed because of intensities). P 190, Bohemia.

| | 1. | | 2. | | 3. | | 4. | |
|---|---|---|---|---|---|---|---|---|
| *Indices.** | *d.* | *I.* | *d.* | *I.* | *d.* | *I.* | *d.* | *I.* |
| 221 | 1·946 | vw | | | 1·935 | 1 | 1·95 | ½ |
| $\bar{1}33$ | 1·886 | vw | | | 1·88 | ½ | | |
| $\bar{2}04$ | 1·872 | w | 1·8738 | ½ | 1·87 | ½ | 1·875 | 1+† |
| 310 | 1·837 | vvw | | | 1·83 | 1 | | |
| $\bar{2}41$, 132, 042 | 1·807 | m | 1·8062 | ¼ | 1·80 | ½ | 1·81 | 2 |
| $\bar{2}42$, $\bar{1}14$ | — | — | — | — | 1·77 | ½ | — | — |
| $\bar{3}32$ | 1·740 | vvw | | | 1·74 | ½ | | |
| 240 | 1·720 | s | 1·7215 | 3 | 1·720 | 4 | 1·72 | 5 |
| 202, $\bar{3}14$ | 1·705 | m | 1·7054 | ½† | 1·705 | 1½ | 1·705 | 1 |
| 113 | 1·684 | vvw | | | | | | |
| | 1·671 | vvw | | | | | | |
| | 1·656 | m | 1·6573 | 3− | 1·655 | 3 | 1·655 | 3 |
| 004 | 1·602 | vvw | | | 1·605 | 1− | | ½ |
| | 1·557 | m | 1·5571 | ½ | 1·555 | 1 | 1·555 | 2 |
| | 1·539 | vvw | | | 1·535 | ½ | | ½ |
| $\bar{3}31$ | 1·522 | vvw | | | 1·520 | ½ | | ½ |
| | 1·510 | vvw | | | 1·510 | ½ | | ½ |
| | 1·495 | vvw | | | 1·495 | ½ | | ½ |
| | 1·479 | m | 1·4804 | ½ | 1·48 | 2 | 1·48 | 2 |
| | 26 more lines (all w or less) | | | | | | | |

4. Same as last, except P 174, Rhodesia.

* Computed graphically by the Peacock–Bloss technique (Amer. Min., 1952, vol. 37, p. 588).

† Broad and diffuse line.

## Addendum

The optical properties of the Slavkov triplites listed in the first two columns of table I have recently been determined by two of my students using the double variation technique on the universal stage, with results as follows:

| | *Dark triplite** | | | | *Light triplite*† | | | |
|---|---|---|---|---|---|---|---|---|
| λ. | *C.* | *D.* | *E.* | *F.* | *C.* | *D.* | *E.* | *F.* |
| α | 1·6785 | 1·6802 | 1·6824 | 1·6845 | 1·6592 | 1·6626 | 1·6668 | 1·6707 |
| β | 1·6868 | 1·6883 | 1·6903 | 1·6922 | 1·6625 | 1·6662 | 1·6711 | 1·6755 |
| γ | 1·6999 | 1·7012 | 1·7031 | 1·7049 | 1·6752 | 1·6787 | 1·6832 | 1·6873 |
| $V_A$‡ | 38·3 | 38·3 | 38·3 | 38·3 | 29·1 | 29·0 | 28·9 | 28·8 |
| $V_B$‡ | 39·4⁵ | 39·1 | 38·6 | 38·1⁵ | 30·9 | 30·4 | 29·8 | 29·2 |
| 2V | 77·7⁵ | 77·4 | 76·9 | 76·4⁵ | 60·0 | 59·4 | 58·7 | 58·0 |

* α, β, and V measured by S. Ghose; γ calculated from these results by D. J. F.; thus the γ-values would presumably have rather large errors if there were even small ones in the α or β figures. Later actual measurements by Ghose show that these γ values are substantially correct, at least in the D–E range.

† All values measured by G. Chao (except V for F light).

‡ The differences in the two V-values determined for each wave-length confirm the presence of inclined dispersion (thus $b \rightarrow \beta$) with $r > v$.

A. S. Povarennykh (1950) has described triplite and apatite in the hydrothermal veins of southern Kazakhstan. Here the apatite is also post-triplite. At depth the apatite forms borders of the triplite masses, but in the upper horizon the apatite almost completely replaces the triplite. This is a mangan-triplite with only very minor amounts of Ca and Mg. On the other hand the analysis of the apatite shows 2·17 % MgO. This is so unusual that the writer is inclined to suspect that this apatite may contain some isokite.

### *References.*


Cornu (F.), 1905. Tschermaks Min. Petr. Mitt., vol. 24, p. 334.

Deans (T.) and McConnell (J. D. C.), 1955. Min. Mag., vol. 30, p. 681.

Fiala (F.), 1947. Věstník Státního geologického ústavu Č.S.R. (Praha), vol. 32, p. 101.

Groth (P.), 1870. Zeits. deut. geol. Gesell., vol. 22, p. 381.

Heinrich (E. W.), 1951. Amer. Min., vol. 36, p. 256.

Kratochvil (J.), 1943. Archiv pro Přírodovědecký Výzkum, vol. 21 (2), p. 1485. Also see vol. 21 (4), p. 574 (1948).

Lazarevič (M.), 1910. Centr. Min., p. 385.

Otto (H.), 1936. Tschermaks Min. Petr. Mitt., vol. 47, p. 89.

Phillips (J. A.), 1896. Treatise on Ore Deposits (2nd edn. by H. Louis), 943 pp. Macmillan and Co., London.

[Povarennykh (A. S.)] Поваренных (А. С.), 1950. Зап. Всесоюз. Мин. Общ. [Mem. All-Union Min. Soc.], ser. 2, vol. 79, p. 226; abstr. by A. Mirtsching, Zentr. Min., 1954 (for 1952), pt. 1, p. 83.

Schmid (H.), 1955. Neues Jahrb. Min., Abh., vol. 88, p. 309.

Sellner (F.), 1924. Zeit. Krist., vol. 59, p. 504; and vol. 60, p. 275.

Stelzner (A. W.), 1906. Die Erzlagerstätten (completed by A. Bergeat). II. Hälfte, pp. 471–1330. A. Felix, Leipzig.

Strunz (H.), 1952. Neues Jahrb. Min., Abh., vol. 84, p. 77.

Volborth (A.), 1954. Ann. Acad. Sci. Fenn., Ser. A III, no. 39.

Weber (A.), 1948. Rozpravy České Akad., vol. 58, no. 1 [M.A. **11**–51] (Czech); Bull. Internat. Acad. tchèque Sci., vol. 49, no. 1 [M.A. **11**–121] (abbreviated English version).

## SHORT COMMUNICATIONS

### *A note on the composition of staurolite from the Caenlochan schists.*

The Caenlochan schists occur along the north-west side of the Duchray Hill gneiss. They form a belt of country about 1 mile wide extending north-east from the Glen Shee diorite towards the Tolmount situated in the north-west corner of Forfarshire. These schists were named and described by Barrow (1912*a*, p. 22), who correlated them with the Ben Lawers schists of Perthshire. The dominant constituent of the Caenlochan schists is a finely banded, soft, micaceous rock; the lighter bands are specially rich in granulitic quartz and oligoclase while the darker are mainly composed of mica with biotite in excess of muscovite, garnets, iron ores, and secondary chlorite. Intimately associated with these pelitic and psammopelitic schists are some thin bands of quartzite and some impure limestone. The schists occur within the garnet zone (Barrow, 1912*b*), but as the older granites of the Duchray Hill gneiss are approached there is a marked increase in grain size coupled with the appearance of kyanite and staurolite. Particularly good exposures of coarsely crystalline kyanite–staurolite gneiss occur on the Crags of Cannes at the head of Glen Isla. Staurolite is very abundant and forms crystals up to 3 cm. in length. It is very resistant to weathering, and crystals, weathering out of the gneiss, have accumulated in small hollows on the glaciated rock surface to form patches of staurolite gravel. In thin section this staurolite gneiss is seen to be composed of quartz, oligoclase, biotite, garnet, kyanite, and staurolite, with a little muscovite. Garnet and biotite occur as felts, interleaving quartz–felspar strings, lenticles, and augen. Porphyroblasts of staurolite and kyanite are more or less regularly distributed throughout the rock. Most of the staurolites are riddled with inclusions of quartz. Although the coarse grain size of these rocks can probably be attributed to the adjacent older granites, it is uncertain whether there has been any addition of material for though the gneiss is rich in oligoclase, the normal fine-grained pelitic and psammopelitic schists also contain appreciable amounts of oligoclase.

An analysis of the staurolite from these schists gave: $SiO_2$ 28·33, $TiO_2$ 0·86, $Al_2O_3$ 52·85, $Fe_2O_3$ 3·41, FeO 10·92, MnO 0·04, MgO 2·13, CaO 0·22, $H_2O+$ 1·91, $H_2O-$ nil, sum 100·67 %. Refractive indices

(Na light) $\alpha$ 1·741, $\beta$ 1·746, $\gamma$ 1·755 (all $\pm$0·003). Ferrous iron was determined by fusion of the mineral in sodium metafluoroborate, following the procedure given by Groves (1951); water by a modified Penfield method, the mineral sample being heated in a silica tube for half an hour by an oxy-coal gas burner, the temperature reached being about 1300° C. The number of metal atoms have been calculated on the basis of 48(O,OH) to the unit cell: Si 7·807, Al 17·163, Fe‴ 0·706, Ti 0·178, Mg 0·874, Fe″ 2·515, Mn 0·015, Ca 0·064, OH 3·510; Al+Fe‴ 17·869; Fe″+Ti &c., 3·646. If Ti and Ca are grouped with Fe″, Mg, and Mn, the resultant formula agrees best with that proposed by Juurinen (1956), namely $Fe_4Al_{18}Si_8O_{44}(OH)_4$.

*Research School of Physical Sciences,*
*Australian National University,*
*Canberra, Australia.*
N. J. Snelling.

Barrow (G.) *et al.*, 1912*a*. Explanation of Sheet 65. Mem. Geol. Surv. Scotland.
Barrow (G.), 1912*b*. Proc. Geol. Assoc., vol. 23, p. 274.
Groves (A. W.), 1951. Silicate Analysis. 2nd edn., London.
Juurinen (A.), 1956. Ann. Acad. Scient. Fenn., ser. A, vol. 3, no. 47.

## *Serpierite from the Lake District.*

Serpierite, a basic sulphate of copper, zinc, and calcium, was first described in 1881 from the Camareza section of the Laurium mines in Greece; in 1927 Sir Arthur Russell[1] described a second occurrence at Ross Island, Killarney, Co. Kerry, in Ireland, this being the first and hitherto only known locality in the British Isles. One other locality, in Kazakhstan, in the U.S.S.R., has since been recorded, but it is a rare mineral.

We have recently found and confirmed the occurrence of serpierite at two localities in the northern part of the Lake District. First, at Driggith Mine, Caldbeck, where in some massive, intergrown chalcopyrite and blende, derived from the 30-fathom level, serpierite occurs in narrow veinlets or coating surfaces of joints; it forms aggregates of tiny, pale-blue, lath-like crystals, with a pearly lustre, and at first sight could be confused with aurichalcite. Its identity was confirmed by powder-photographs which exactly match that of authenticated serpierite from Laurium. On some of the specimens from Driggith mine the serpierite is intimately associated with another pale-blue, pearly mineral, in minute hexagonal plates, which gives an entirely different but well-defined powder-pattern, but has so far remained unidentified.

The second occurrence is in a small copper vein near Potts Gill, which has produced an astonishing variety of secondary copper, lead, and zinc minerals and which we hope to describe shortly. At this locality the serpierite forms tufts of minute, pale-blue needles and resembles the Ross Island and some of the Laurium material; it is associated with smithsonite, malachite, aurichalcite, and other secondary copper minerals.

*Department of Mineralogy, University of Oxford.* ARTHUR W. G. KINGSBURY

*Department of Geology, University of Leeds.* J. HARTLEY

[1] Min. Mag. 1927, vol. 21, p. 386.

---

## *γ-Manganese dioxide from Mysore, India.*

DURING an examination under the ore-microscope of manganese ore from Mysore (My 4, Bidarematti, Kumsi area), I noticed a few clumps of slightly fibrous and platy, greyish-white mineral associated with pyrolusite. An X-ray powder photograph of the mineral using Fe-*K* radiation gave a different pattern from that of pyrolusite. The spacings observed and tabulated below agree fairly well with the values of McMurdie and Golovato[1] for $\gamma$-$MnO_2$;[2] the intensities are estimated, and *b* indicates broad lines:

| *d*, Å. | 3·15 | 2·41 | 2·15 | 1·83 | 1·64 | 1·53 | 1·34 |
|---|---|---|---|---|---|---|---|
| *I* | 1 | 10*b* | 9*b* | 1 | 8*b* | 2 | 4*b* |

A synthetic, electrolytically deposited $\gamma$-$MnO_2$ from Japan was furnished for my study by the Winchester research laboratory, New Haven, Connecticut; it gave a pattern in fair agreement with the above spacings.

Differential thermal curves were obtained for both the synthetic and the naturally occurring mineral from Mysore; both show a significant endothermic peak at 600° C. and minor peaks at 250–300° C. and 950° C. The steep peak exhibited at 600° by the synthetic material is probably due to its fineness and purity.

'$\gamma$-Manganese dioxide' is unstable at high temperatures. X-ray photographs of the mineral taken after heating to 500° C. showed a pyrolusite pattern, hence the $\gamma$-dioxide could be considered as poorly crystallized pyrolusite, but the exact nature of it is still uncertain.

The oxide is of considerable industrial value. Recent research in

dry-cell technology has indicated that $\gamma$-dioxide forms a very high-grade material for the manufacture of batteries. Its occurrence has been reported[1] from the ores of Ghana, California, and New Guinea, but this is the first report of the oxide from the ores of Mysore, India.

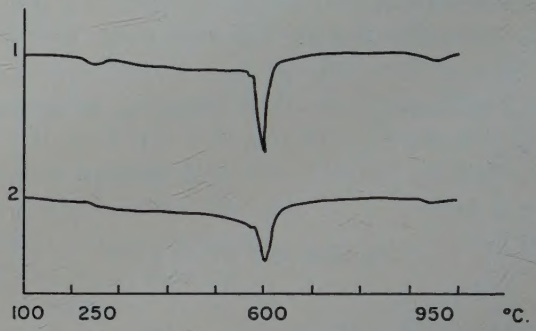


Differential thermal analyses: (1) synthetic $\gamma$-manganese dioxide, (2) $\gamma$-manganese dioxide from Mysore.

I am very grateful to Prof. Alan M. Bateman and Prof. Horace Winchell for their guidance and help in this work.

*Laboratory of Economic Geology,* B. L. Sreenivas
*Yale University,*
*New Haven,*
*Connecticut, U.S.A.*

[1] H. F. McMurdie and E. Golovato, Journ. Res. Nat. Bur. Stand., 1948, vol. 41, p. 589.

[2] $\gamma$-$MnO_2$ was first described by O. Glemser, Ber. deut. chem. Gesell., 1939, vol. 72, Abt. B, p. 1879 [M.A. **9**–227].